Exploring feedbacks between air pollution and climate policy

Clifford Darah Chuwah

Exploring feedbacks between air pollution and climate policy

C.D. Chuwah

2015

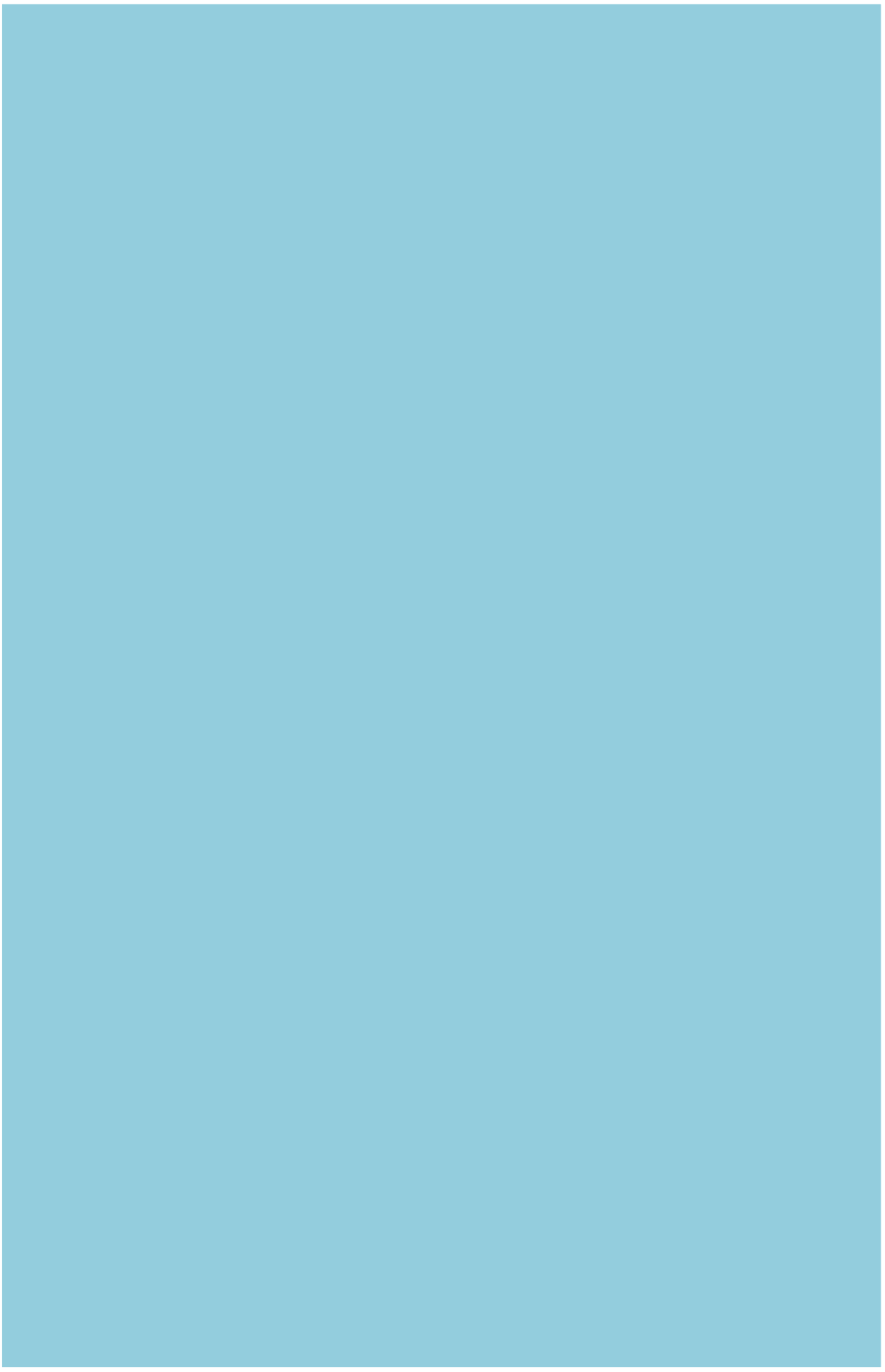

Exploring feedbacks between air pollution and climate policy

Clifford Darah Chuwah

Thesis committee

Promotors
Prof. Dr W. Hazeleger
Professor of Climate Dynamics
Wageningen University

Prof. Dr D. van Vuuren
Professor of Integrated Assessment of Global Environmental Change
Utrecht University

Co-promotor
Dr T.P.C. van Noije
Senior scientist
Royal Netherlands Meteorological Institute (KNMI), De Bilt

Other members
Prof. Dr J. Lowe, University of Reading, UK
Prof. Dr M. Huijbregts, Radboud University Nijmegen
Prof. Dr R. Leemans, Wageningen University
Prof. Dr B. Bregman, Radboud University Nijmegen

This research was conducted under the auspices of the SENSE Research School

Exploring feedbacks between air pollution and climate policy

Clifford Darah Chuwah

Thesis
submitted in fulfilment of the requirements
for the degree of doctor
at Wageningen University
by the authority of the Rector Magnificus
Prof. Dr A.P.J. Mol,
in the presence of the
Thesis Committee appointed by the Academic Board
to be defended in public
on Tuesday 3 November 2015
at 11 a.m. in the Aula.

Clifford Darah Chuwah
Exploring feedbacks between air pollution and climate policy,
125 pages.

PhD thesis, Wageningen University, Wageningen, NL (2015)
With references, summary in English

ISBN 978-94-6257-554-7

The research described in this thesis was financially supported by the Netherlands Organisation for Scientific Research (NWO)

Summary

The climate of the Earth is changing in response to natural and anthropogenic forcing agents. Emissions of greenhouse gases and air pollutants have led to significant changes in the Earth's climate systems and projections indicate that further extensive changes are likely. Increased scientific understanding into the processes responsible for climate change and the possible consequences of assumptions regarding future climate and air pollution policy is important to formulate effective response strategies based on mitigation and adaptation. Earth System Models (ESMs) can be used to make climate projections based on emissions or concentrations projections for greenhouse gasses and aerosols derived from socio-economic scenarios. Such scenarios are produced by Integrated Assessment Models (IAMs), based on detailed descriptions of population growth, energy demand and land use.

There has been increasing interest in coupling different disciplines involved in climate research. The current cooperation efforts among scientists from different disciplines have led to an improved representation of climate forcings in ESMs, and of climate responses impacts in IAMs. In this thesis, we contribute to this cooperation by exploring the consequences of emission scenarios under different assumptions regarding air pollution and climate policy.

To do so, we utilize a set of scenarios similar to the Representative Concentration Pathways (RCPs), developed using the IAM IMAGE. These scenarios combine scenarios with radiative forcing targets in 2100 of 2.6 W/m^2 and 6.0 W/m^2 with different assumptions for air pollution policies (low/high). These scenarios are subsequently used in the global atmospheric chemistry and transport model TM5. Results reveal that both climate and air pollution control policies have large-scale impacts on pollutant concentrations, often of comparable magnitude. We also find that air pollution control measures could, on a global scale, significantly reduce the warming induced by tropospheric ozone and black carbon and the cooling resulting from sulphate in the coming decades. These effects tend to cancel each other on a global scale.

Next, we evaluate the equilibrium climate response to aerosol reductions in different parts of the world in 2050, using the global climate model EC-Earth. Reductions in aerosol concentrations increase downward surface solar radiation and surface temperature concomitantly in various parts of the world. The increase in surface temperature is dominated by the reduced cooling effect of sulphate which in some areas is partially compensated by the decreased warming effect of black carbon. Also, we find that aerosol reductions can significantly affect climate at high latitudes especially in the winter, mostly as a result of teleconnections between the low and high latitudes.

Due to the inhomogeneous spatial distributions of air pollutants, changes in their emissions can have strong regional climate impacts. Using EC-Earth, we assess in Chapter 4 the effectiveness of different aerosol forcing agents in causing climate change in 2050. Our results show that different anthropogenic aerosol components may have a broad range of

efficacies. The results also reveal that there are large interhemispheric differences in aerosol forcings, which result in changes in circulation patterns.

By using surface ozone concentrations simulated by TM5 as input to IMAGE, we estimate ozone impacts on crop production, and subsequent impacts on land use and carbon fluxes in 2005 and 2050. In the absence of new climate and air pollution policies, higher ozone concentrations could lead to an increase in crop damage in 2050 compared to present day. This may lead to a global increase in crop area notably in Asia. Implementation of air pollution policies and climate policies (co-benefits of reducing ozone precursor emissions) could limit future crop yield losses due to ozone in the most affected regions. At the local scale, the changes can be substantial.

Contents

CHAPTER 1

Introduction

1.1 General Introduction

The emissions of greenhouse gases (GHGs) and air pollutants of anthropogenic origin have increased substantially since the industrial revolution. CO_2 emissions from fossil fuel burning and cement manufacturing form the main category, contributing to around 375 GtC in the atmosphere, or 68% of the total anthropogenic CO_2 emissions over the last 150 years (IPCC, 2013). 180 GtC of CO_2 has been released to the atmosphere through deforestation and other land use changes. In general, the atmospheric concentrations of CO_2 in 2011 was about 390 ppm which is 40% higher than in 1750 (Hartmann et al., 2013). Also, the emissions and concentrations of other important GHGs like methane (CH_4), nitrous oxide (N_2O) and some manufactured halogenated gases (CFCs) have increased over the last 150 years due to human activity. For instance, the concentrations of N_2O in 2011 (324.2 ppb) was 20% higher than 1750 and that of methane (1803.2 ppb) 150% greater than before 1750 (Hartmann et al., 2013).

The increases in the atmospheric concentrations of GHGs have contributed to human induced climate change (IPCC, 2013). Generally, GHGs absorb thermal radiation from the Earth's surface and re-emit radiation back toward the surface and lower atmosphere. This results in a reduction in outgoing thermal radiation and forces an imbalance at the top of the atmosphere (TOA) radiation budget. The forcing imbalance at the top of the atmosphere (TOA) induced by changes in GHGs lead to systematic change in the climate system, since the energy balance at the TOA will lead to changes in temperature in the lower atmosphere, on land, and in the oceans. Changes in land surface temperature are evident in observations (Hansen et al., 2010; Jones et al., 2012; Rohde et al., 2013). These changes in the climate system in response to the forcing can also be computed with a fully coupled atmosphere-ocean-land-sea ice model which allow all feedbacks to operate and temperature at the surface, in the ocean and the atmosphere to adjust to the forcing perturbation. The increase in GHG concentrations have led to an increase in global mean surface temperature between 0.5°C to 1.3°C between 1951 to 2010 (IPCC, 2013).

The most common approach to estimate this radiative forcing perturbation due to a given forcing agent, is to estimate the net flux change at the tropopause after allowing the stratospheric temperatures to adjust to a new radiative equilibrium (Ramaswamy et al., 2001). The resulting net flux change is called the adjusted radiative forcing (F_a). This radiative forcing concept has been used in the Intergovernmental Panel on Climate Change (IPCC) assessments to represent an externally imposed perturbation in the energy budget of the Earth's climate system and the concomitant climate responses (e.g. Ramaswamy et al., 2001; Forster et al., 2007; Myhre et al., 2013). Fig 1.1 shows the estimated global mean adjusted radiative forcing of different atmospheric constituents.

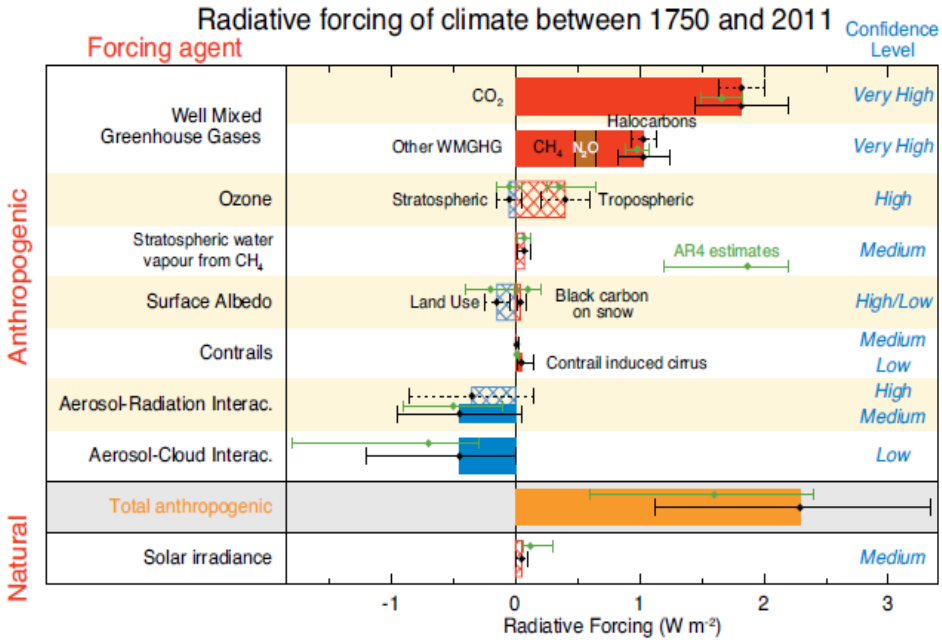

Fig. 1.1. Global mean radiative forcings (W/m^2) of various atmospheric constituents between the start of the industrial era (1750) and 2011 (IPCC, 2013).

Among the GHGs, the increases in the atmospheric concentrations of CO_2 contribute most to the total radiative forcing, compared to CH_4, N_2O and halogenated gases. The stratospheric radiative adjustments operate on fast atmospheric timescales while the adjustment in the troposphere might take up to a decade as a result of the interaction with the ocean, which has a large heat capacity (Boucher et al., 2013). The equilibrium climate sensitivity parameter (λ) is defined as:

$$\lambda = \frac{\Delta T_s}{F_a}, \qquad (1.1)$$

where ΔT_s is the long-term global mean change in surface air temperature (usually taken at 2 m) in response to the radiative forcing F_a. In the standard definition, the climate sensitivity is defined with respect to a doubling of the CO_2 concentration. This can be generalized to include all forcings (not only CO_2). However, when calculated using the above definition in terms of the adjusted forcing F_a, the resulting value for the climate sensitivity would differ considerably across different forcing agents (Forster et al., 2007). The temperature response to forcing from a given agent compared to the response to forcing from CO_2 has been defined as efficacy (Hansen et al., 2005). To better estimate the long-term climate response to a given forcing agent, Hansen et al. (2005) introduced an alternative measure of climate forcing known as the fixed SST forcing (F_s), termed effective radiative forcing (ERF) in the IPCC fifth assessment report (e.g. see Boucher et al., 2013; Myhre et al., 2013). F_s is defined as the net flux change at the top of the atmosphere (TOA) after the forcing agent is added to the atmosphere with sea surface temperature (SST) and sea ice (SI) fixed. It is given by:

$$F_s = F_0 + \delta T_0 / \lambda, \qquad (1.2)$$

where F_o and δT_o are the global mean radiative flux change at the TOA and the global mean change in surface air temperature, in response to the forcing perturbation with SST and SI held constant, and λ the model equilibrium climate sensitivity to CO_2. As part of this warming is caused by feedbacks in the climate system, by including many of the rapid adjustments that differ across forcing agents, the ERF concept includes much of their relative efficacy. This therefore leads to a more uniform climate sensitivity across agents (IPCC, 2013).

The strongest radiative feedback is associated with the Planck response to the warming. This is a negative feedback, since the increase in surface temperature implies larger amounts of outgoing longwave radiation (see e.g. Lacagnina et al., 2014 and references therein). The albedo, cloud, water vapour/lapse rate feedbacks (involved in moist atmospheric processes associated with clouds) are also important determinants of equilibrium climate sensitivity. For example, since the saturation vapour pressure of air increases in conjunction with temperature, the amount of water vapour in the air has increased in response to the warming, further enhancing the greenhouse effect. These changes have wider implications for the climate system. For instance, there has been significant human influence on large-scale circulation and precipitation patterns (IPCC, 2013).

1.2 Short-lived climate pollutants

Air pollutants, like sulphur dioxide (SO_2), aerosols, carbon monoxide (CO), non-methane volatile organic compounds (NMVOCs), methane and nitrogen oxides (NO_X), are emitted naturally into the atmosphere (e.g. by wildfires, vegetation, and volcanic eruptions). Anthropogenic activities like fossil fuels combustion and land use change have significantly increased the emissions of air pollutants over the last 150 years (see Fig. 1.2).

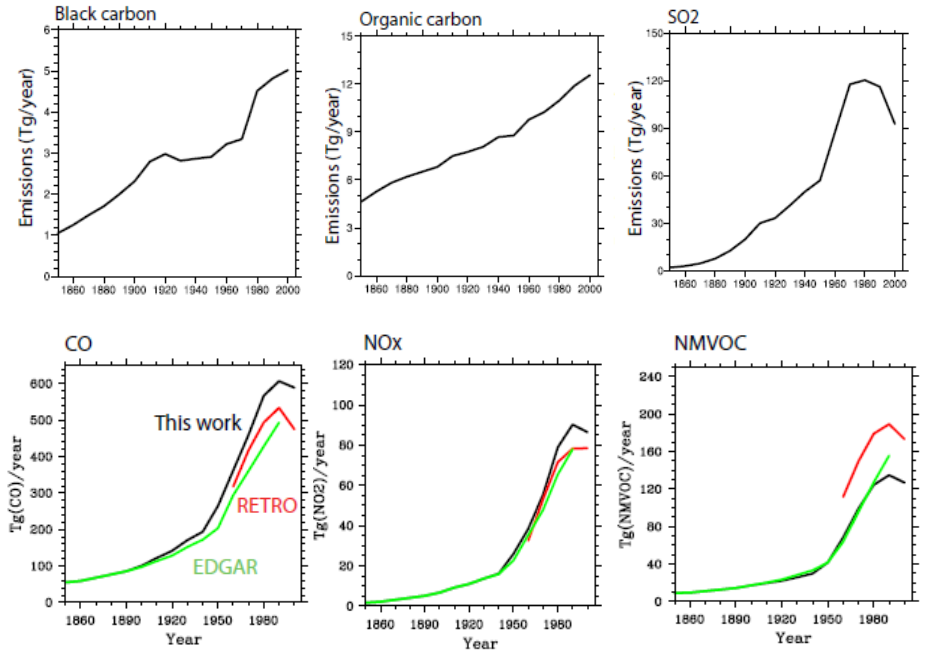

Fig. 1.2. The evolution of global total air pollutant from the beginning of the industrial era to present day (taken from Lamarque et al., 2010). The data are based on EDGAR (green line), RETRO (red line) emissions inventories and Lamarque et al. (2010) as indicated by the black line.

This has led to a significant increase of air pollution levels. The time evolution of air pollutants varies greatly across different region. For example, there has been a threefold increase in the concentrations of tropospheric ozone in the Northern Hemisphere (NH) over the last 100 years, which has made it the third most important anthropogenic GHG after carbon dioxide and methane (Royal Society, 2008, Myhre et al., 2013). Based on satellite and surface based remote sensing, it is very likely that the aerosol optical depth (AOD) has decreased over Europe and the eastern USA since the mid1990s and increased over eastern and southern Asia since 2000 (Hartmann et al., 2013 and references therein)

The anthropogenically driven changes in aerosols have led to a perturbation of the radiation balance of the Earth through scattering and absorption of solar radiation, and also in a number of non-linear ways through their interactions with clouds. For instance, sulphate (SO_4), nitrate, and some forms of organic aerosols reflect solar radiation and therefore cool the climate system (Hansen et al., 1981; Charlson et al., 1990; 1991; Kiehl and Briegleb, 1993; Mitchell et al., 1995). On the contrary, black carbon (BC) particles in the atmosphere absorb solar radiation, radiate energy and therefore warm the atmosphere. Observations and modelling studies have shown that anthropogenic aerosols have exerted a net cooling effect on the climate which has offset some of the warming from GHGs that would have occurred in their absence (Boucher et al., 2013; Stevens, 2015).

As a result of their very short atmospheric residence time varying from a few days to weeks (Hartmann et al., 2013 and references therein), the spatial distributions of aerosols, unlike well-mixed GHGs, are inhomogeneous with higher concentrations typically situated near emission sources. This entails that changes in emissions of aerosols and aerosols precursors can have significant regional climate impacts (e.g. Hansen et al., 2005; Chen et al., 2007; Shindell and Faluvegi, 2009; Shindell et al., 2012). For example, because most changes in anthropogenic aerosol and precursor emissions over the last 150 years occurred in the NH, this has given rise to strong interhemispheric differences in aerosol forcings. A number of modelling studies (e.g. Yoshimori and Broccoli, 2008; Ming and Ramaswamy, 2009; Ocko et al., 2014) have shown that the associated stronger surface cooling in the NH compared to the Southern Hemisphere (SH) can lead to a disruption of circulation patterns and changes in precipitation in the tropics.

Apart from their impacts on climate, air pollutants have significantly impacts on health, ecosystem and crop yields globally (UNEP 2011). Field experiments (e.g., Heck et al., 1983; Fuhrer et al., 1997; Pleijel et al., 2002; Karlsson et al., 2007; González-Fernández et al., 2008; De Bock et al., 2011) have demonstrated that elevated levels of tropospheric ozone can have detrimental impacts on crops, resulting in yield reduction and deterioration of crop quality. The ozone induced decrease in crop yield might result in agricultural intensification on land currently in use or the need for more arable land to meet food demand, therefore resulting in land use changes and other associated environmental problems.

1.3 Modelling and integration

Earth System Models (ESMs) are used to investigate the impact of historical changes or future scenarios of anthropogenic emissions in the climate system by using prescribed time series of emissions or concentrations. Such scenarios are produced by Integrated Assessment Models (IAMs) and usually include detailed representations of anthropogenic activities related to population growth, energy demand and land use. In addition, IAMs have been used to calculate the environmental impacts of different emission scenarios by using output of climate models. In the past, most of the IAMs and ESMs research has been done relatively independently. To get a better overview of ESMs and IAMs models, we give a brief description below.

1.3.1 Integrated Assessment models (IAMs)

IAMs combine knowledge from different disciplines within a single framework to provide more insights on societal problems. They have been developed with the primary aim of tackling societal problems that cut across different traditional disciplines (Schneider, 1997). This means that most IAMs today provide a modelling framework wherein socio-economic, physical and biological factors are combined to make assessments of future changes of the world economy, agriculture, land use, emissions, climate and ecological values. By combining knowledge from different disciplines, IAMs provide a system-based approach in support of decision making processes. They can be used to explore the impacts of current trends, and to analyze the effectiveness of various policy scenarios.

Over the years, different IAMs have been developed for different purposes. The most simple IAMs, mostly used for cost-benefit analysis like DICE (Nordhaus, 1993) and FUND (Tol, 1997), consist of a relatively compact set of equations, describing economic growth, emissions associated with fossil fuel combustion, climate change and associated impacts. Over time, a set of more comprehensive IAMs like IMAGE (Bouwman et al., 2006) has been developed with much better description of future trajectories for emissions from different energy sources and land use. However, the climate and atmospheric chemistry descriptions remain very simplified.

1.3.2 Earth system models (ESMs)

The Earth's climate system is complex and includes many factors that interact on different spatial and temporal scales. In order to unravel these complexities and investigate past and future climatic changes, scientists over the last decades have developed climate models. Climate models can be classified into three main classes based on complexity. These classes are: one-dimensional energy balance models, three-dimensional Earth system models of intermediate complexity with simplified physics and dynamics, and three-dimensional general circulation models (GCMs) with elaborate physics and dynamics. When including (biogeo)chemistry the latter are often referred to as ESMs. Here, we focus on the GCM approach as in this thesis we used a GCM to analyze the regionally differentiated response to anthropogenic greenhouse gas, air pollutant and precursor emissions.

GCMs are numerical models describing physical processes in the atmosphere, land, cryosphere and land surface (IPCC definition). A GCM is made up of both atmospheric GCMs (AGCMs) and oceanic GCMs (OGCMs) which can be coupled together to form a fully coupled general circulation model (AOGCM). In general, coupled GCMs consist of component models of the atmosphere, ocean, cryosphere, and land surface, which are intricately linked through exchange of energy and momentum across the interfaces between them. For instance, the ocean model is driven by the atmospheric fluxes of heat, momentum and freshwater simulated by the atmospheric component. The heat and freshwater fluxes are functions of the sea surface temperatures simulated by the ocean component. In addition, the importance of the carbon cycle for the climate system has resulted in the development of GCMs that include the carbon cycle (ESMs). Such ESMs typically include dynamic vegetation and ocean biogeochemistry. The most advanced ESMs also have options to interactively simulate atmospheric chemistry and aerosols.

GCMs describe the climate using a three-dimensional grid over the globe, normally with a horizontal grid and vertical layers in the atmosphere and the oceans. In GCMs many physical processes, such as those linked to radiation, turbulence, precipitation and clouds, occur at smaller scales and cannot be appropriately simulated. Instead, these processes are described using parameterizations (Randall et al., 2007). This is one source of error in GCMs, which causes uncertainty in projections of future climate. These uncertainties may result in GCMs giving different responses to the same forcing as a result of the way certain processes and feedbacks are simulated.

Some GCMs include an atmospheric chemistry transport model (CTM) which is used to quantify the concentrations and deposition fluxes of atmospheric reactive gases, including GHGs like ozone and methane, and aerosols over space and time by modelling atmospheric chemistry processes. CTMs can be used offline, driven by global meteorological data sets, or online as a module inside GCMs. In the online configuration, radiative properties of short-lived greenhouse gases (ozone, methane) and aerosols for instance, can be ingested back into the radiation module of GCMs to calculate the impact of air pollutants on climate. Aerosol-cloud interactions associated with indirect radiative effects of aerosols can also be included. In CTMs there is a trade-off between the number of tracers and chemical reactions simulated on the one hand, and transport and mixing in the atmosphere on the other hand. For instance, a column chemistry model which is a very simple tool for describing the chemical evolution of species in the atmosphere, might include a lot of chemical reactions but, with a very rudimentary representation of the mixing in the atmosphere. Conversely, a 3D CTM usually includes more physical processes in the atmosphere but fewer chemical reactions and tracers due to computational constraints.

1.3.3 Model integration

In recent years, there is increasing interest in coupling different disciplines involved in climate research. Moss et al. (2010), for instance, explicitly mention the need for a stronger collaboration between the research fields to better account for possible feedbacks between human systems and the earth system on the global scale. In van Vuuren et al. (2012), we

outlined why integration can be important. For instance, research have shown how climate impacts may influence macro-economic development (Tol, 2002; Frankhauser and Tol, 2005), or how (anthropogenic) land use and land cover change can interact with the climate (Voldoire et al., 2007; Bondeau et., 2007; Pitman et al., 2009; Sitch et al., 2005; Schaeffer et al., 2006) and air pollution (Ganzeveld et al., 2010). Also from a policy-making perspective, integration of knowledge is required. The focus towards more integration can also be seen in current research trends. The ESM community, for example, has extended its focus from a primary interest in the climate system itself to related topics such as the carbon cycle, land use, hydrology and even urban systems. At the same time, the IAM communities are also looking into these same topics, partly as part of joint scenario development (Kriegler et al., 2011; van Vuuren et al., 2011). As a result, the research agendas of these communities are starting to overlap and closer collaboration becomes increasingly useful.

Examples of cooperation can already be found. The Representative Concentration Pathways (RCPs) scenarios, which form the basis of Coupled Model Intercomparison Project (CMIP5, Taylor et al., 2012) experiments used in the Fifth Assessment Report (AR5) of the IPCC, were constructed in a collaboration process aim at strengthening the cooperation between the ESM and IAM communities. Still, the information flow in the RCP process was limited to a single hand-off of scenario information of IAM modelers to the ESM community.

There is increasing need for integrating IAM and ESM modelling activities in order to improve the understanding of important linkages between human development and environmental change. We discuss the different forms of linkages between IAM and ESM models, which each have strengths and weaknesses (see Table 1.1).

Collaboration between the IAM and ESM model groups can take many forms ranging from activities that stimulate information exchange, dedicated joint research programs, data collection or even shared model components. Van Vuuren et al. (2012) recognises four possible forms of integration that may help to improve the understanding of the different feedbacks and linkages between human activities and the earth system. These four forms are:

(A) Information can be exchanged in one direction from ESM to IAM models and/or vice versa (as is currently mostly done). Such interaction can be further refined in the spatial, temporal or variable dimension (to take account of more detailed information available within each community).
(B) The representation of the Earth system within IAM models can be further improved by advancing the climate, vegetation, carbon cycle and atmospheric chemistry representation within the IAM models.
(C) The representation of societal elements within ESM models can be further improved by advancing, for instance, the modelling of agricultural and water management options within the ESM models.
(D) IAM and ESM models can be fully coupled online, allowing for more or less instantaneous two-way interactions.

Method	*Advantages*	*Disadvantages*
A (Off-line information exchange, one-way)	• work with existing terminology and tools • transparent information exchange • flexibility • separate research strategies	• Feedbacks are only captured via single of multiple iterations. • potential inconsistencies
B (Improved IAMs)	• allows for good representation of uncertainty • model complexity tailored to question • detail in treatment of socio-economic processes	• lack of detail in treatment of biophysical processes (often meta modeling)
C (Improved ESMs)	• higher resolution analyses than in IAMs • detail in treatment of biophysical processes	• lack of detail in treatment of socio-economic processes • limitation of model runs limits representation of uncertainty
D (Full coupling)	• assessment of feedbacks • highest degree of consistency	• technical difficulties • lack of representation of uncertainty • inflexibility • complexity/intransparency • limitations in knowledge may hamper progress

Table 1.1. Advantages and disadvantages of the different types of IAM-ESM collaboration (van Vuuren et al., 2012).

These four different forms of integration also correspond to increasing levels of complexity (from A to D). A summary of the advantages and disadvantages of each form of integration is shown in Table 1.1 (see van Vuuren et al., 2012 for more details).

1.3.4 The Representative Concentration Pathways (RCPs)

The Representative Concentration Pathways (RCPs) are four alternative pathways of future greenhouse gas and air pollutant emissions and land-use change based on existing scenarios published in the literature. The four RCPs represent the range of scenarios in the literature, i.e. RCP2.6 is representative of a stringent climate policy scenario, RCP4.5 and RCP6.0 form 2 intermediate stabilisation scenarios and RCP8.5 is representative of the highest forcing scenarios in the literature. The RCPs were developed using 4 different Integrated Assessment Models and form the basis of research for Earth System Models, General Circulation Models and other climate models. The RCPs form an important input in the report of Working Group 1 for the fifth Assessment Report. They have also been used by other research communities such as for air pollution research.

Interestingly, all RCPs assume that worldwide ambitious air pollution control policies will be implemented. For this reason, the RCPs have been criticised by the atmospheric modelling community for being too optimistic on air pollution. While the RCPs as a set compare relatively well with other emission inventories for the present day (Granier et al., 20011; Lamarque et al., 2011), Van Vuuren et al. (2011) conclude that it shows a smaller range of possible outcomes for the future with regard to air pollutant emissions than other scenario sets, such as the IPCC SRES scenarios (see fig. 1.3). While this narrow range may well represent the most likely trajectory of future air pollutant emissions, it does not cover counterfactual scenarios in which no new air pollution policies are introduced. This limits the use of the RCPs for projecting future changes in air quality and climate forcing from short-lived air pollutants. There is a possibility that higher air pollutant scenarios may represent situations in which important feedbacks and linkages exist between human systems and the Earth system that are not adequately represented by low air pollutant scenarios.

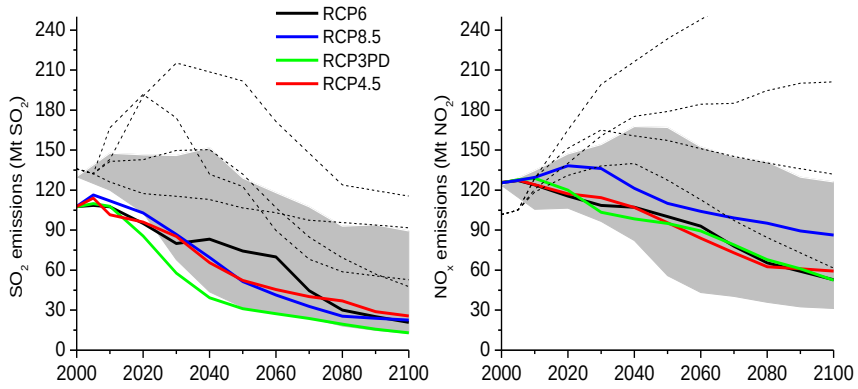

Fig. 1.3. Emissions of SO_2 and NO_x across the RCPs. Grey area indicates the 90th percentile of the range of estimates found in the literature. Dotted lines indicate the SRES scenarios used in the third and fourth assessment reports of the IPCC (Van Vuuren et al., 2011).

1.3.5 Potential human dimension–physical system interactions

Here, we introduce and discuss some IAM–ESM interactions that we explore in this thesis. Firstly, the interaction between climate policy and air pollution control has received increasing attention. In many cases, the impacts of air pollution control on climate are highly non-linear and require further improvement in terms of the representation of spatial and temporal variability in emissions, dispersion, and deposition of pollutants. For instance, while climate change mostly focuses on long-lived GHGs, for air quality issues fine geographic scales and short time scales are relevant. It therefore seems logical to further pursue assessments to the first-order interactions between these two global issues by using type A form of cooperation.

Often scenarios are designed by selecting a long-term climate target. In reality, however, it is much more likely that policy decisions are based on short-term trends and observations. In IAM research, it has been investigated how observations may reduce uncertainty after some time, influencing the optimal decisions on climate policy (Yohe, 2004). Using more complex climate models adds the opportunity to focus on more intricate linkages and feedbacks which

are often represented in a simple way in IAMs. This can be achieved by using a type A/C form of cooperation.

Another class of interactions is formed by those between emission of air pollutants, deposition, concentration levels and vegetation processes. For instance, ozone concentrations can have a considerable impact on the crops yield. This, in turn, could lead to different trends in the agricultural production and subsequently, land use changes. However, hardly any attention has been given to the link between surface ozone concentrations, crop production and land use. Therefore, a type A/B form of cooperation would be most useful to explore the strength of these different impacts.

To explore these possible interactions and linkages, we used a consistent modelling chain from the IAM (IMAGE, Bouwman et al., 2006) to the CTM (TM5, Huijnen et al., 2010; Noije et al., 2014) to the ESM (EC-Earth, Hazeleger et al., 2012) to create new scenarios (with different policy assumptions) and calculate the consequences for air quality and climate. Subsequently, we also calculated the ozone impact on crop using a closed loop from IMAGE to TM5 and again to IMAGE (see fig. 1.4).

1.4 Research questions and outline

Our main objective is to explore important linkages between anthropogenic emissions and the atmospheric composition and climate system that are not adequately represented by the approach used in the development of the RCPs. We attempt to bridge the gap between ESM and IAM model components by exploring the consequences of detailed emission scenarios for air quality, atmospheric composition and climate in the 21st century. We conclude this chapter by introducing the key research questions and an overview of human dimension-physical system interactions that have been investigated in this study.

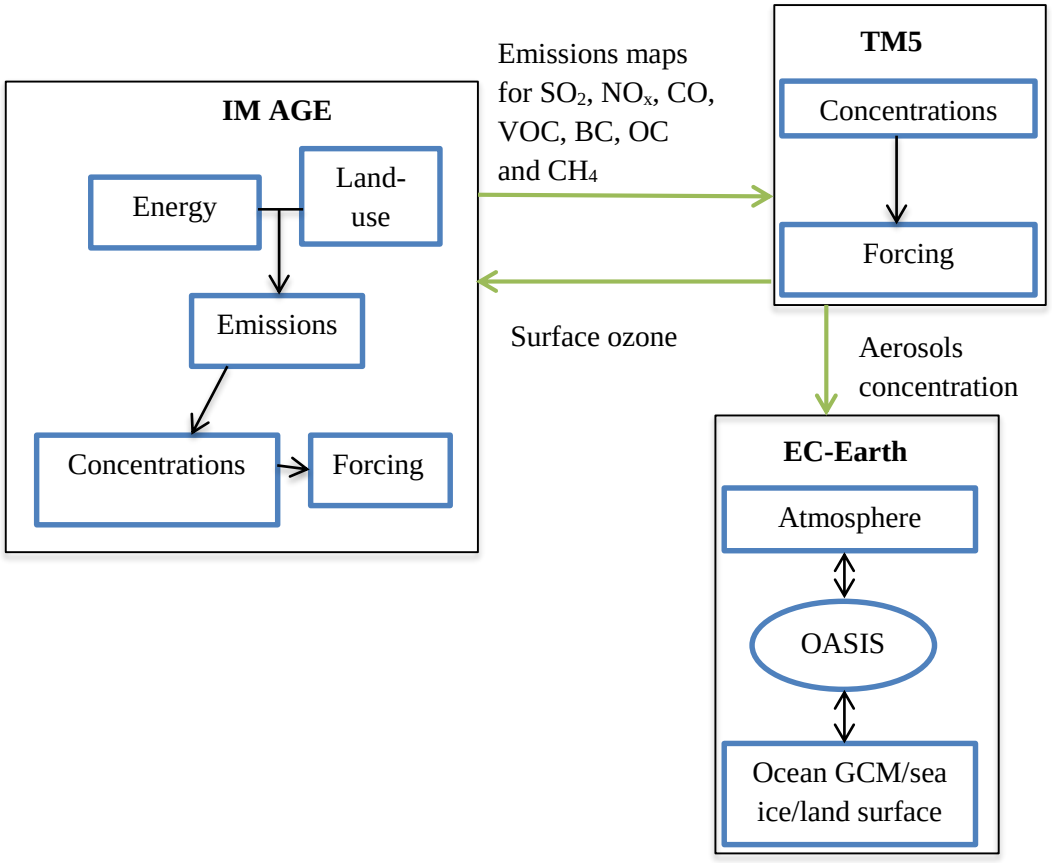

Fig. 1.4. Modelling framework used in this thesis showing the major components of IMAGE, TM5 and EC-Earth. The green arrows indicate the variables output from one model that is (are) used in the other.

Implications of alternative assumptions regarding future air pollution control in scenarios similar to the Representative Concentration Pathways

In Chapter 2, we explore how different assumptions on future air pollution policy and climate policy lead to different concentrations of air pollutants for a set of RCP-like scenarios developed using the IMAGE IAM. Here, we use a systematic framework of air pollution and climate policy, wherein emissions data from IMAGE is used as input to the CTM TM5. The main question we seek to address in this chapter is:

Q1 *What would be the possible ranges of future air pollutants concentrations and climate forcings under a wider range of assumptions regarding air pollution emissions compared to the RCP scenarios?*

Global and regional climate impacts of future aerosol mitigation in an RCP6.0-like scenario in EC-Earth

In Chapter 3, we evaluate the equilibrium climate response to possible future aerosol reductions in different parts of the world, using the GCM EC-Earth and emission data from IMAGE for an RCP-like scenario with modest climate policy. In this chapter the following research question is addressed:

Q2 What could be the climate impacts of future changes in emissions of aerosols and aerosol precursors for different air pollution and climate policy assumptions in an RCP-like scenario?

Efficacy of aerosol forcings in an RCP6.0-like scenario

Chapter 4 investigates the climate efficacy of different aerosol components using EC-Earth and RCP-like scenarios with modest climate policy from IMAGE. In this chapter the following research question is answered:

Q3 How effective are different aerosol components in causing climate change relative to carbon dioxide?

Global impacts of surface ozone changes on crop yields and land use

Chapter 5 explores the ozone impacts on crop production and subsequent impacts on land use and carbon fluxes, between present day and the future, using surface ozone fields from TM5 in IMAGE. In this chapter the following research question is answered:

Q4 What are the impacts of future changes in surface ozone on agricultural yields and land use under different assumptions for future air pollution and climate policies?

Lastly, a synthesis of the thesis is presented in Chapter 6. A discussion of the main conclusion from the other chapters is provided with focus on the research questions listed above as well as an outlook for future research.

CHAPTER 2

Implications of alternative assumptions regarding future air pollution control in scenarios similar to the Representative Concentration Pathways

Abstract

The uncertain, future development of emissions of short-lived trace gases and aerosols forms a key factor for future air quality and climate forcing. The Representative Concentration Pathways (RCPs) only explore part of this range as they all assume that worldwide ambitious air pollution control policies will be implemented. In this study, we explore how different assumptions on future air pollution policy and climate policy lead to different concentrations of air pollutants for a set of RCP-like scenarios developed using the IMAGE model. These scenarios combine low and high air pollution variants of the scenarios with radiative forcing targets in 2100 of 2.6 W/m^2 and 6.0 W/m^2. Simulations using the global atmospheric chemistry and transport model TM5 for the present-day climate show that both climate mitigation and air pollution control policies have large-scale effects on pollutant concentrations, often of similar magnitude. If no further air pollution policies would be implemented, pollution levels could be considerably higher than in the RCPs, especially in Asia. Air pollution control measures could significantly reduce the warming by tropospheric ozone and black carbon and the cooling by sulphate by 2020, and in the longer term contribute to enhanced warming by methane. These effects tend to cancel each other on a global scale. According to our estimates the effect of the worldwide implementation of air pollution control measures on the total global mean direct radiative forcing in 2050 is +0.09 W/m^2 in the 6.0 W/m^2 scenario and -0.16 W/m^2 in the 2.6 W/m^2 scenario.

This chapter has been published as: Chuwah, C.D., van Noije, T., van Vuuren, D.P., Hazeleger, W., Strunk, A., Deetman, S., Mendoza Beltran, A., van Vliet, J., 2013. Implications of alternative assumptions regarding future air pollution control in scenarios similar to the Representative Concentration Pathways. Atmospheric Environment 79, 787–801.

2.1 Introduction

Recently, the research community has developed a set of scenarios (Representative Concentration Pathways, RCPs) to improve understanding of the complex linkages between human activities and the climate system (Moss et al., 2010; van Vuuren et al., 2011a). These scenarios form the basis of the current generation of climate model runs as part of the Atmospheric Chemistry and Climate Model Intercomparison Project (ACCMIP, Lamarque et al., 2013) and Coupled Model Intercomparison Project (CMIP5, Taylor et al., 2012), which will be used in the fifth assessment report of the Intergovernmental Panel on Climate Change (IPCC). The RCP set consists of four scenarios (RCP2.6, RCP4.5, RCP6.0 and RCP8.5) each of which describes a different trajectory for emissions of long-lived greenhouse gases (LLGHGs) and short-lived air pollutants, the corresponding concentration levels, land use and radiative forcing. Together the four RCPs span a range of possible climate forcings varying from 2.6 W/m^2 to 8.5 W/m^2 in 2100 (van Vuuren et al., 2011a). It should be noted that the four RCPs have been produced by four different integrated assessment models (IAMs) (see Masui et al., 2011; Riahi et al., 2011; Thomson et al., 2011; and van Vuuren et al., 2011b).

The emissions trajectories of air pollutants are determined by three important factors: the level of economic activities, the assumed degree of air pollution control and the assumed level of climate policy (van Vuuren et al., 2011a). The relationship with climate policy originates from the fact that LLGHGs and air pollutants have a number of common sources. As such, policies aimed at curbing LLGHGs often lead to reduction in air pollutants (e.g. van Vuuren et al., 2008; Koornneef et al., 2010). In the RCPs, all modeling teams assumed that higher income levels lead to the implementation of more stringent air pollution control measures. Overall, this implies that in each RCP air pollutant emission factors gradually decline during the course of the century. Van Vuuren et al. (2011c) conclude that the RCP set shows a smaller range of possible outcomes with respect to air pollutant emissions than other scenario sets, such as the IPCC SRES scenarios (Nakićenović et al., 2000), used in Prather et al. (2003), and scenarios from the International Institute for Applied Systems Analysis (IIASA), utilized by Dentener et al. (2006b) and Kloster et al. (2008). This narrow range may limit the use of the RCPs for projecting future changes in air quality and climate forcing from short-lived components.

Given the importance of the RCPs, the key research question that is addressed in this study is: what would be the possible ranges of future air pollutant emissions, associated concentrations and climate forcings if a wider range of air pollution assumptions is included. In order to systematically distinguish the impacts of climate policy (different LLGHG emission profiles corresponding to RCP forcing levels) and air pollution control, it is most interesting to investigate this within a single model framework. Therefore, we explore the impact of alternative assumptions regarding air pollutant emissions using a set of RCP-like scenarios developed using the IMAGE integrated assessment model. While these are RCP replications (designed in a different model framework), the exact reproduction is not important for answering the research questions listed above.

In the past, several studies have already analyzed the implications of climate and air pollution policies on air pollutants (e.g. Kloster et al., 2008; van Aardenne et al., 2010; Shindell et al., 2012; Bond et al., 2013). In general, these studies show that climate and air pollution policies implementation have co-benefits on air pollutant concentrations and climate forcing from short-lived components. We do add to this literature by the direct relation with the RCPs and the systematic framework of air pollution and climate policy scenarios described in the next section.

The paper is structured as follows: Sect.2.2 describes the modeling system and the methods used to develop the new scenarios. In Sect. 2.3, we compare the evolution of the emissions and methane concentrations in our scenarios and the RCPs, and we present results for surface concentrations and radiative forcing. A discussion and conclusions of our results are given in Sect. 2.4.

2.2 Models and methods

The modeling framework used in this study is schematically illustrated in Fig. 2.1b and consists of the Integrated Model to Assess the Global Environment (IMAGE, Bouwman et al., 2006) and the atmospheric chemistry and transport model TM5 (Huijnen et al., 2010).

The IMAGE model is used to develop a set of consistent scenarios (IM2.6-low, IM2.6-high, IM6.0-low and IM6.0-high). These scenarios explore the impact of very different assumptions in terms of both climate policy (IM2.6 versus IM6.0) and air pollution control (high and low variants, see Fig. 2.1a). The IM6.0-low scenario is an IMAGE variant of the RCP6.0 produced by the Asian-Pacific Integrated Model (AIM) leading to a 2100 forcing level of 6.0 W/m^2. For both climate scenarios, variants were made assuming air pollution control policies following similar assumptions as the RCPs (low) and an alternative scenario assuming no improvement in the implementation of air pollution control measures whatsoever (high). This hypothetical assumption forms an upper bound on possible emission trajectories, providing a natural reference level for the impact of air pollution policy. In reality, very high air pollution levels are likely to evoke a policy response, but the main purpose here is to provide an indication of the range of possible air pollution levels under different assumptions in the integrated assessment model IMAGE.

The TM5 model is used for a detailed grid-level representation of the atmospheric chemistry and to estimate the effect of future emission changes on the concentrations of air pollutants and aerosol optical depth, based on the present-day climate. Emission changes are the most important driver of changes in tropospheric ozone and aerosols in the coming decades. The effects of climate change are still very uncertain and model dependent, but are expected to be generally smaller (Stevenson et al., 2006; Lamarque et al., 2011; Fiore et al., 2012; Young et al., 2013). The model was driven by meteorological data from the ERA-Interim reanalysis (Dee et al., 2011) of the European Centre for Medium-Range Weather Forecasts (ECMWF). Simulations were carried out for the years 2005, 2020 and 2050, using meteorological fields

for 2005. Based on the TM5 simulations, we recalculate the radiative forcing of aerosols and tropospheric ozone (see Sect. 2.2.4).

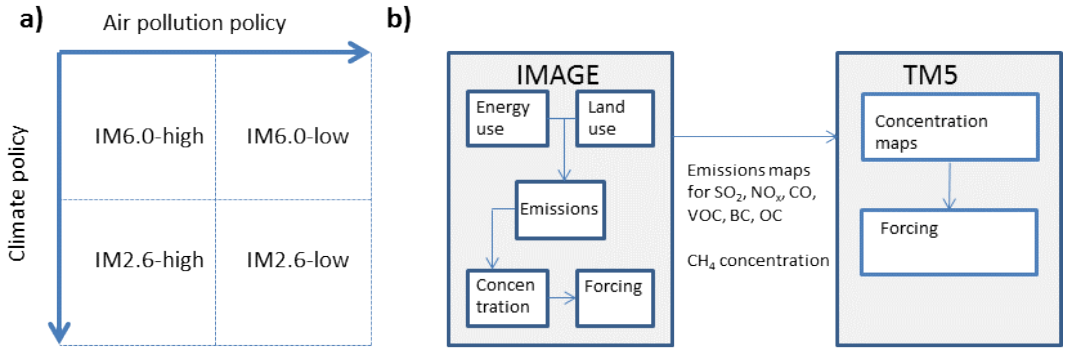

Fig. 2.1. (a) A matrix of the four IMAGE scenarios analyzed in this study illustrating the different degrees of climate and air pollution policies. (b) The major components of the IMAGE and TM5 models and the IMAGE output variables used in TM5.

2.2.1 IMAGE

The IMAGE model contains a description of the world energy system, land-use and land-cover change, the carbon cycle and the climate system (Bouwman et al., 2006). Human activities and climate policy are represented in 26 world regions while the climate, land-cover and land-use change related processes are represented on a 0.5 x 0.5 degree grid. The model can be used to describe the baseline scenario (i.e. in the absence of climate policy) as well as alternative mitigation scenarios and associated costs, based on reduction measures in the energy and land use systems. Here, two scenarios are designed leading to two cost-optimal paths to radiative forcing targets at 2.6 and 6.0 W/m^2 (for a description of the approach, see van Vuuren et al., 2011b and the references therein).

In IMAGE, the climate system is represented using the MAGICC6 model (Meinshausen et al., 2011a). The concentration and forcing of most agents are calculated using the parameterizations included in MAGICC6 – with the exception of the carbon cycle for which IMAGE includes a detailed, grid-level description. The regional emission trajectories are downscaled to national and grid levels by using different algorithms described in detail in van Vuuren et al. (2007). The different emission scenarios are harmonized to historic 2000 values (Granier et al., 2011) at the species and sector level, by applying a scaling factor that changes linearly to one between 2000 and 2100. The IMAGE output consists of 2-D annual total emission fields for the different sectors used in the RCPs (see van Vuuren et al., 2011a) as well as global mean methane concentrations. The methane concentrations are estimated following the MAGICC6 parameterization, in which the chemical lifetime of methane in the troposphere changes from year to year due to changes in the methane concentration itself, the total annual emissions of nitrogen oxides (NO_x), carbon monoxide (CO) and non-methane volatile organic compounds (NMVOCs), and the global mean surface temperature (see Appendix A in Meinshausen et al., 2011a).

2.2.2 TM5

The version of TM5 used in this study simulates tropospheric photo-chemistry and aerosol microphysics and optical properties. The gas-phase chemistry scheme is based on a modified and updated version of the carbon bond mechanism 4 (Gery et al., 1989). The simulated aerosol types include sulphate (SO_4), black carbon (BC) and organic carbon (OC), sea salt and mineral dust. These are represented by a modal aerosol microphysics scheme (M7; Vignati et al., 2004). Gas-aerosol partitioning of ammonium and nitrate is described by a thermodynamic equilibrium model.

Aerosol optical properties are calculated based on Mie theory. The refractive indices of sulphate, black carbon and sea salt have been taken from OPAC (Hess et al., 1998) whereas those of organic matter and mineral dust are based on the values used in ECHAM-HAM (Kinne et al., 2003), and that of water on Segelstein (1981). In the optics module nitrate is treated as sulphate in the soluble accumulation mode (Aan de Brugh et al., 2010). The optical properties of internally mixed particles are calculated using effective medium theory as described in Aan de Brugh et al. (2013).

Further details about the implementation of the aerosol modules are given by Aan de Brugh et al. (2010). The chemistry and other general aspects of the model are documented in Huijnen et al. (2010). In this study we applied a global resolution of 3 x 2 degrees (longitude x latitude) and 34 vertical levels. For each scenario and time slice (2005, 2020, and 2050), we conducted a one year spin-up simulation in order to derive the equilibrium conditions for our one-year final simulations.

In the calculations, global methane concentrations were prescribed for 2005 using zonal mean values based on observations. In the future simulations, the concentrations were scaled using the ratio between the projected global mean methane concentration for 2020 and 2050, respectively, and the 2005 value. Anthropogenic and biomass burning emissions of CO, NOx, NMVOCs, sulphur dioxide (SO_2), ammonia (NH_3), black carbon (BC) and organic carbon (OC) are based on the annual total emission estimates provided by IMAGE, which for NMVOCs included only the total NMVOC amounts. For use in TM5, we applied the seasonal cycles and VOC splits from the RCPs. In the case of aircraft emissions, we used only the global annual total from IMAGE and used this to scale the monthly 3-D distribution from the RCPs. Production of NOx by lightning and oceanic emissions of dimethyl sulfide (DMS) and sea salt were calculated online (Huijnen et al. 2010; Vignati et al., 2010). Emissions of desert dust were prescribed using a monthly dataset for the year 2000 (Dentener et al., 2006a). Most other natural emissions were prescribed based on a monthly dataset for the present day compiled by the Monitoring Atmospheric Composition and Climate (MACC) project, including NMVOC emissions from vegetation based on the MEGAN model (Guenther et al., 2012). The emission heights of anthropogenic, biomass burning and natural emissions have been revised compared to the description given in Huijnen et al. (2010).

TM5 has been extensively evaluated against observations, for instance by Huijnen et al. (2010) for tropospheric and surface ozone and by Aan de Brugh et al. (2010) for aerosol concentrations and optical depths over Europe. The same model version with similar emissions as applied in this study for present day participated in the ACCMIP (Stevenson et al., 2013; Naik et al., 2013) and AeroCom projects (Myhre et al., 2013). The simulated aerosol concentrations and optical depths from this model version have been evaluated in a number of studies (e.g. Von Hardenberg et al., 2012). A comparison of surface ozone concentrations from our 2005 simulation with in-situ observations at a number of representative background stations is presented in Fig. S2.1.

2.2.3 Scenarios development process

The scenarios used in this study are derived from the baseline scenario developed for the OECD Environmental Outlook (OECD, 2012). On the basis of the baseline, mitigation scenarios were developed targeting a 2100 radiative forcing level of 2.6 and 6.0 W/m^2 (Fig. 2.1a). In the scenarios with stringent air pollution control (IM2.6-low and IM6.0-low), it is assumed that emission factors (emissions per unit activity per sector and fuel type) of air pollutants decline up to 2030 assuming implementation of current and planned air quality policies. After 2030, further abatement measures are implemented as a function of the increasing income levels by applying gross domestic product (GDP) thresholds for medium and advance levels of air quality control (Lucas et al., 2007; van Vuuren et al., 2007). In the two high scenarios labeled IM2.6-high and IM6.0-high, the implementation of current and planned air quality legislations is presumed till 2010 after which we assume constant emission factors onwards. In summary, the two climate policy variants (IM2.6 and IM6.0) differ with respect to energy use and land use, while the air pollution variants (high and low) refer to different emission factors.

2.2.4 Radiative forcing

In the design of the four scenarios, the radiative forcing (RF) levels are calculated in IMAGE. We also include a post-calculation of the aerosol and tropospheric ozone forcing using the TM5 output. In both cases, the calculations are based on the MAGICC6 approach (Appendix A; Meinshausen et al., 2011a). In the case of ozone (O_3), a mean forcing efficiency of 0.042 Wm^{-2} DU^{-1} is used to convert the simulated tropospheric burden changes to RFs, in agreement with the recent estimate by Stevenson et al. (2013). Monthly mean tropospheric O_3 columns are determined using the 150-ppb O_3 level to define the tropopause height. This is done using the fixed 2005 monthly mean O_3 mixing ratio fields in the demarcation of the tropopause for all scenarios. With respect to methane, we calculate the RF from the concentration using the simplified expression applied in MAGICC (see e.g. Meinshausen et al., 2011a).

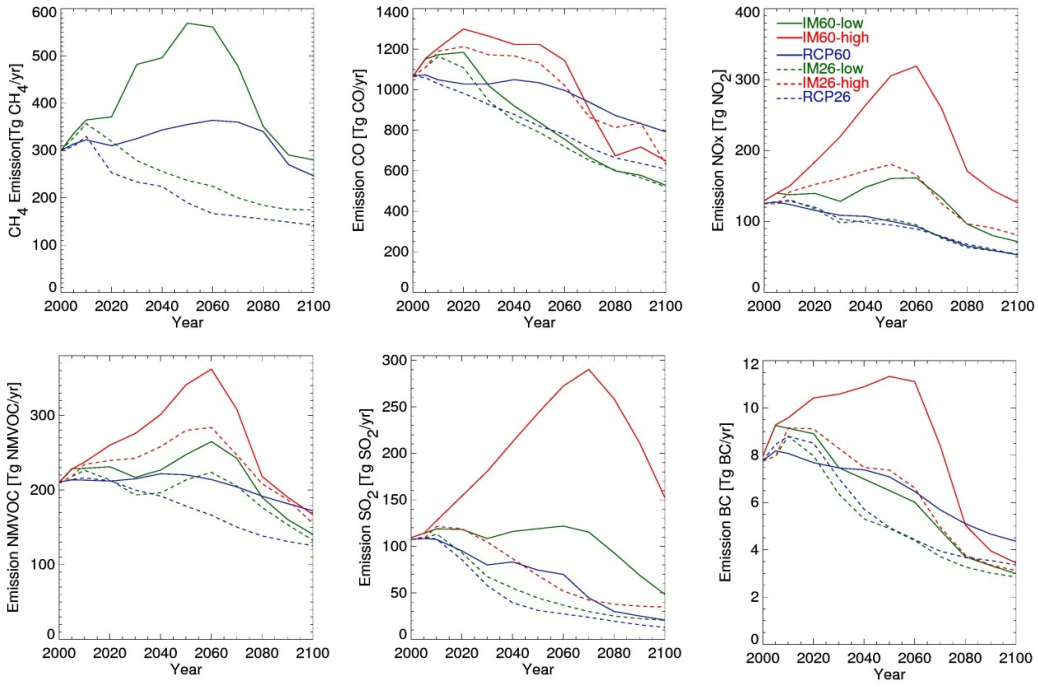

Fig. 2.2. Annual total anthropogenic emissions of CH_4, CO, NO_x, NMVOC, SO_2, and BC in the new IMAGE scenarios and the corresponding RCPs. Emissions from biomass burning are included in the totals.

Our projections of changes in the RF by aerosols include only contributions from direct radiative effects. The chemical composition and consequently the optical properties of the different aerosol types might change as a result of climate change, but such climate-driven changes are not considered in this study. It is therefore justified to assume a linear relationship between the direct radiative effect of an individual aerosol component and its optical depth. Thus, to estimate the future RFs of the various aerosol components we make use of the present-day RF calculations from the GISS model E simulations by Hansen et al. (2005) and apply a simple linear scaling based on the anthropogenic contributions to the aerosol optical depths (AODs) of the various components simulated in TM5. This procedure is similar to the method applied in MAGICC6, but we use scaling ratios defined in terms of optical depths at 550 nm instead of emissions of aerosols or aerosol precursor gases.

As in MAGICC6, we apply a hemispheric approach wherein we apply separate scaling factors over the land and ocean areas in both hemispheres. At this aggregated level, potential mismatches related to different spatial distributions of the AODs in TM5 and GISS (e.g. due to different emission distributions) will largely average out. Thus, the global mean future radiative forcing per aerosol component i is calculated as

$$\mathrm{RF_i(year)} = \overline{\mathrm{RF_{i,r}^{GISS}} \times \frac{\mathrm{AOD_{i,r}^{anthro}(year)}}{\mathrm{AOD_{i,r}^{anthro}(2005)}}}. \qquad (2.1)$$

Here $RF_{i,r}^{GISS}$ is the present-day radiative forcing estimate for component i and region r from Hansen et al. (2005), $AOD_{i,r}^{antrho}$ is the anthropogenic AOD of component i averaged over region r, and the overbar represents the area weighted averaging over the four regions (land and ocean in both hemispheres). It is important to note that the radiative forcing from tropospheric ozone and aerosols varies regionally (e.g. Stevenson et al.; 2013; Myhre et al., 2013). The aggregated approach described here does not give any information about the magnitude of these regional variations.

2.3 Results

2.3.1 Emission projections

Fig. 2.2 shows the pathways for the global total emissions of methane (CH_4), carbon monoxide (CO), nitrogen oxides (NO_x), non-methane volatile organic compounds (NMVOCs), sulphur dioxide (SO_2), and black carbon (BC). Regional totals for four main industrialized regions, viz. North America (NA), Europe (EU), East Asia (EA) and South Asia (SA), are presented in the supplementary material (Figs. S2.2 and S2.3) The definition of these regions follows the definition applied by the Task Force on Hemispheric Transport of Air Pollution (HTAP; see Wild et al., 2012).

The emission pathways of individual components in the scenarios analyzed here are somewhat different from the RCPs (Fig. 2.2). The differences between the RCP2.6 and IM2.6-low scenarios are small and originate from the updated baseline and model version (for instance, more rapid baseline growth in China has been assumed (OECD, 2012)). The differences between the IM6.0-low and RCP6.0 scenarios are larger as they are produced by two different IAMs (IMAGE and AIM). The AIM model produces lower methane emissions in Asia than IMAGE (Figs. S2.4 and S2.5). This is caused by different assumptions on activity levels for agriculture (livestock and rice) and energy production (coal mining). Both scenarios are, however, bounded by the radiative forcing target which means that for the combination of greenhouse gases a similar profile emerges.

In the IM2.6-high and IM6.0-high scenarios, the emissions of CO_2, CH_4, and other LLGHGs are the same as in the corresponding low air pollution scenarios, but air pollutant emissions are considerably higher due to the assumptions on emission factors. Clear differences can be noted in SA and EA (see Figs. S2.4 and S2.5), where rapid growth in economic activities leads to a corresponding increase in pollutant emissions, if air pollution policies are not tightened. Nevertheless, even in the high emission scenarios emissions mostly decrease in the second half of the century as a result of reduced direct use of fossil fuels (for instance, in transport, the scenarios assume increased use of hydrogen power resulting in much lower emissions than with oil-based fuels).

2.3.2 Methane concentrations

Projections for methane concentrations are shown in Fig. 2.3. The concentrations in IM2.6-low are slightly higher than in the RCP2.6 as

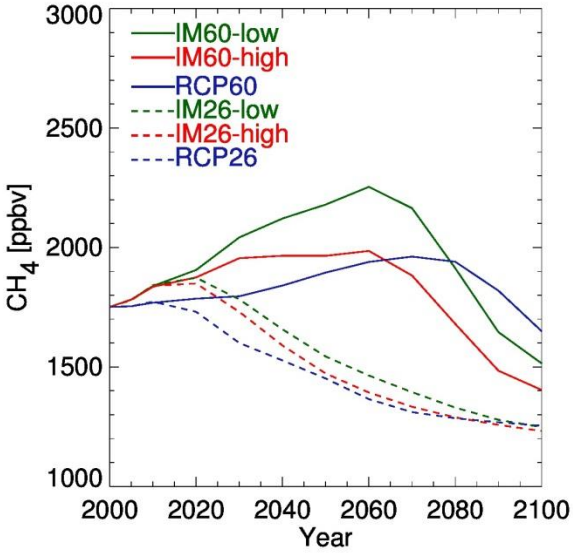

Figure 2.3. Global mean methane concentrations in the new IMAGE scenarios and the corresponding RCPs.

result of changes in the IMAGE model version and baseline assumptions (see Fig. 2.2). The higher concentrations in IM6.0-low compared to RCP6.0 are also a result of higher methane emissions (and reflect the differences in the AIM and IMAGE projections). Comparing the high and low air pollution scenarios, we find lower concentrations in the high scenario variants, especially in 2050. In other words, the effect of the higher NO_x emissions dominates over the opposing effects of the higher CO and NMVOC emissions. Higher NO_x concentrations in the high air pollution scenarios lead to enhanced recycling of the hydroxyl radical (OH) and thus to higher abundances of OH in the troposphere. This tends to reduce the methane lifetime compared to the low air pollution scenarios, which results in lower methane concentrations despite the fact that the methane emissions are the same in both scenario variants.

2.3.3 Future air quality

Annual mean surface concentrations of ozone, sulphate and black carbon simulated with TM5 are presented for 2020 and 2050, and compared to the reference year 2005.

2.3.3.1 Surface ozone concentrations

The projected surface ozone concentrations vary over a very wide range as they are found to be sensitive to the implementation of air quality and climate policies, even in the short term (Figs. 2.4 and 2.5). In the IM6.0-high scenario, the annual mean ozone concentrations are projected to increase over almost the entire globe. In 2050, increases as high as 30 ppbv are observed near the Indian subcontinent. Some exceptions are noted where concentrations decrease, most notably in the northeastern part of China. With low emission factors (IM6.0-low) the situation changes: now ozone concentrations are projected to decrease in the eastern

United States, parts of the Mediterranean, the Black Sea, Kazakhstan and surrounding regions, and, in 2050, in regions of the Amazon and Central Africa where biomass burning plays a dominant role (see Fig. 2.4). In the latter regions the differences between the high and low scenario variants are mostly due to the influence from the surrounding regions, as the emissions from biomass burning are the same in both variants.

Interestingly, in eastern China ozone concentrations are projected to decrease in both IM6.0 scenarios despite increases in NO_x emissions. This indicates that this region is in a hydrocarbon-limited regime wherein surface ozone production is limited by NMVOCs. Local titration of ozone mainly during winter may also play a role in the observed decrease in surface ozone over eastern China (see also Pozzer et al., 2012).

In the IM2.6-high scenario, the ozone concentrations will first increase in most parts of the world, but by the middle of the century decreases are simulated in large parts of the continents, including the United States, China, and South Africa. In the lowest emission scenario (IM2.6-low), the ozone concentrations are still projected to increase in 2020 in most of the Southern Hemisphere (SH) as well as in India and Southeast Asia. In contrast, the IM2.6-low scenario leads to decreased concentrations in large parts of the Northern Hemisphere (NH), as a result of reductions in ozone precursor emissions in the industrialized regions. In the longer term (2050), the ozone concentrations in this mitigation scenario will be reduced over almost the entire globe with the strongest reductions reaching 10 ppbv at northern mid-latitudes. Regionally averaged annual mean concentration values for NA, EU, EA and SA and the different scenarios are presented in Fig. 2.6. The corresponding global mean values are given in the supplementary material (Table S2.1).

The differences in ozone concentrations as a result of the assumed differences in air pollution control and those in climate policy are qualitatively similar (Fig. 2.5). The largest differences are observed in the NH subtropics and mid-latitudes. As expected, air pollution control is most effective in reducing the ozone concentrations when there is less climate policy in place. Similarly, the co-benefits of climate policy for the ozone air quality are largest when air pollution control is weak. However, the highest future reductions in ozone concentrations are achieved under the IM2.6-low scenario, emphasizing the importance of the co-benefits of climate policy for ozone concentrations.

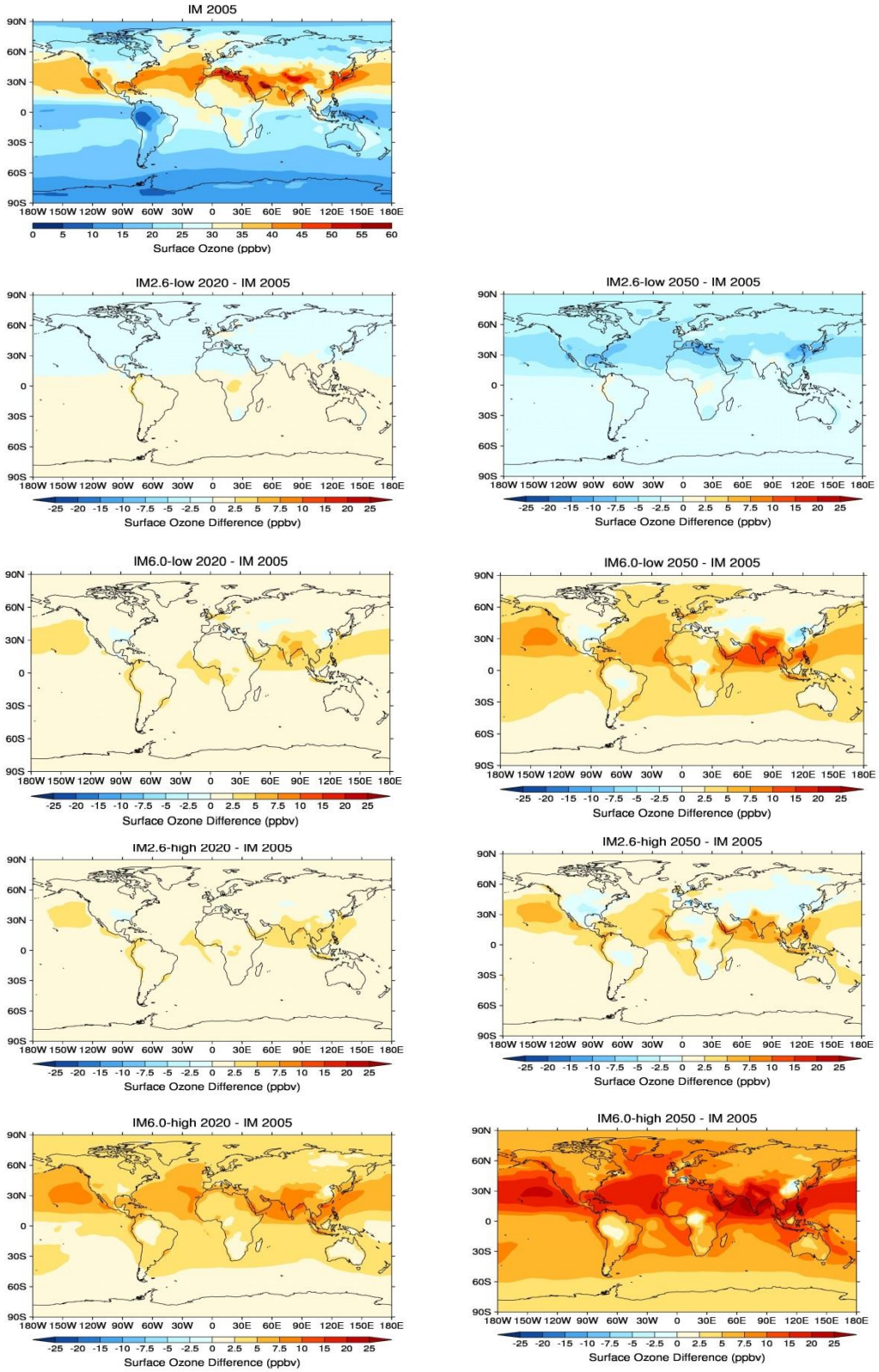

Fig. 2.4. Simulated annual mean surface ozone concentrations in 2005 and the changes in 2020 and 2050 relative to 2005 for the different scenarios.

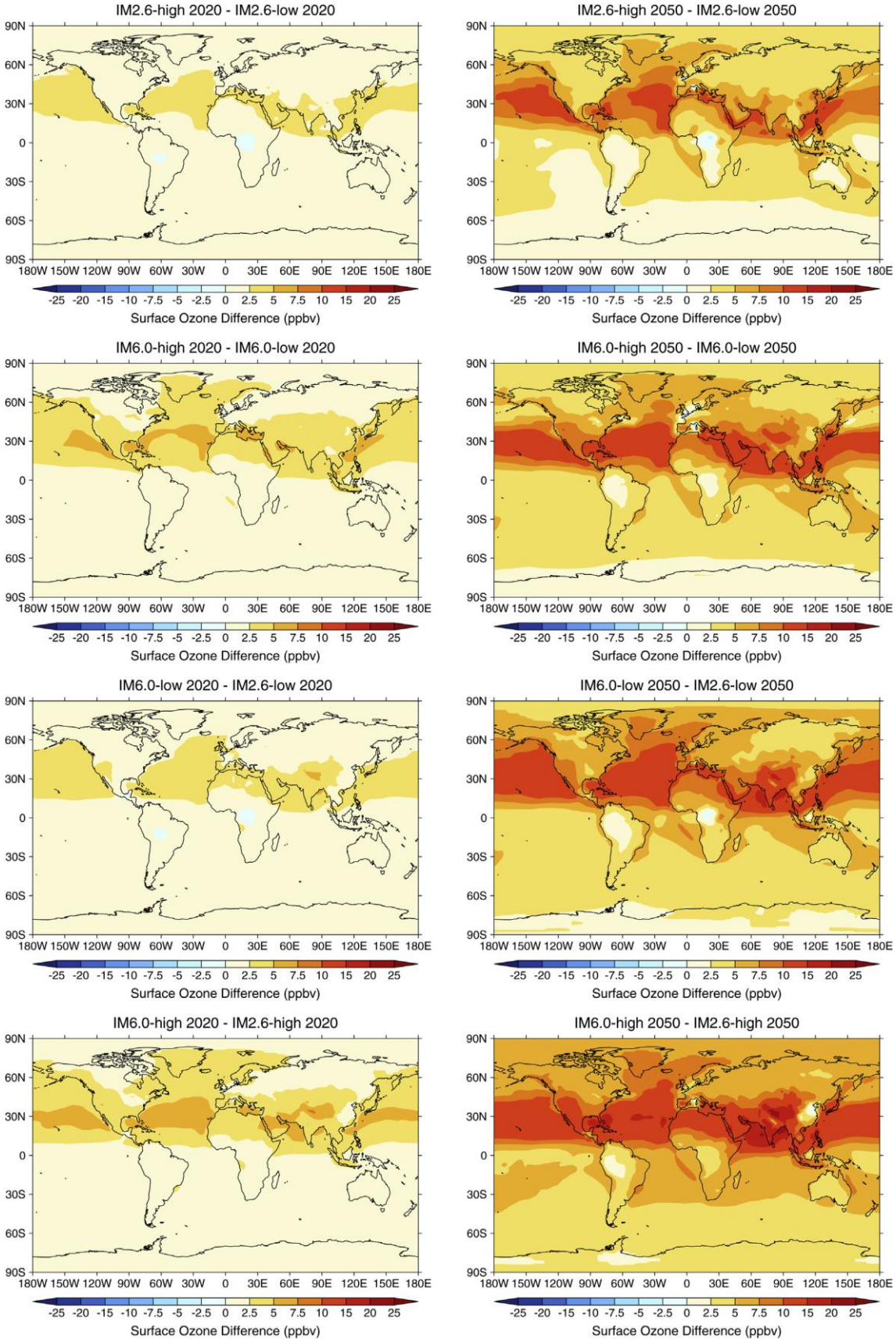

Fig. 2.5. Differences in the annual mean surface ozone concentration between the high and low air pollution scenarios (top panels) and the weak and strong climate policy scenarios (bottom panels) for 2020 and 2050.

2.3.3.2 Surface concentrations of sulphate

The results for surface concentration of sulphate (SO_4) depend on the region, time period and scenario. An increase is observed in the short term (2020) in all four scenarios in the Asian regions, mainly as a result of increasing energy demand and reliance on coal. At the same time, in all scenarios in 2020 a decrease is observed for North America, the North Atlantic, western Europe, and Australia, mainly due to SO_2 emission reductions achieved in the power sector (Fig. 2.7).

In the highest emission scenario (IM6.0-high), the increase in concentration continues in the period up to 2050 in many developing regions (Middle East, Asia, Africa, and South America, and over the tropical and subtropical oceans) (see also Fig. 2.6 for the NA, EU, EA and SA regions). The largest increases are projected in southern and eastern Asia, where annual mean concentrations in some places increase by more than 25 μg/m^3 in 2050. In contrast, under IM6.0-low in 2050 the sulphate concentrations at northern mid- and high latitudes are reduced, even in the northern parts of China. In IM2.6-high the concentrations in 2050 decline in most parts of the world except in the north of India, parts of central Africa and the west coast of Latin America. In IM2.6-low the increases in these regions are further reduced, while the concentrations in eastern China are reduced by up to about 5 μg/m^3.

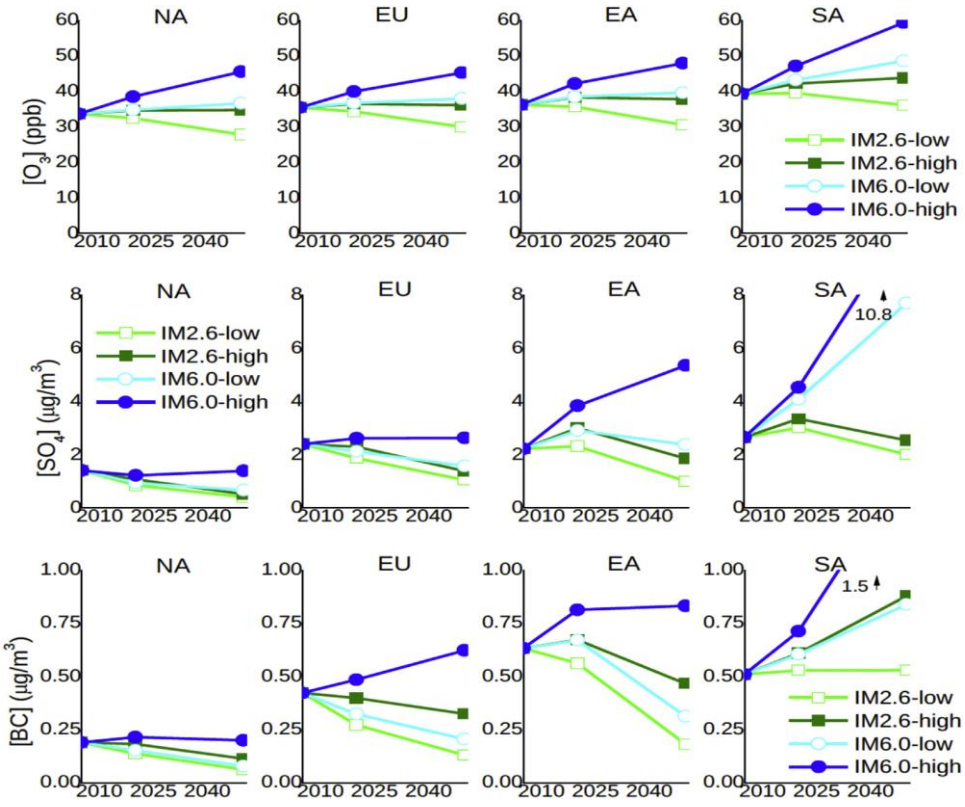

Fig. 2.6. Simulated regional and annual mean surface ozone, sulphate and black carbon concentrations in 2005, 2020 and 2050 for North America (NA) (60°W-125°W × 15°N-55°N), Europe (EU) (10°W-50°E × 25°N-65°N), East Asia (EA) (95°E-160°E × 15°N-50°N) and South Asia (SA) (50°E-95°E × 5°N-35°N).

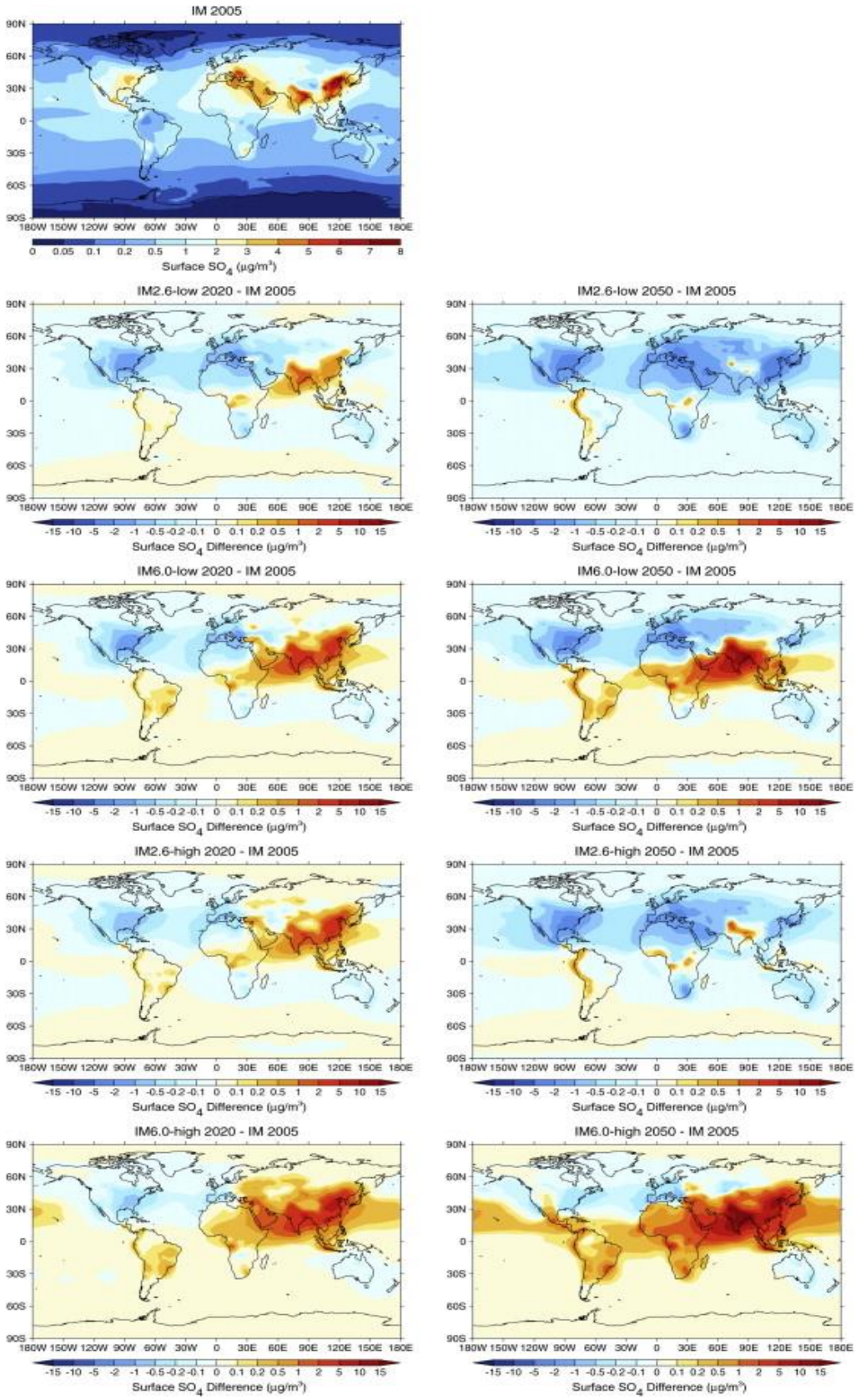

Fig. 2.7. Simulated annual mean surface SO_4 concentrations in 2005 and the changes in 2020 and 2050 relative to 2005 for the different scenarios.

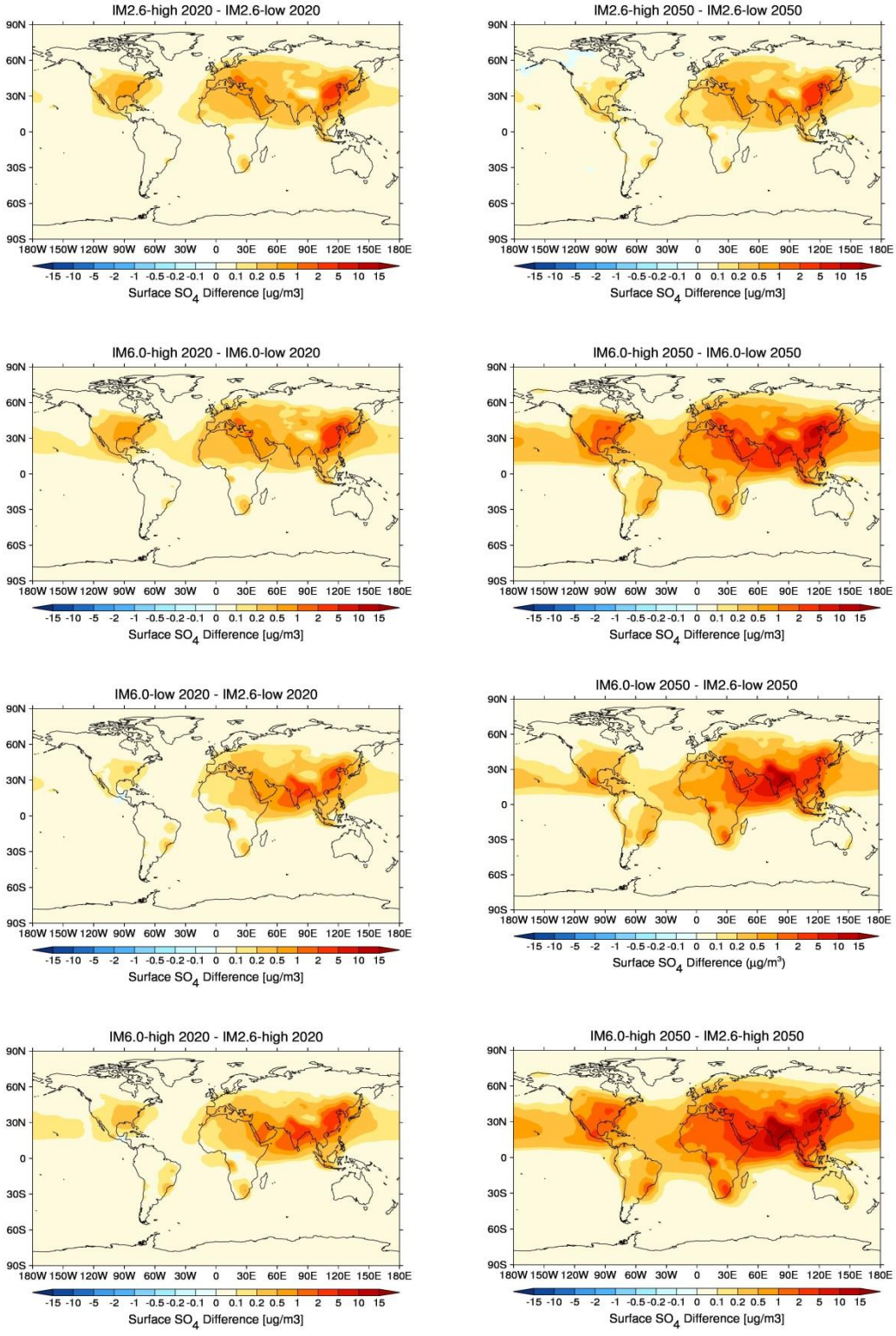

Fig. 2.8. Differences in the annual mean surface SO_4 concentrations between the high and low air pollution scenarios (top panels) and the weak and strong climate policy scenarios (bottom panels) for 2020 and 2050.

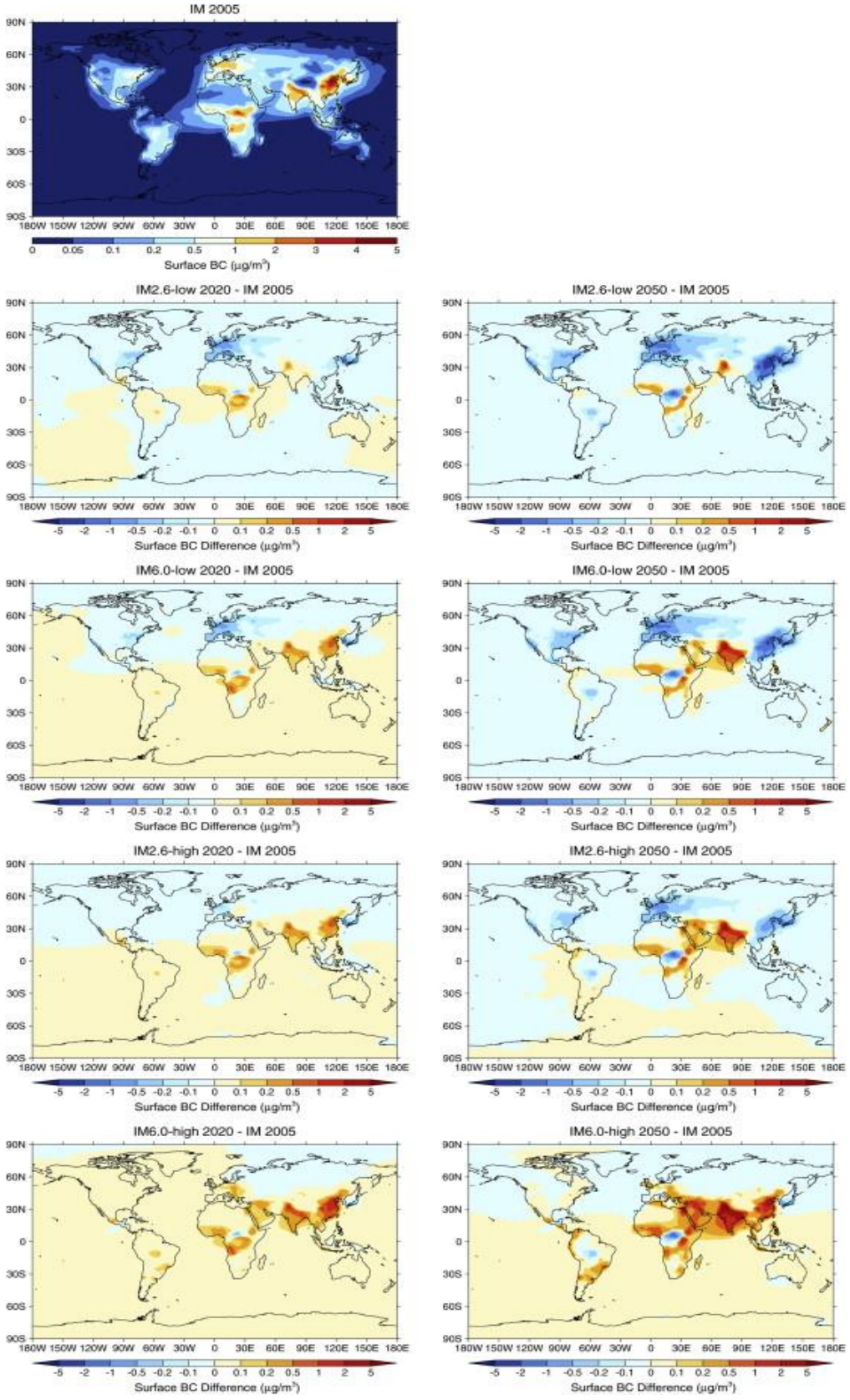

Fig. 2.9. Simulated annual mean surface BC concentrations in 2005 and the changes in 2020 and 2050 relative to 2005 for the different scenarios.

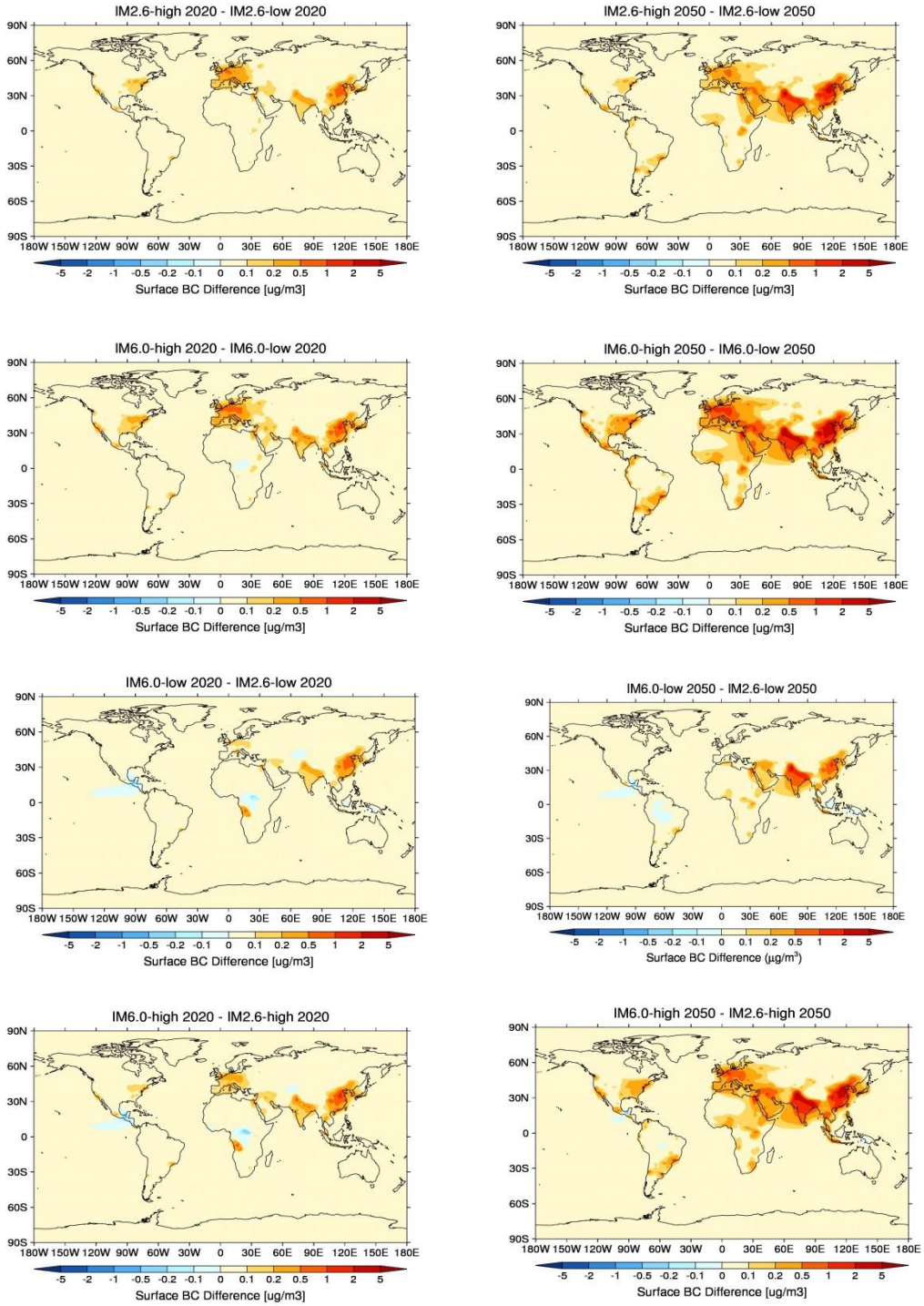

Fig. 2.10. Differences in the annual mean surface BC concentrations (µg/m^3) between the high and low air pollution scenarios (top panels) and the weak and strong climate policy scenarios (bottom panels) for 2020 and 2050.

Clearly, the impact of air pollution policy assumptions on sulphate concentrations is less in the IM2.6 than in the IM6.0 scenario (Fig. 2.8). The reason is that a large part of the SO_2 emissions are caused by coal fired power plants, which are progressively being phased out in the 2.6 W/m^2 scenario. The largest effects are observed in India and eastern China, where a rapid increase in energy demand and a high dependence on coal lead, in the absence of further control, to high SO_2 emissions. Significant effects can also be observed in the Middle East, parts of Eastern Europe, the Mediterranean region, the eastern US, Mexico, and parts of Latin America and Africa.

It should be noted that the assumptions of the IM6.0-high scenario lead to extremely high sulphate concentrations in Asia, as a result of increasing coal use in this region. This shows that further tightening of air pollution standards in Asia is needed.

2.3.3.3 Surface concentrations of black carbon

In the highest emission scenario (IM6.0-high) the surface concentrations of black carbon (BC) strongly increase in many world regions, including the Middle East, Eastern Europe, the eastern US, and in parts of Latin America, Africa and especially eastern China and India (Fig. 2.9). In contrast, in the IM6.0-low and IM2.6-high scenarios BC concentrations are reduced in North America and Europe, and by the middle of the century also in China. In the lowest emission scenario (IM2.6-low), the BC concentrations are reduced in most parts of the world, even in China in 2020. However, increased concentrations are still observed in 2050 in this scenario in northern India and Pakistan and parts of Africa. Fig. 2.6 shows the regionally averaged BC concentrations for NA, EU, EA and SA.

As for ozone, starting from the IM6.0-high scenario air pollution and climate policies have quantitatively similar effects on the BC concentrations, both in 2020 and 2050 (Fig. 2.10). Large reductions of up to about 5 μg/m^3 can be achieved by both types of policies in the most polluted parts of India and China. Indeed, the regional total BC emissions in SA and EA follow similar pathways under the IM6.0-low and IM2.6-high scenarios (see Figs. S2.4 and S2.5). The implementation of air pollution control is also effective in reducing the BC concentrations in case of the stringent climate policy scenario (IM2.6-high scenario). We note that in our modelling study the co-benefits of climate policy are relatively small if climate mitigation measures are introduced in a situation of already existing stringent air pollution policies, especially in Europe and the United States. However, the co-benefits are much more important in achieving further improvement in air quality in India and China.

2.3.4 Future radiative forcings

The global mean radiative forcings are estimated from the IMAGE methane concentrations and TM5 ozone concentrations and component-specific aerosol optical depths and include only the direct radiative effects (Table 2.1).

For methane, we project a slight increase in the RF in 2020 in all scenarios. However, the projected radiative forcing in the longer term clearly depends on whether stringent climate

policies are introduced (increases in IM6.0 and a decrease in IM2.6). As observed in Sect. 2.3.2, the methane RFs are lower in the high than in the corresponding low air pollution scenarios, especially in 2050.

The different scenarios for ozone lead to very different forcings. For the IM2.6-low scenario we find a negligible change in 2020 and a reduction of 0.12 W/m^2 in 2050 compared to today. In all other scenarios, the global mean ozone RF is expected to increase. The strongest increases are produced in the IM6.0 scenarios, especially in the high air pollution variant where the ozone RF is increased by 0.34 W/m^2 in 2050.

Tracers	IM2.6 Low 2020	IM2.6 High 2020	IM6.0 Low 2020	IM6.0 High 2020	IM2.6 Low 2050	IM2.6 High 2050	IM6.0 Low 2050	IM6.0 High 2050
CH_4	0.034	0.026	0.045	0.034	-0.091	-0.12	0.14	0.066
O_3	-0.001	0.040	0.066	0.15	-0.12	0.022	0.13	0.34
SO_4	0.081	-0.045	-0.055	-0.22	0.31	0.19	-0.20	-0.84
OC	-0.003	-0.009	-0.013	-0.018	0.038	0.031	0.016	0.003
BC	-0.046	0.047	0.032	0.15	-0.22	-0.039	-0.037	0.39
$CH_4 + O_3$	0.033	0.065	0.11	0.18	-0.21	-0.098	0.27	0.41
Aerosol	0.032	-0.006	-0.036	-0.090	0.12	0.18	-0.22	-0.44
Total RF	0.066	0.059	0.076	0.090	-0.082	0.081	0.054	-0.033

Table 2.1. Estimated global mean direct radiative forcings (W/m^2) of methane, tropospheric ozone and aerosols in 2020 and 2050 relative to 2005

The direct RF contributions from individual aerosol components are projected to go in very divergent directions as a function of the policy assumptions. In IM2.6-low, the sulphate cooling effect on the climate is projected to decrease by 0.08 W/m^2 in 2020 and by 0.31 W/m^2 in 2050 (i.e. the negative forcing becomes smaller). Also if the stringent air pollution policies are dropped, the cooling by sulphate is reduced by 0.19 W/m^2 in 2050 (but there is a small peak in 2020). Finally, in the IM6.0 scenarios the sulphate cooling is enhanced both in 2020 and 2050 (by maximally 0.84 W/m^2 in IM6.0-high in 2050).

For black carbon (BC), both climate and air pollution policies are relevant in determining the final change in forcing. In the IM2.6-low scenario the warming effect of BC is projected to decrease by 0.05 W/m^2 in 2020 and by 0.22 W/m^2 in 2050. Conversely, in both the IM2.6-high and IM6.0-low scenarios, the BC RF first peaks in 2020 and slightly declines in 2050.

Finally, in the IM6.0-high scenario the warming by BC is projected to increase by 0.15 W/m2 in 2020 and by 0.39 W/m2 in 2050.

For organic carbon (OC), much smaller changes in the RF are projected than for sulphate and BC (Table 2.1). The abundance of the semi-volatile ammonium-nitrate aerosol may change regionally in response to local changes in ammonia (NH_3) emissions and sulphate concentrations. The effect on the global mean RF is uncertain, but for our scenarios we estimate it to be smaller than for the other components. The total aerosol direct RF is therefore determined by the changes in the contributions from sulphate and BC. Changes in the cooling by sulphate are generally dominant, but are still partly compensated by the changes in the warming by BC. Thus, the changes in the combined aerosol RF are much smaller than in the separate contributions from sulphate and BC. As a result, the aerosol RF remains close to present-day levels in 2020. For 2050 the aerosol RF is projected to increase in the IM2.6 scenarios (by 0.12 W/m^2 in IM2.6-low and by 0.18 W/m^2 in IM2.6-high), and to decrease in the IM6.0 scenarios (by 0.22 W/m^2 in IM6.0-low and by 0.44 W/m^2 in IM6.0-high).

Interestingly, the impacts described above also lead to strong cancellation of the contributions of methane, ozone and aerosols to the total global mean RF. The absolute change in the total RF of these components is maximally 0.09 W/m^2 (IM6.0-high in 2020).

Similarly, the global climate effect of worldwide implementation of air pollution control is determined by the balance between the reduced warming by ozone and BC versus the reduced cooling by sulphate and the enhanced warming by methane. In both climate scenarios the net effect on the total global mean RF in 2020 is small. In the longer term, the reduced cooling by sulphate dominates in the IM6.0 scenario, whereas the reduced warming by ozone and BC dominates in the IM2.6 scenario. As a result, the global mean RF in 2050 changes by +0.09 W/m^2 in IM6.0 and by -0.16 W/m^2 in IM2.6 as a result of air pollution control. It is important to emphasize that the cancellation of the contributions of the individual components to the RF may not occur at regional and local scales.

2.4 Discussion and conclusions

This study has explored the impact of different assumptions regarding air pollution control in RCP-like scenarios on both air quality and direct radiative forcing of climate in 2020 and 2050. In our scenarios, air pollution control and climate mitigation policies both have large-scale effects on the concentrations of air pollutants, often of similar magnitude. The scenario with both stringent climate policy and air pollution control policies, therefore, results in the lowest concentrations. The results also show that in our modelling study the co-benefits of climate policies for air quality become lower for higher levels of air pollution control. Clearly, this study indicates that while climate mitigation policies do have important co-benefits for air quality, they alone are not enough to resolve air quality problems. The results confirm that the range of air pollutant emissions and concentration levels associated with the RCPs is indeed constrained by the assumed air pollution policies in these scenarios. If no

further air pollution policies would be implemented, air pollutant concentration levels could be considerably higher than in the RCPs, especially in Asia.

The co-benefits of worldwide implementations of air pollution control policies for mitigating global warming was analyzed in terms of its effect on the direct radiative forcing of methane, tropospheric ozone, and aerosols (sulphate, BC and OC). Air pollution control leads to substantially reduced warming by ozone at regional to continental scales, which at the global scale is partially compensated by increased warming by methane. Also, we project strong reductions in the cooling by sulphate and in the warming by BC, and much smaller changes in the RF by OC. The combined effect of air pollution policy on the global mean direct RF of the aerosols together is a small positive forcing in both climate scenarios in 2020. In the longer term (2050) it leads to a small negative RF by aerosols in the 2.6 W/m^2 scenario due to reductions in BC, and a substantial positive RF of 0.22 W/m^2 by aerosols in the 6.0 W/m^2 scenario, where air pollution control will significantly reduce sulphate emissions, especially in Asia. The combined global mean RF from methane, ozone and aerosols together is hardly affected by air pollution policies in the short term. By the middle of the century, air pollution control is projected to change the total global mean RF by +0.09 W/m^2 in the 6.0 W/m^2 scenario, mostly due to reductions in the sulphate RF, and by -0.16 W/m^2 in the 2.6 W/m^2.

The projections presented in this study are based on a number of assumptions. First, the methane concentrations pathways calculated in the IMAGE model are based on the parameterization applied in MAGICC6, which is based on a chemistry transport model intercomparison study performed for the IPCC Third Assessment Report (Ehhalt et al., 2001). Recently, Prather et al. (2012) presented improved methane concentration projections and associated uncertainties for the RCP emission pathways and compared their results with the official RCP concentration projections based on MAGICC6 (Meinshausen et al., 2011b). They found very good agreement for both RCP4.5 and RCP6.0, but concluded that MAGICC6 based concentration projections for RCP2.6 and RCP8.5 are at the high resp. the low end of their range of uncertainty.

We also applied the same meteorological data based on the ERA-Interim reanalysis in our TM5 simulations for the future and the present day. In reality, the future climate will change depending on the scenario assumed for emissions and land use, and future changes in meteorological parameters are expected to have an effect on the surface concentrations of air pollutants. Also, natural emissions of ozone and aerosol precursors are likely to evolve differently under future climatic conditions. However, the impacts of these anticipated future changes are still highly uncertain.

Furthermore, our estimates of the future changes in the direct RFs of the various aerosol components are based on the scaling approach described in Sect. 2.2.4, which involves aggregation of the simulated aerosol optical depth fields to sufficiently large scales. It should also be noted that our RF estimates don't include any indirect aerosol effects. Including those would make the sulphate effects relatively more important.

Compared to the RCP set of scenarios, the scenarios presented in this study give a much broader range of possible outcomes with respect to the future evolution of air pollutants. It is imperative to emphasize that though the RCPs include short-lived tracers and aerosols, they were not designed to assess future changes in air quality. Instead, they were produced to assess how different climate forcing targets can be reached by the end of the century, while assuming a continuation of the current trend towards more stringent air pollution control. This paper is meant to explore the potential impacts of varying air pollution policies. In this light, integrated emission scenarios focusing on short lived components as presented in this study are required to make representative projections of future changes in air quality and climate forcing.

Electronic Supplementary Material A

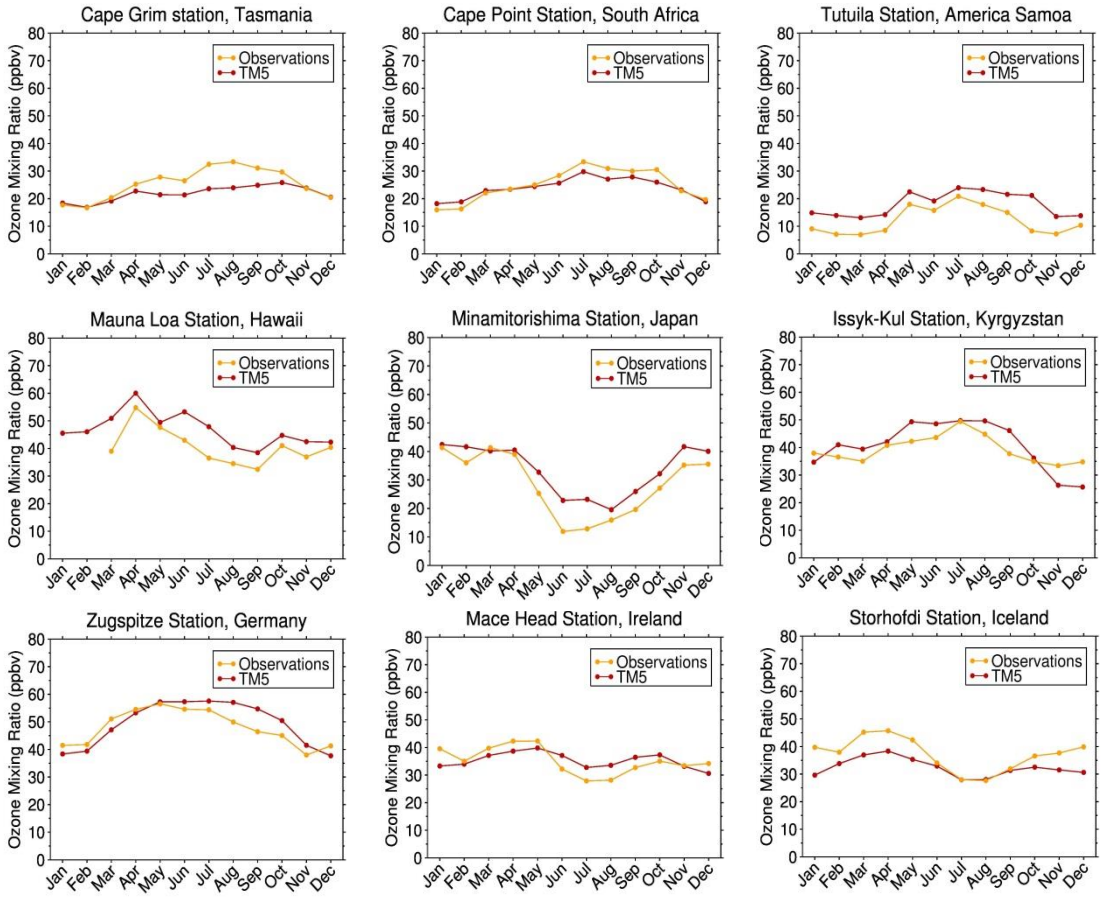

Fig. S2.1. Comparison of monthly surface ozone mixing ratios from the TM5 simulation for 2005 with observations at a number of representative background stations. The stations have been selected from the networks coordinated by the NOAA Global Monitoring Division (GMD), the World Data Centre for Greenhouse Gases (WDCGG), and the European Monitoring and Evaluation Programme (EMEP).

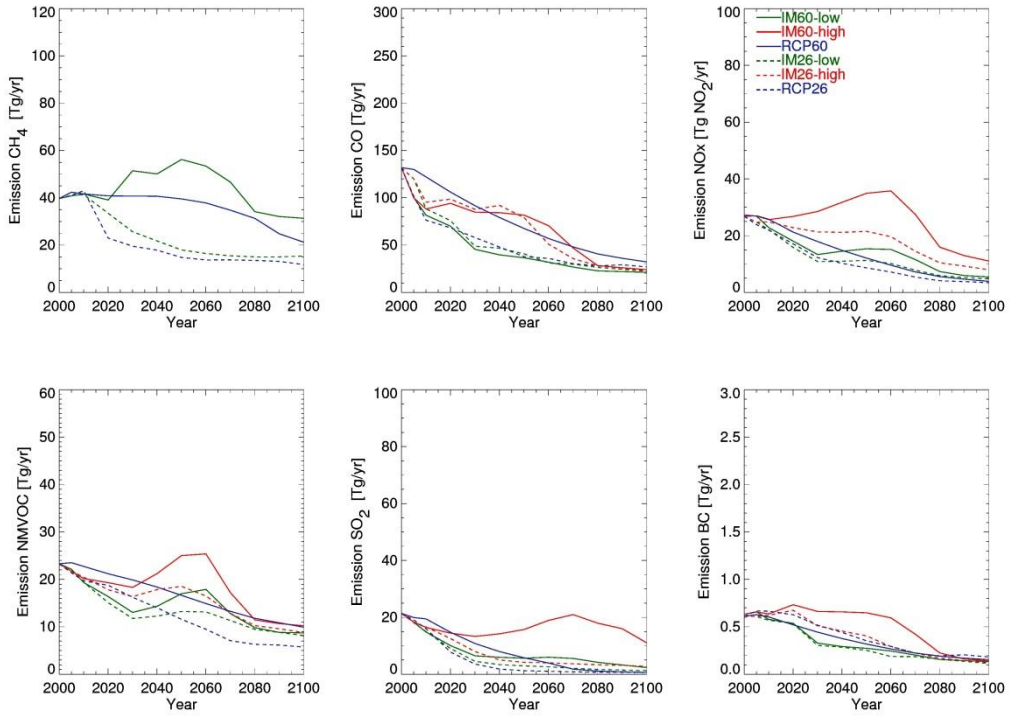

Fig. S2.2. Annual total anthropogenic emissions of CH_4, CO, NO_x, NMVOC, SO_2, and BC in the new IMAGE scenarios and the corresponding RCPs for North America (60°W-125°W × 15°N-55°N). Emissions from biomass burning are included in the totals.

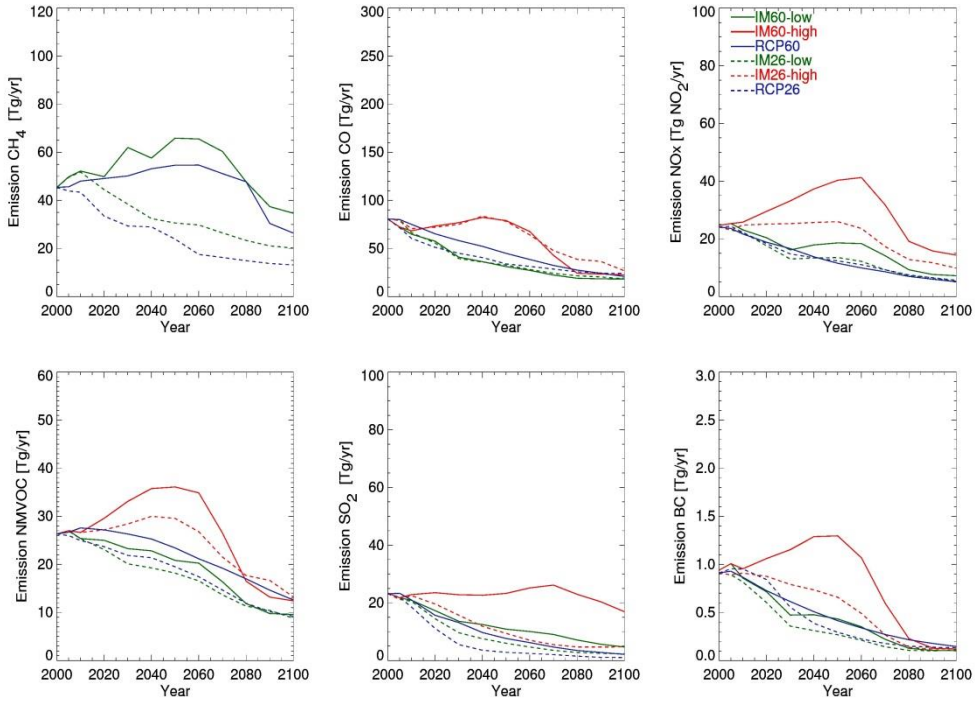

Fig. S2.3. Annual total anthropogenic emissions of CH_4, CO, NO_x, NMVOC, SO_2, and BC in the new IMAGE scenarios and the corresponding RCPs for Europe (10°W-50°E × 25°N-65°N). Emissions from biomass burning are included in the totals.

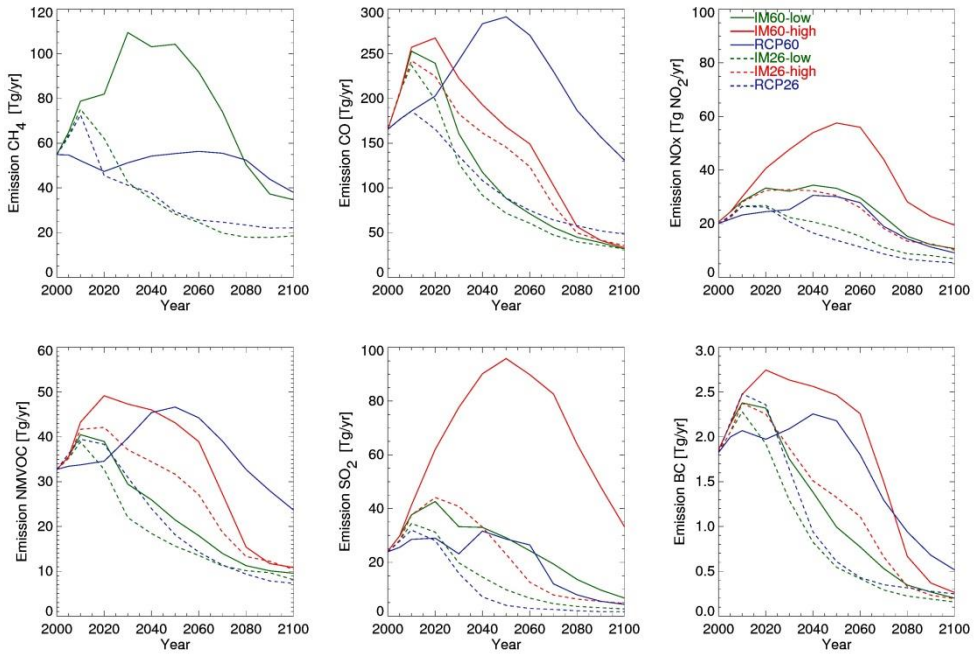

Fig. S2.4. Annual total anthropogenic emissions of CH_4, CO, NO_x, NMVOC, SO_2, and BC in the new IMAGE scenarios and the corresponding RCPs for East Asia (95°E-160°E × 15°N-50°N). Emissions from biomass burning are included in the totals.

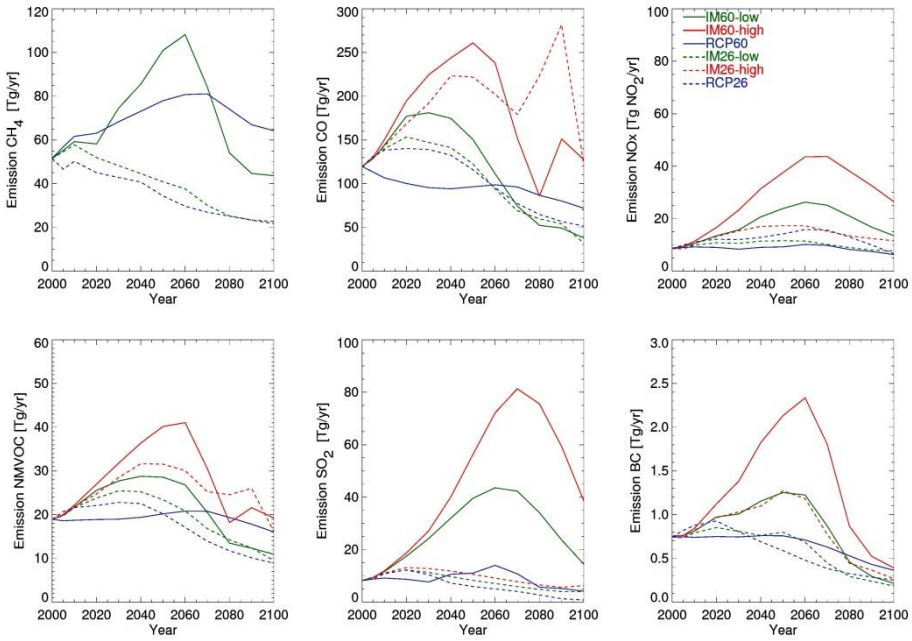

Fig. S2.5. Annual total anthropogenic emissions of CH_4, CO, NO_x, NMVOC, SO_2, and BC in the new IMAGE scenarios and the corresponding RCPs for South Asia (50°E-95°E × 5°N-35°N). Emissions from biomass burning are included in the totals.

Tracers	2005	IM2.6 Low 2020	IM2.6 High 2020	IM6.0 Low 2020	IM6.0 High 2020	IM2.6 Low 2050	IM2.6 High 2050	IM6.0 Low 2050	IM6.0 High 2050
O_3 (ppbv)	25.61	25.67	27.05	27.22	29.48	22.90	27.57	29.17	34.89
SO_4 ($\mu g/m^3$)	0.793	0.722	0.832	0.843	0.984	0.489	0.608	0.927	1.420
BC ($\mu g/m^3$)	0.137	0.125	0.146	0.141	0.169	0.085	0.134	0.114	0.208

Table S2.1. Simulated global annual mean surface concentrations of ozone, sulphate and black carbon in 2005, 2020 and 2050.

CHAPTER 3

Global and regional climate impacts of future aerosol mitigation in an RCP6.0-like scenario in EC-Earth

Abstract

Future changes in aerosol concentrations will influence the climate system over the coming decades. In this study we evaluate the equilibrium climate response to aerosol reductions in different parts of the world in 2050, using the global climate model EC-Earth. The aerosol concentrations are based on a set of scenarios similar to RCP6.0, developed using the IMAGE integrated assessment model and exploring stringent and weaker air pollution control. Reductions in aerosol concentrations lead to an increase in downward surface solar radiation under all-sky conditions in various parts of the world, especially in Asia where the local brightening may reach about 10 Wm^{-2}. The associated increase in surface temperature may be as high as 0.5°C. This signal is dominated by the reduced cooling effect of sulphate which in some areas is partially compensated by the decreased warming effect of black carbon. According to our simulations, the mitigation of BC may lead to decreases in mean summer surface temperature of up to 1°C in central parts of North America and up to 0.3°C in northern India. Aerosol reductions could significantly affect the climate at high latitudes especially in the winter, where temperature increases of up to 1°C are simulated. In the Northern Hemisphere, this strong surface temperature response might be related to changes in circulation patterns and precipitation at low latitudes, which can give rise to a wave train and induce changes in weather patterns at high latitudes. Our model does not include a parameterization of aerosol indirect effects so that responses could be stronger in reality. We conclude that different, but plausible, air pollution control policies can have substantial local climate effects and induce remote responses through dynamic teleconnections.

This chapter is in press as: Chuwah, C.D., van Noije, T., van Vuuren, D.P., Le Sager, P., Hazeleger, W., 2015. Global and regional climate impacts of future aerosol mitigation in an RCP6.0-like scenario in EC-Earth, Climatic Change.

3.1 Introduction

Changes in the amount, distribution and composition of aerosols in the atmosphere over the last 150 years are mainly caused by anthropogenic activities related to energy and land use. These changes have influenced the transfer of radiation and spatial distribution of moist static energy through the atmosphere with a large impact on weather and climate (Boucher et al., 2013). Sulphate (SO_4), nitrate, and some forms of organic aerosols reflect solar radiation and thus have a cooling effect on the climate (Hansen et al., 1981; Charlson et al., 1991; Kiehl and Briegleb, 1993; Mitchell et al., 1995). Black carbon (BC), on the other hand, absorbs solar radiation, thereby reducing the amount of solar energy that reaches the earth's surface. This results in a local warming of the atmosphere and a cooling of the underlying surface (Hansen et al., 2005; Bond et al., 2013). Besides these direct radiative effects, aerosols also influence the climate by changing the properties and lifetimes of clouds, and changes in diabatic heating can cause remote changes through atmospheric teleconnections. Field observations and modelling studies have shown that overall increases in aerosols have had a net cooling effect on the climate, especially at the surface (Boucher et al., 2013).

The aerosol-induced scattering and absorption of solar radiation, which results in dimming at the surface, reduces the amount of solar energy available for evaporation, thereby slowing down the hydrological cycle (Wild et al., 2005 and references therein; Hartmann et al., 2013). There are indications that this dimming has recently been reversed in some parts of the world (Wild et al., 2005), resulting in local warming that is larger than the warming of greenhouse gases alone (Van Oldenborgh et al., 2009). This could be the result of reduction of aerosol concentrations due to the implementation of stringent air pollution policy. While the implementation of air quality control measures has reduced emissions of aerosols and aerosol precursors in Europe and North America, emissions have increased in the rapidly growing economies in South Asia and East Asia. While it is expected that stronger air pollution control policies will also be implemented here, it is yet unclear how pollution levels in Asia will evolve in the decades ahead.

A number of studies have looked at the impact of aerosol mitigation on future climate using the Representative Concentration Pathways (RCPs) (Chalmers et al., 2012; Gillett and Von Salzen, 2013; Rotstayn et al., 2013) and emission scenarios from the International Institute for Applied Systems Analysis (IIASA) (Kloster et al., 2010, Sillmann et al., 2013). In general, these studies show that the mitigation of aerosols and precursor emissions could result in brightening at the surface and an increase in surface temperature.

In chapter 2, we explored the implications of different assumptions regarding future air quality and climate policy for air pollutant concentrations, using a set of RCP-like scenarios developed with the IMAGE integrated assessment model (Bouwman et al., 2006). The scenarios showed a wide range of aerosol concentration pathways corresponding to substantially different radiative forcings, even on a global scale. The study found that the implementation of more stringent air pollution control (compared to current legislation) in a scenario with weak climate policy (similar to RCP6.0) would lead to a global mean net

positive aerosol direct radiative forcing of 0.22 Wm^{-2}, mainly due to substantial reductions of aerosol concentrations in Asia. Among the different aerosol components, the reduction of the cooling effect of SO_4 was found to be the strongest signal (0.64 Wm^{-2}), but that effect is partially compensated by the decline in the warming effect of BC (-0.35 Wm^{-2}).

Our scenarios cover a much broader range of possible outcomes with regard to future air pollutants than the RCPs. The climate impacts have not yet been evaluated in a general circulation model. In this study, we use the global climate model EC-Earth to assess the climate impacts of aerosol reductions in the RCP6.0-like scenarios shown in chapter 2 for 2050. We thereby separate the climate impacts due to reductions in SO_4 and BC, respectively. EC-Earth is derived from a numerical weather prediction model and has a comparatively high resolution compared to other models that participated in CMIP5 (Taylor et al., 2012). As a consequence it simulates atmospheric dynamics comparatively well (e.g. Zappa et al., 2013). Our model does not include a parameterization of aerosol indirect effects. Although these are very uncertain and not well constrained by observations, responses to aerosol reductions could therefore be higher in reality, especially in the case of SO_4.
.

The paper is structured as follows: Section 3.2 describes the methodology. In Section 3.3 we present results on local and remote climate impacts of aerosol mitigation. A discussion and conclusions of our results are given in Section 3.4.

3.2 Methodology

3.2.1 Model description

In this study, we use the EC-Earth model version 2.3 which participated in the Coupled Model Intercomparison Project (CMIP5, Taylor et al., 2012). The atmosphere and land surface components in EC-Earth are simulated using the Integrated Forecasting System (IFS) from the European Centre for Medium-Range Weather Forecasts (ECMWF). In this version of EC-Earth, IFS version 31r1 is used with some modifications as described by Hazeleger et al. (2012). The IFS component is configured to run at a horizontal spectral resolution of T159 (triangular truncation at wavenumber 159) and a vertical resolution of 62 layers. The ocean is simulated with the Nucleus for European Modelling of the Ocean (NEMO) version 2, with a horizontal resolution of about 1 degree and 42 vertical layers (Madec, 2008). Sea ice is modelled inside NEMO using the Louvain-la-Neuve sea ice model (LIM) version 2. The ocean/sea ice and the atmosphere/land components communicate via the OASIS3 coupler (Valcke, 2013). Here we used the fully coupled EC-Earth model that allows for dynamic response and feedbacks from interactions between the atmosphere, land surface, sea ice, and the ocean. It is important to note that in this version of EC-Earth the description of clouds is not coupled to changes in aerosol concentrations. Also, the impact of BC deposited on snow or ice is not accounted for. In that sense, indirect aerosol effects are not accounted for. The absorption of solar radiation by BC modifies the atmospheric temperature structure and therefore cloud distributions (semi-direct effect). In EC-Earth, the impact of changes in cloud distributions on radiation induced by this semi-direct effect is accounted for.

3.2.2 Emissions scenarios

From the four scenarios presented in chapter 2, we selected two scenarios that explore high and low aerosol forcing as a result of different levels of air pollution control. These scenarios, developed using the IMAGE integrated assessment model (Bouwman et al., 2006), have the same greenhouse gas emissions, but different emission factors (emissions per unit activity per sector and fuel type) for air pollutants (scenarios LOW and HIGH). In terms of greenhouse gas emissions, the scenarios are similar to the original RCP6.0 (Masui et al., 2011). Thus the global radiative forcing in our scenarios gradually increases throughout the century and reaches a value of around 6.0 Wm^{-2} in 2100.

The official RCP scenarios all assume successful implementation of air pollution policy (see Van Vuuren et al., 2011). This is simulated in our scenario LOW, in which the emission factors are assumed to decline in accordance with the implementation of current and planned air pollution legislations until 2030 and thereafter as a function of income levels. In contrast, in the HIGH scenario we assume that emission factors are held constant at the 2010 levels providing a reference scenario, which enables us to systematically assess the potential impacts of future air pollution policy on aerosol concentrations and regional climate conditions by comparing the LOW and HIGH scenario. As a set, the two scenarios therefore explore the impact of air pollution emissions for a wider range than included in the RCPs. A detailed description of the underlying assumptions of the LOW and HIGH scenarios and comparison with the RCPs can be found in chapter 2. Some important results of the scenarios are shown in the supplementary material (Fig. S3.1).

3.2.3 Experimental setup

The climate response to the reduced aerosol concentrations is investigated using time slice simulations with EC-Earth for 2050. The initial conditions were set to the 2005 results from a CMIP5 compliant simulation of EC-Earth with prescribed historical forcings. Here, we used prescribed monthly mean aerosol fields for our simulations which is in line with simulations conducted in other studies (e.g. Teng et al., 2012). In our time slice simulations, the forcings for well-mixed greenhouse gases, ozone, volcanic aerosols, and the solar cycle were fixed to their 2050 levels irrespective of the model year. All simulations were continued for 180 years to allow the model to adjust to the imposed forcings. The output of our simulations was analysed for the last 80 years when the model's climate has reached a quasi-steady state (Fig. S3.2).

The aerosol fields used in EC-Earth version 2.3 for CMIP5 are based on simulations with the chemistry-climate models CAM3.5 (Lamarque et al., 2010). The CAM aerosols consist of hydrophobic and hydrophilic BC and OC, SO_4, sea salt and mineral dust. In order to account for the aerosol direct radiative effects according to the HIGH and LOW scenarios for 2050, we scale the CAM mixing ratios of BC, OC, and SO_4 using the vertically integrated burdens from the atmospheric chemistry and transport model TM5, used in chapter 2. Note that the TM5 future aerosol concentrations were calculated using present-day (2005) meteorological fields from ERA-Interim reanalysis (Dee et al., 2011) of the European Centre for Medium-

Range Weather Forecasts (ECMWF). To use our TM5 aerosol fields in EC-Earth, we apply scaling ratios for SO_4, BC, and OC to the corresponding aerosol fields for 2005 computed in CAM. Thus, the mixing ratios X_i of the various aerosol components *i* used in our simulations are given by

$$X_i(\underline{r}, 2050) = \frac{B_i^{\mathrm{TM5}}(\underline{x}, 2050)}{B_i^{\mathrm{TM5}}(\underline{x}, 2005)} \times X_i^{\mathrm{CAM}}(\underline{r}, 2005), \qquad (3.1)$$

where B_i denote the vertically integrated burdens for the different aerosol components, and $\underline{r}$ and $\underline{x}$ are the 3-D and 2-D coordinates.

We performed four different simulations with different aerosol concentrations as shown in Table 3.1. The first two simulations correspond to the LOW and HIGH scenarios respectively. To assess the individual contributions of BC and SO_4 to the simulated climate response we performed two additional experiments: BC-LOW and SO_4-LOW. In these experiments the HIGH scenario is assumed, but with concentrations of BC and SO_4, respectively, from the LOW scenario. The data presented in this study represent averages over the last 80 years of our simulations. Statistical significance of the differences in climate response between our scenarios is evaluated using student's *t*-test at a significance level of 0.05.

Simulation	**BC concentrations**	**OC concentrations**	**SO_4 concentrations**
LOW	Low	Low	Low
HIGH	High	High	High
LOW-BC	Low	High	High
LOW-SO_4	High	High	Low

Table 3.1. Overview of the EC-Earth simulations performed in this study.

3.3 Results

3.3.1 Impacts of aerosol reductions on radiation

The top panels of Fig. 3.1 show the differences in annual mean downward surface solar radiation (SSRD) under all-sky conditions between the LOW and HIGH pollution scenarios (left) and the contribution from reductions in SO_4 aerosols only (SO_4-LOW compared to HIGH) (right). While the air pollution control policies assumed in the LOW scenario strongly reduce air pollution levels, they also lead to a significant brightening at the surface, most notably in the Northern Hemisphere (NH) subtropics and mid-latitudes. The largest changes, with an increase in annual mean SSRD reaching 9.9 Wm^{-2}, are found in India and China, where aerosol concentrations are projected to increase strongly in the HIGH scenario and pollution control is most effective in reducing absolute concentrations levels. Significant changes in annual mean SSRD due to aerosol reductions can also be seen in most parts of the United States (US), Mexico and Europe, and in some parts of the Middle East and Northern

Africa. Comparison with the SSRD differences due to changes in SO_4 only reveals that the SSRD increases are dominated by the scattering effect of SO_4, with the contributions from reductions in other aerosol components being much smaller.

The reduction of aerosol concentrations by air pollution policy as assumed in the LOW scenario leads to increases in annual mean net solar radiation at the top of the atmosphere (TSR) under clear-sky conditions (Fig. 3.1, bottom panels), especially in eastern China where increases of around 3 Wm^{-2} are estimated. Here, the reduced upward scattering by SO_4 dominates the calculated increase in the clear-sky TSR, which is partially compensated by a decrease in BC absorption. However, under all-sky conditions we see a decrease in annual mean TSR, especially in parts of eastern China where we simulate decreases of up to 7 Wm^{-2}. Further analysis indicates that the aerosol-induced brightening at the surface increases the amount of potential convective energy, thereby enhancing the development of convective clouds, which increases the upward scattering effect of clouds. This is evident in the increase in the computed annual mean liquid water path (Fig. S3.4, bottom left) and in convective precipitation, especially during the boreal summer (Fig. S3.4, bottom right). The mitigation of aerosols result in an increase in precipitation of up to 1 mm per day over China which is similar to the findings of Levy et al. (2013). This computed increase in available potential convective energy and convection is consistent with previous studies (see Persan et al., 2012; Kim et al., 2014) and demonstrates how aerosol direct radiative effects can have an impact on clouds and the hydrological cycle. In contrast, Niemeier et al. (2013) found that the hydrological sensitivity is decreased by solar radiation management, especially for aerosol-based techniques such as artificial sea salt emissions.

3.3.2 Local impacts of aerosol reductions on climate

Our results indicate that the impact of air pollution policy on surface temperature could be significant, especially in South and East Asia (Fig. 3.2). The abatement of aerosols in the LOW vs. HIGH scenario results in an increase of up to 0.5°C in surface temperature in parts of North America, India and China. The significant changes in surface temperature that we find over the US appear qualitatively similar to results reported in Mickley et al. (2012). Our results also show that the reduced scattering effect of SO_4 (SO_4-LOW compared to HIGH) explains most of the estimated increases in surface temperature especially in most parts of eastern China and central US, with a maximum increase of up to 0.5°C. Levy et al. (2013) also found that the temperature response to aerosol changes in RCP4.5 is dominated by sulphate in their model. On the other hand, a 0.3°C decrease in surface temperature due to the effect of reductions in BC (BC-LOW with respect to HIGH) in the northern parts of India during the boreal summer is also visible (Fig. 3.2, third row, left panel). Also, we find a significant decrease in summer mean surface temperature of up to 1°C in parts of central North America (Fig. 3.2, bottom right) as a result of the mitigation of BC. Teng et al. (2012) found qualitatively similar temperature changes over the United States in response to changes in carbonaceous aerosol concentrations over Asia. Interestingly, we find that BC reductions lead to surface warming in parts of the US and a region stretching from the Sea of Japan to

the east, which may be related to the simulated surface brightening. In Europe the changes in surface temperature are less significant.

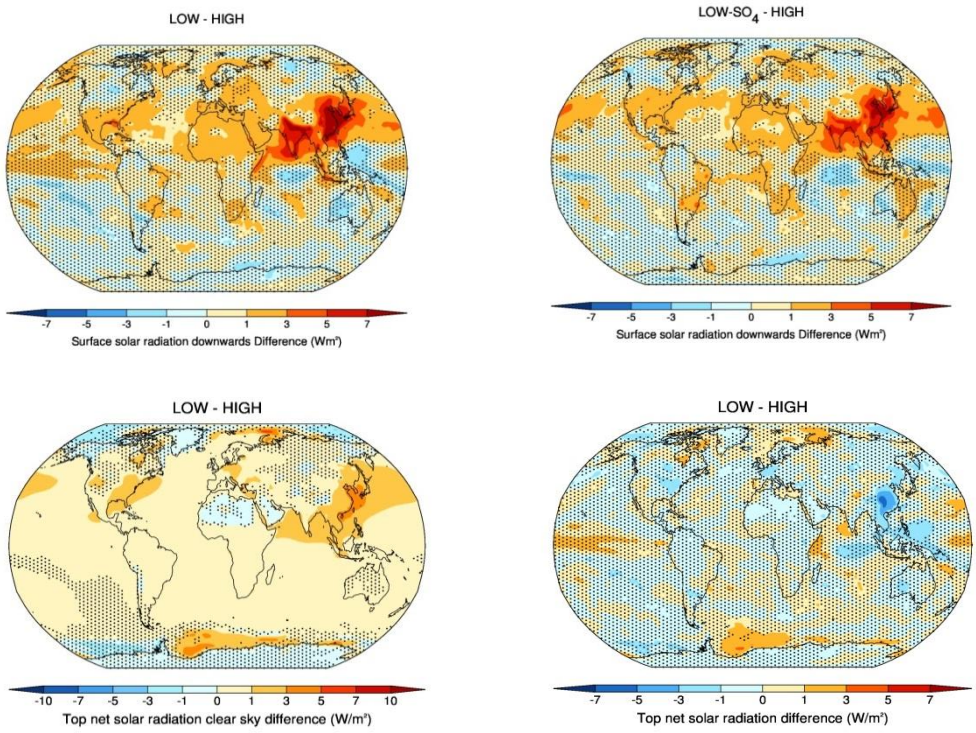

Figure 3.1. Differences in annual mean downward surface solar radiation under all-sky conditions between the LOW and the HIGH scenario (top left panel) and the contributions from reductions in SO_4 aerosols only (top right panel). The bottom panels show the corresponding differences in annual mean top of atmosphere net solar radiation under clear-sky (left) and all-sky (right) conditions. The stippled areas show regions where the differences are not significant at the 5% level, and this applies to all the other figures as well.

3.3.3 Remote impacts of aerosol reductions on climate

Although most of the aerosol changes occur in the subtropics and NH mid-latitudes, a substantial climate response is found in the Arctic and Antarctic (Fig. 3.3). In the Arctic the annual mean surface temperature increases by about 0.5°C due to aerosol reductions. This surface temperature increase is higher in winter (up to 1°C).

Results from the SO_4-LOW and BC-LOW compared to the HIGH scenario show that BC and SO_4 can have opposite effects on surface temperature in the Arctic. For example, decreases in SO_4 concentrations increase annual mean surface temperatures in the Arctic by up to 1°C. On the contrary, reductions in BC tend to lead to surface cooling of the Arctic. Locally, this contribution can be as high as 0.5°C in the annual mean and 1°C in winter.

The reduction of aerosol concentrations results in a decrease in annual mean surface temperature by 1°C in parts of the Weddell Sea. At the same time, increases in annual mean

surface temperature of up to 1°C can be seen in small parts of the Ross Sea and in large parts of the Southern Ocean to the west of the Ross Sea. The changes found in the high latitudes may be caused by remote responses induced by changes in aerosol concentrations through teleconnections. However, the region where such responses are simulated is rather small. It is important to reiterate that most of the aerosols reductions take place in the NH mid-latitudes and the tropics. This suggests that the overall climate response at high latitudes is strengthened by processes described below.

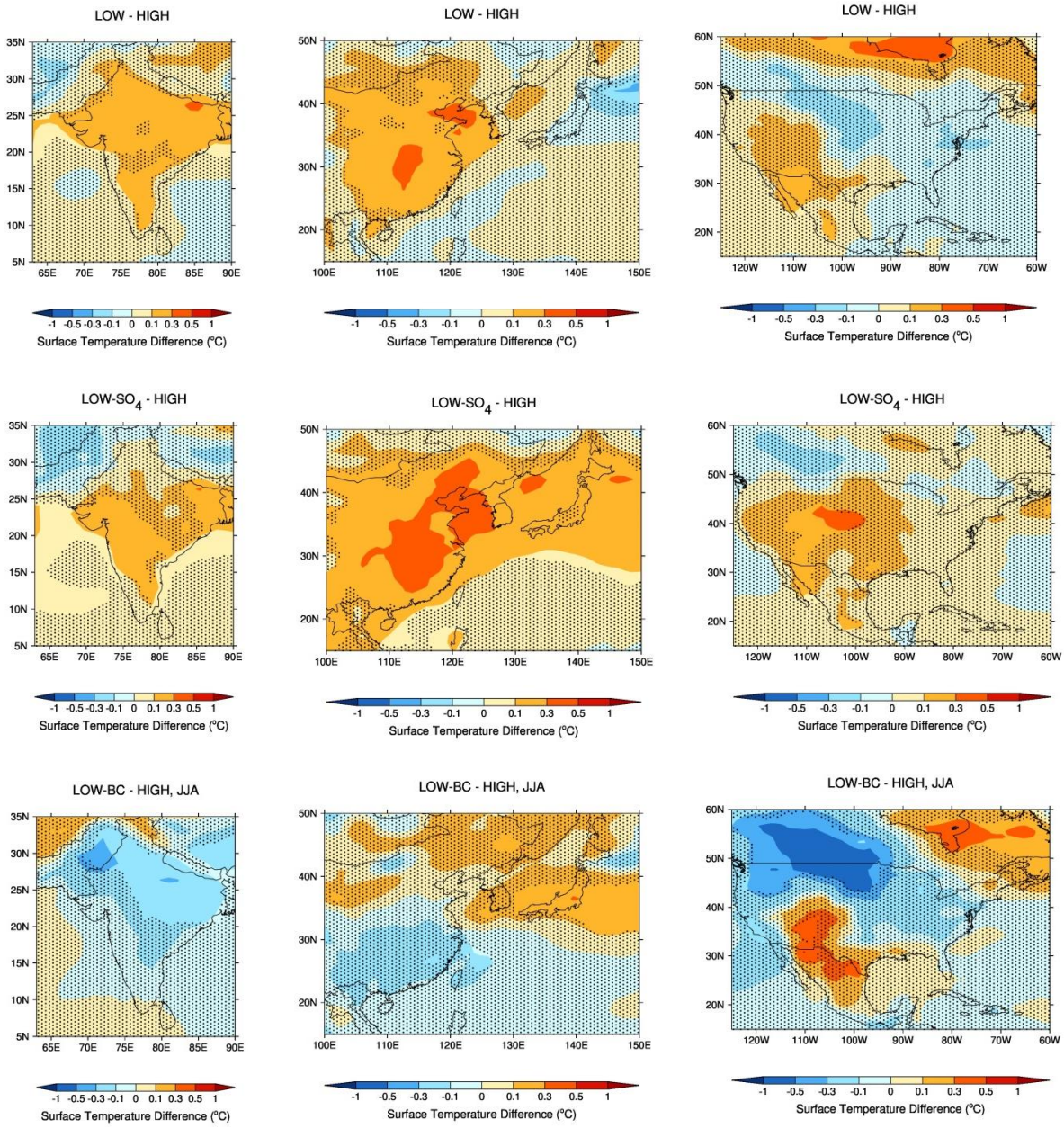

Figure 3.2. Differences in annual mean temperature over India (left panels), China (middle panels) and the United states (right panels) between the LOW and the HIGH scenario (upper panels), the contributions from reductions in sulphate only (second row panels) and the effects of reductions in BC in the summer (JJA, third row panels).

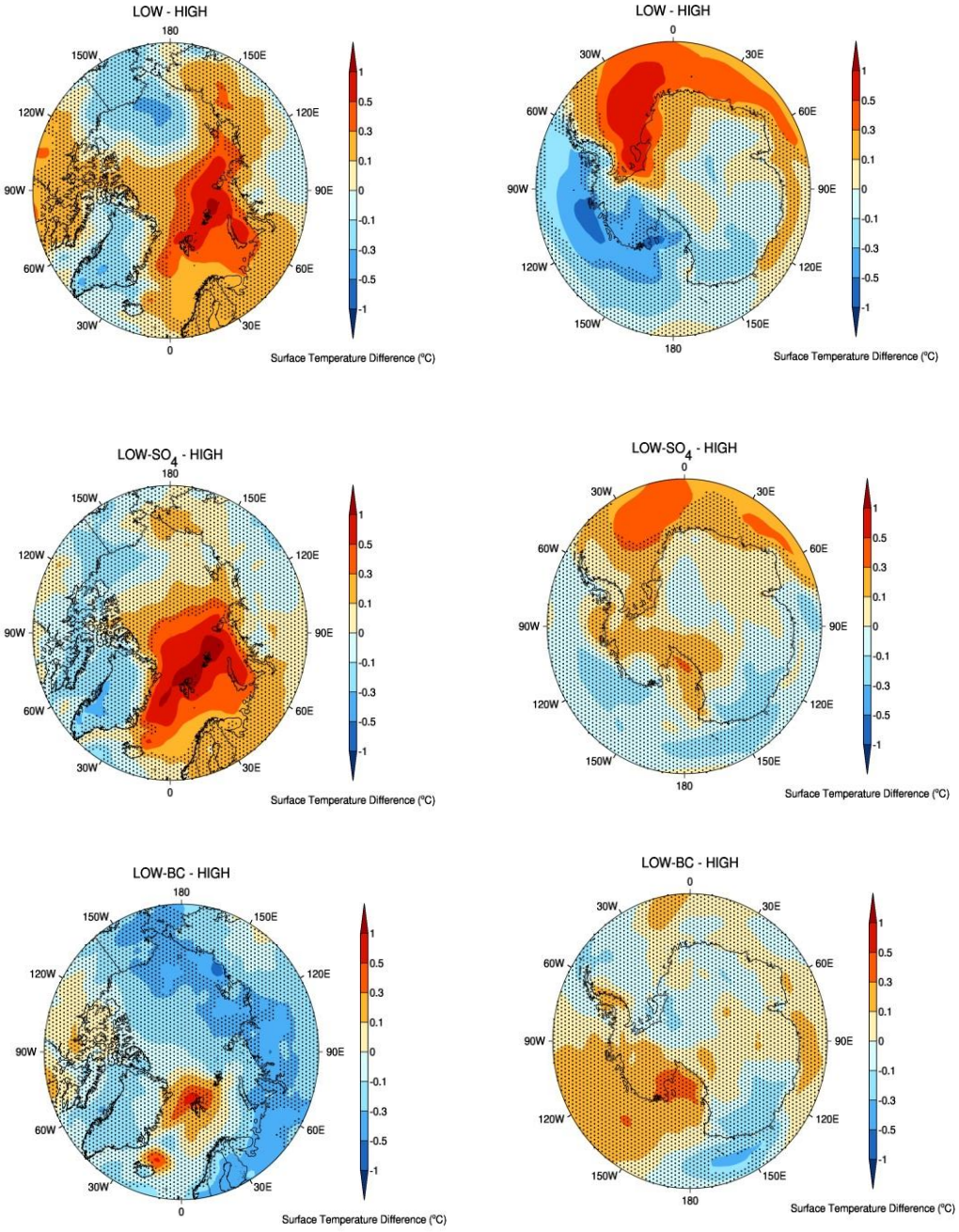

Fig.3.3. Differences in annual temperature in the Arctic (left panels) and Antarctic (right panels) between the LOW and the HIGH scenario (upper panels), and the contributions from reductions in SO_4 (middle panels) and BC (bottom panels) only.

Previous studies have shown that Arctic temperatures are strongly influenced by NH mid-latitude forcings (e.g. Shindell et al., 2007; Shindell et al., 2010; Sand et al., 2013; Rotstayn et al., 2014). Part of the strong surface temperature response that we find in the winter at the poles is linked to the local ice albedo feedback carried over from the summer (see Screen and Simmonds, 2010, and references therein). Here, the reduced sea ice cover in the summer enhances the warming of the surface ocean, which further harnesses sea ice loss and more

energy uptake by the ocean. The additional heat stored in the ocean is released in the winter, thereby hampering the expansion of winter sea ice. In the Arctic, the largest temperature changes are found in the Barentsz and Kara Seas, which have been noted to have very large climate variability and strong local feedbacks (Kim et al., 2014). However, there are important differences between the externally mixed aerosols used in our model and the internally mixed representation in Kim et al. (2014), which might limit the comparison of our results to their findings.

Nonlocal effects through atmospheric teleconnections likely play a role as well. In Fig. 3.4 we present changes in zonal mean precipitation and the meridional overturning mass streamfunction for boreal summer under the LOW and SO_4-LOW scenarios relative to the HIGH scenario. Increases in zonal mean precipitation of up to about 0.07 mm per day are found, with the strongest responses in the tropics and NH mid-latitudes. The precipitation changes are dominated by changes in convective precipitation, especially in the tropics. Also, we see changes in the Hadley cell circulation pattern which is strongly related to precipitation at low latitudes (Yoshimori and Broccoli, 2008). Previous studies (Rotstayn et al., 2014 and references therein) have indicated that higher aerosol forcings in the NH result in the enhancement of the Hadley cell circulation, an increase in precipitation in the SH and a decrease in the NH tropics. Our results show a weakening of the ascending and descending branches of the Hadley cell circulation, especially during the boreal summer (Fig. 3.4, bottom panels).

The simulated increases in precipitation in the tropics can cause anomalies in high-level wind divergence which acts as a Rossby wave source (Hoskins and Karoly, 1981). For instance, Yuan and Martinson (2000), using Pacific precipitation as an indicator of tropical climate variability, showed that there is a link between the Antarctic sea ice extent and changes in Pacific precipitation. It is possible that the increase in convection as highlighted by an increase in convective precipitation in the tropics induced by aerosol reductions might affect the sea ice cover and the climate in the polar regions. The anomalies in geopotential height indicate a Pacific-North American (PNA) response and a North Atlantic Oscillation-like response in the Northern Hemispheric during the winter. (Fig. 3.5, top panels). These teleconnection patterns are known to be driven by anomalous divergence in the Pacific warm pool region. However, the Pacific South American-like response appears less significant in austral winter. While our results indicate that some of the climate responses simulated in the Arctic might be driven by climatic changes in the tropics, it is not clear from our findings if the climate responses seen in the Antarctic are related to the changes in circulation patterns and precipitation at low latitudes, as demonstrated by Yuan and Martinson (2000). While our findings are consistent with previous research (Kloster et al., 2010; Chalmers et al., 2012), additional research is needed to better comprehend the mechanisms responsible for the aerosol induced climatic responses simulated in the Antarctic.

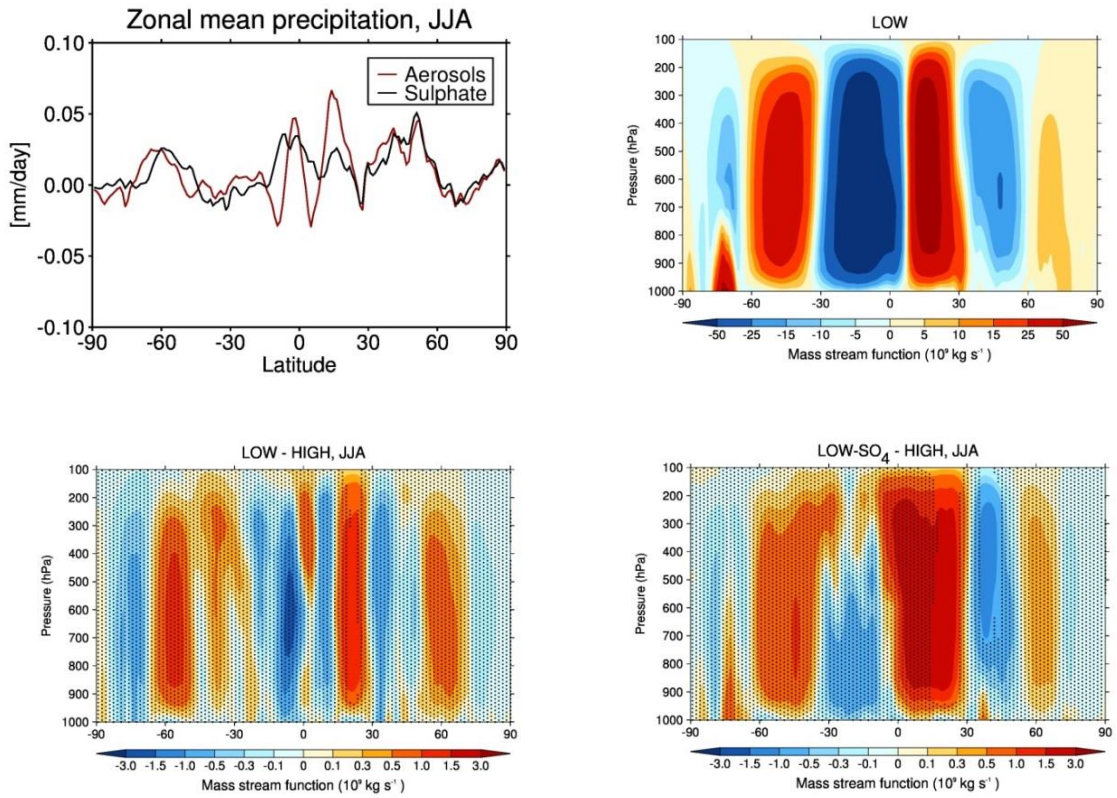

Fig. 3.4. Zonally integrated precipitation (top left panel) and mass stream function (top right panel) in boreal summer (JJA), and the corresponding differences in mass stream function between the LOW and the HIGH scenario (bottom left panel), and the contribution from reductions in SO_4 only (bottom right panel).

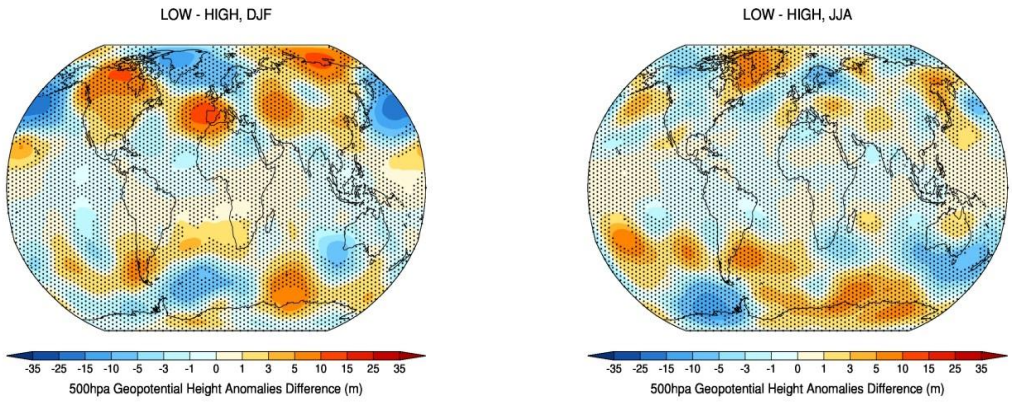

Fig. 3.5. Differences in boreal winter (DJF) and summer (JJA) geopotential height anomaly with respect to the zonal mean, between the LOW and the HIGH scenario.

3.4 Discussion and Conclusions

This study has assessed the impacts of reduction of aerosol and aerosol precursor emissions (as a result of air pollution policies) on climate using the ocean-atmosphere coupled general circulation model EC-Earth (Hazeleger et al., 2012). EC-Earth has a relatively high spatial resolution and well represents atmospheric dynamics. We performed long equilibrium simulations with fixed boundary conditions for 2050. In total, we completed four simulations based on two concentration scenarios, describing a contrasting LOW and HIGH trajectory of aerosol concentrations for an RCP6.0-type scenario shown in chapter 2. These scenarios are used to estimate the combined climate impact of reductions in SO_4, BC, and OC. Also, we compute the climate impact of reducing BC and SO_4 separately. By comparing the different simulations, we are able to assess possible climate impacts of aerosols mitigation and the separate contributions of SO_4 and BC.

The equilibrium climate responses presented in this study take into account the direct and semi-direct radiative effects of the imposed aerosol changes, and the subsequent response of the climate system. Other studies (Kloster et al., 2010; Levy et al., 2013; Rotstayn et al., 2013) have taken into account aerosol effects on cloud albedo and cloud lifetime. This could make the sulphate effects relatively more important. For instance, Levy et al. (2013) found that both temperature and precipitation show much stronger responses when aerosol indirect effects are included. In addition, the use of prescribed monthly mean aerosol fields ignores correlations introduced by synoptic variability, for example related to wet removal and interactions with clouds. This tends to reduce the simulated aerosol direct radiative effects under clear-sky conditions, and in the case of BC above clouds.

In addition, we did not account for changes in nitrate aerosols in our simulations. The impact of nitrate on future climate will become relatively more important as concentrations of other aerosol components will decrease (Bellouin et al., 2011; Shindell et al., 2013). Bellouin et al. (2011) indicated that nitrate aerosols are likely to become the dominant species in Europe and Asia and decelerate the decrease in global mean aerosol forcing. They estimated that increases in nitrate aerosols could make aerosol radiative forcing 2 to 4 times stronger by 2100, depending on the RCP. However, it is important to note that nitrate concentrations are quite difficult to model, especially with global models, because of its semi-volatile character and the strongly localized pattern of ammonia emissions.

The climate impacts have been evaluated in terms of changes in the solar radiation budget, surface temperature and elements of the hydrological cycle. The results show that the reductions in aerosol concentrations will lead to a substantial increase in SSRD under all-sky conditions on regional and continental scales, especially in Asia. This increase is mainly caused by reduced scattering by sulphate. The direct radiative effects of aerosols also have an impact on clouds. This can be seen in the computed TSR over eastern China, where the increase in clear-sky downward surface solar radiation results in more convective clouds, precipitation and a decrease in simulated TSR. Also, it has been shown that the reduced absorption of incoming solar radiation by BC has a semi-direct effect on clouds and climate

(Boucher et al., 2013) by cooling the surrounding atmosphere and reducing the evaporation of cloud droplets.

A decrease in both scattering and absorbing aerosols leads to a change in surface temperature in some parts of the world by up to 1°C. The surface temperature response is qualitatively similar to the effect of declining aerosols on climate reported in the global modelling studies of Rotstayn et al. (2013) and Levy et al. (2013) and the regional modelling study for the US by Mickley et al. (2012). For instance, some of the strongest surface temperature responses are found at high latitudes, where the changes in aerosol concentrations are small. This indicates the sensitivity of this region to changes in the tropics and mid-latitudes. Other studies (Shindell and Faluvegi, 2009; Screen and Simmonds, 2010; Kim et al., 2014) have also shown that the climate response in the Arctic is correlated with mid-latitude forcing, notably outside the summer season, as a result of the large-scale dynamics influencing the climate of this region.

A decrease in sulphate concentrations alone results in surface warming, while decreases in BC concentrations might decrease or increase the local surface temperature depending on the location. It has been demonstrated in previous studies (Shindell and Faluvegi, 2009; Sand et al., 2013; Yang et al., 2014) that increases in BC at mid-latitudes may contribute substantially to surface warming in the Arctic, through increased transport of heat into the Arctic which leads to a decrease in sea ice. However, it is important to note that we do not take into account the direct role of BC in producing surface warming when it is deposited on ice or snow. Previous studies (e.g. Hansen et al., 2005; Bond et al., 2013 and references therein) have shown that BC deposited on snow or ice decreases the reflectivity of these surfaces, resulting in an increase in solar radiation absorption, and may play an important role in Arctic warming. Here, we also find a substantial surface temperature response in the Antarctic. This could be related to increased convection in the Western Pacific, which propagates in a wave train modulating the westerlies over the South Pacific and thereby influencing the variations of Antarctic sea ice over the Pacific and Atlantic sectors (Trenberth et al., 2007). Further research is needed to analyse these nonlocal effects in more detail.

This study clearly shows that there are continental and regional scale climate impacts following the implementation of aerosol mitigation measures. Our analysis indicates that the warming induced by sulphate mitigations dominate under the 6.0 Wm^{-2} scenario considered in this study and are therefore representative of scenarios with similar climate policy assumptions. However, under a scenario with stronger climate policies such as the 2.6 Wm^{-2} scenario similar to RCP2.6 discussed in chapter 2, the climate effects induced by BC reductions through air pollution control measures are expected to become more important as a lot of sulphate precursor emissions are already phased out by climate policies, while BC aerosol emissions could be much less affected by this.

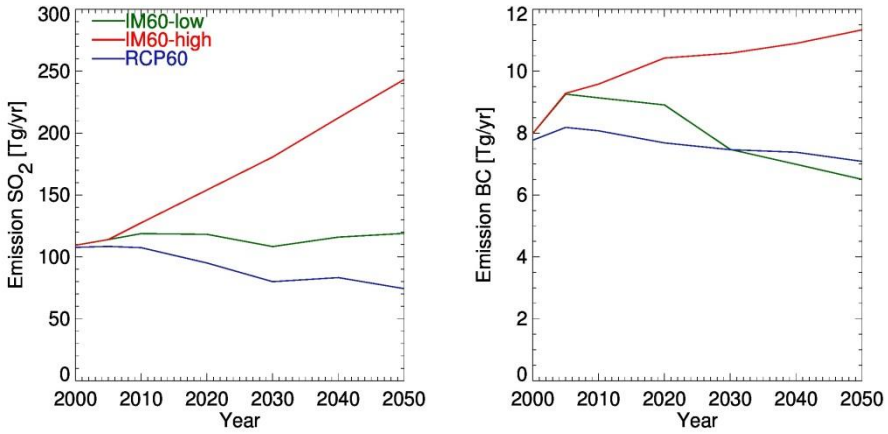

Figure S3.1. Annual total anthropogenic emissions of SO_2 and BC in the IMAGE scenarios and the corresponding RCP. Emissions from biomass burning are included in the totals.

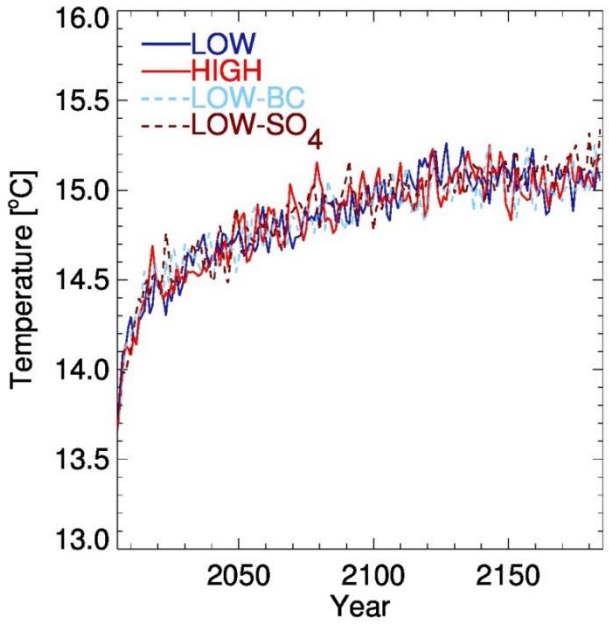

Figure S3.2. Annual global mean 2-meter temperatures for the four simulations for the full 180 years of simulation.

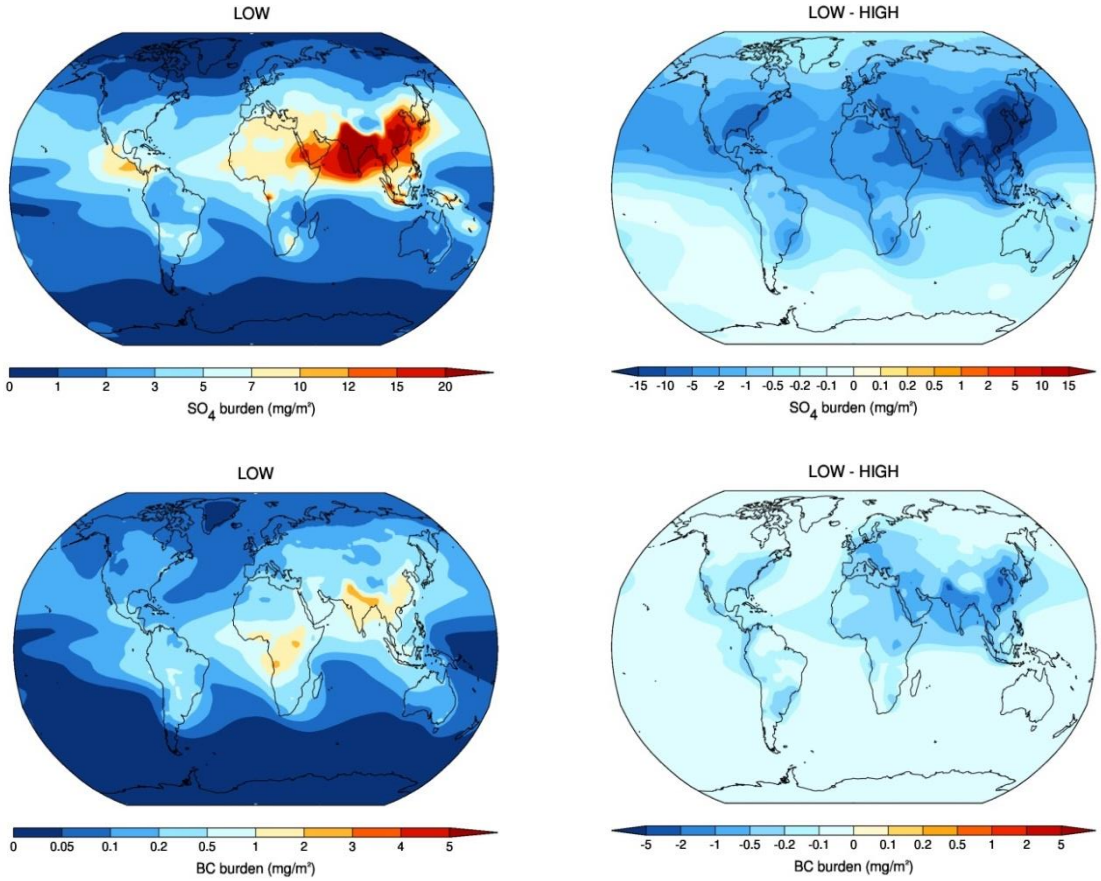

Figure S3.3. Imposed SO_4 and BC burdens for the LOW scenario (left panels) and the corresponding differences between the LOW and the HIGH scenario (right panels).

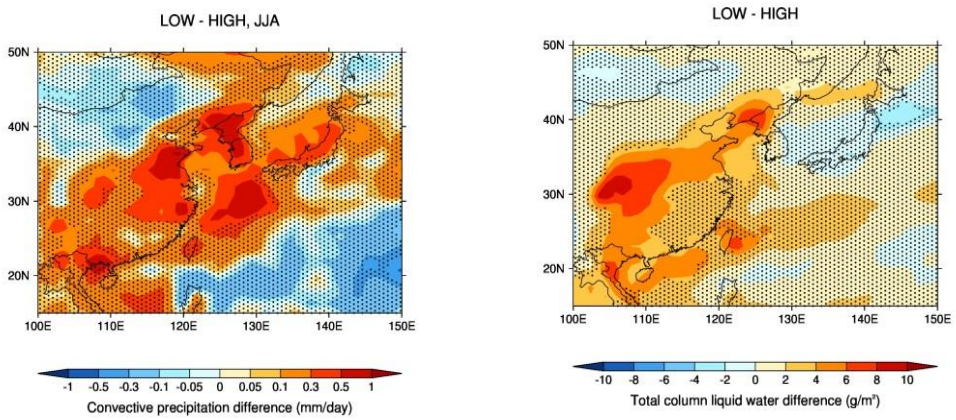

Fig. S3.4. Differences in annual mean total liquid water column (left) and convective precipitation (right) between the LOW and the HIGH scenario under all-sky conditions over East Asia.

CHAPTER 4

Efficacy of aerosol forcings in an RCP6.0-like scenario

Abstract

Anthropogenically induced changes in the concentrations of aerosols strongly alter the transmission of solar radiation through the atmosphere, thereby affecting the climate. In this study we assess the effectiveness of different aerosol forcing agents in causing climate change in 2050 using the global climate model EC-Earth, which includes direct radiative effects of aerosols. We use aerosol and precursor emission scenarios similar to RCP6.0, but with either constant or declining emission factors for air pollutants (developed using the IMAGE integrated assessment model). Our results show a broad range of efficacies for different anthropogenic aerosol components. We find an aerosol efficacy of 286% for the combined aerosols, 112% for sulphate and 41% for black carbon. Our results confirm that large interhemispheric differences in aerosol forcings result in changes in circulation patterns, which gives rise to strong regional feedbacks and climate responses. According to our simulations, changes in aerosol concentrations alter the Hadley cell circulation, which leads to a decrease in precipitation and cloud cover and provides a negative climate feedback at northern mid-latitudes.

4.1 Introduction

Human-induced changes in the concentrations of aerosols have led to a perturbation of the radiation balance of the Earth by affecting the scattering and absorption of solar radiation. Aerosols also affect the climate indirectly by modulating cloud microphysical processes that influence cloud properties such as albedo, lifetime and precipitation efficiency (Boucher et al., 2013). Due to the short residence time of aerosols in the atmosphere, their spatial distributions are inhomogeneous, with higher concentrations mostly located near emission sources. This implies that changes in emissions of aerosols and aerosol precursors can have strong regional climate impacts (e.g. Charlson et al., 1991; 1992; Mitchell et al., 1995; Ramanathan et al., 2001; Hansen et al., 2005; Chen et al., 2007; Shindell and Faluvegi, 2009; Shindell et al., 2012). Understanding the global and regional climate impacts of different forcing agents is therefore important to formulate effective mitigating and adaptation strategies.

The rate and magnitude of climate response in relation to the perturbed energy balance is determined by the radiative forcing, climate feedbacks and the storage of heat by the climate system (IPCC, 2013). Several studies (Ramaswamy et al., 2001; Hansen et al., 2005; Yoshimori and Broccoli, 2008; Boucher et al., 2013; Kummer and Dessler, 2014) have evaluated the radiative forcing changes and concomitant climate responses using different definitions of radiative forcing. The most common approach is to define the radiative forcing perturbation due to a given forcing agent as the net flux change at the tropopause after allowing the stratospheric temperatures to adjust to a new radiative equilibrium (Ramaswamy et al., 2001). The resulting net flux change is called the adjusted radiative forcing (F_a). Models used for the computation of F_a are configured such that temperature is fixed everywhere in the troposphere, while the stratospheric temperature is allowed to adjust to the forcing.

The stratospheric radiative adjustments operate on fast atmospheric timescales while the adjustment in the troposphere might take up to a decade due to the interaction with the ocean, which has a large heat capacity (Boucher et al., 2013). In order to get a better estimate of the long-term climate response to a given forcing agent, Hansen et al. (2005) introduced an alternative measure of climate forcing known as the fixed SST forcing (F_s). F_s is defined as the net flux change at the top of the atmosphere (TOA) after the forcing agent is added to the atmosphere with sea surface temperature (SST) and sea ice (SI) fixed (see section 2.4). Here, the temperature in the entire atmosphere is allowed to change in response to the forcing. Specifically, this approach allows fast feedbacks in the atmosphere (e.g. related to clouds and water vapour) to come into play before the flux is calculated. F_s is therefore more directly related to the long-term climate response than F_a (Hansen et al., 2005). The long-term climate response to the forcing is computed with a fully coupled atmosphere-ocean-land-sea ice model which allow all feedbacks to operate and temperature at the surface, in the ocean and the atmosphere to adjust to the forcing perturbation.

A number of studies (Hansen et., 2005; Yoshimori and Broccoli, 2008; Shindell and Faluvegi, 2009; Shindell et al., 2012; Kummer and Dessler, 2014) have shown that global mean forcings of the same magnitude, but with different spatial distributions, may give rise to different climate responses. In order to account for this effect, Hansen et al., (2005) introduced the efficacy concept. Efficacy refers to the global mean temperature response per unit forcing of a given forcing agent relative to the response produced by a CO_2 concentration perturbation to the same unperturbed state. So far, both F_a and F_s definitions of radiative forcing have been used to calculate the adjusted efficacy (E_a) and fixed SST efficacy (E_s), respectively, for different forcing agents. Hansen et al. (2005) showed that the estimated efficacies for both F_a and F_s can be significantly different from unity indicating that different forcing agents can be more or less effective in causing climate change compared to CO_2. For example, because most anthropogenic aerosol and precursor emissions occur in the Northern Hemisphere (NH), this leads to strong interhemispheric differences in aerosol forcings, while the forcing due to the increase in CO_2 is more uniformly distributed. Several studies (Yoshimori and Broccoli, 2008; Ming and Ramaswamy, 2009; Ocko et al., 2014) indicated that this inhomogeneous hemispheric distribution of aerosol forcings results in surface cooling in the NH, a southward shift of the Inter Tropical Convergence Zone (ITCZ), a disruption of circulation patterns, an increase of precipitation in the Southern Hemisphere (SH) and a decrease in the NH tropics. Also, Hansen et al. (2005) revealed that the efficacy of black carbon (BC) depends on the vertical distribution. They showed that the efficacy of BC decreases rapidly with altitude, as heating by BC reduces cloud cover (semi-direct effect of BC) in the layer where it is situated and inhibits convection from the layer below.

In general, regional variations in radiative forcings and feedbacks can lead to efficacies that deviate from unity. Hansen et al. (2005) showed that the efficacy of aerosols is closer to one when the forcing is defined by F_s rather than F_a. By allowing fast feedbacks in the atmosphere to operate before the radiative flux perturbation is calculated, F_s provides a better estimate of the expected climate response than F_a.

In chapter 2, we simulated aerosol concentration changes for different air pollution and climate policy regimes using a set of future emission scenarios similar to the Representative Concentration Pathways (RCPs; van Vuuren et al., 2011a). Based on a simple calculation of direct radiative forcing, it was estimated that changes in aerosol concentrations in 2050 due to air pollution control can lead to a global mean F_a of 0.22 Wm^{-2} under a scenario with weak climate policy similar to the RCP6.0. In addition, this study discussed how the net forcing in these scenarios is a result of often much larger forcings for individual components with opposite signs: while the radiative cooling by sulphate is the dominant effect, its impact is partly compensated by the warming effect of BC. Using the same RCP-like scenarios in the coupled atmosphere-ocean general circulation model EC-Earth, chapter 3 showed that the equilibrium climate response in 2050 is significantly different for these different air pollution regimes. For instance, it was estimated that the mitigation of aerosols could increase annual mean temperatures in 2050 by up to 0.5°C in Asia and 1°C during winter at high latitudes.

The mitigation of aerosols also resulted in substantial changes in the hydrological cycle and precipitation, especially in the tropics.

A number of studies (Hansen et al., 2005; Yoshimori and Broccoli 2008; Kummer and Dessler, 2014) have calculated the efficacy of different forcing agents. However, the number of climate models for which such an analysis has been carried out is limited and model spread is significant. More so, the physical mechanisms leading to the global and regional responses need further study. Here we determine efficacies of different aerosol components (sulphate, black carbon and organic aerosol combined, as well as sulphate and black carbon individually) in the EC-Earth model using the RCP-like scenarios mentioned above. We use the fixed SST approach of Hansen et al. (2005) to compute changes in forcing at the top of the atmosphere. The corresponding long-term climate response is obtained from the fully coupled atmosphere-ocean simulations shown in chapter 3.

This chapter is structured as follows: Section 4.2 describes the model and methodology. In Section 4.3 we present results on efficacies and climate response. A discussion and conclusions of our results are given in Section 4.4.

4.2 Methodology

4.2.1 Model description

The model used in this study is the EC-Earth model version 2.3 which was also used in the Coupled Model Intercomparison Project (CMIP5, Taylor et al., 2012). The atmospheric part is based on the Integrated Forecasting System (IFS) cycle 31r1 with some modification as described in Hazeleger et al. (2012). It runs at a horizontal spectral resolution of T159 (triangular truncation at wavenumber 159) and a vertical resolution of 62 layers. IFS can be configured to run with fixed SST and sea ice, or coupled to the Nucleus for European Modelling of the Ocean (NEMO) version 2, with a horizontal resolution of about 1 degree and 42 vertical layers (Madec, 2008). Sea ice is modelled inside NEMO using the Louvain-la-Neuve sea ice model (LIM) version 2. The ocean/sea ice and the atmosphere/land components communicate via the OASIS3 coupler (Valcke, 2006). It is important to note that indirect aerosol effects related to interactions between aerosols and clouds are not accounted for in this version of EC-Earth.

4.2.2 Emissions scenarios

The emissions and land use scenarios used in this study were developed using the IMAGE integrated assessment model (Bouwman et al., 2006), as described in chapter 2. Here, we present results of two selected scenarios that explore high and low aerosol forcing as a result of different levels of air pollution mitigation. These scenarios, called ‘LOW’ and ‘HIGH’, have different emission factors (emissions per unit activity per sector and fuel type) for air pollutants, but the same emissions of long-lived greenhouse gases. They resemble the original RCP6.0 (Masui et al., 2011), thus leading to a radiative forcing of around 6.0 Wm^{-2} at the end of the century. As a set, the two scenarios therefore can be used to explore the impact of air pollution emissions for a wider range than included in the RCPs. A detailed description of the

underlying assumptions of the LOW and HIGH scenarios and comparison with the RCPs can be found in chapters 2 and 3.

4.2.3 Experimental setup

The efficacy of aerosols in causing climate change is investigated using EC-Earth time slice simulations for 2050. Here, we analyse results from both coupled and uncoupled simulations. Results from the coupled runs were presented in chapter 3. For the 2050 time slice runs, the concentrations of long-lived greenhouse gases, ozone, volcanic aerosols, and the solar cycle were fixed to their 2050 levels irrespective of the model year. An overview of the different experiments performed is shown in Table 4.1 and additional information can be found in chapter 3. For the uncoupled runs, we used similar settings, except for the fact that we used prescribed SSTs and sea-ice cover for 2005 from a historical CMIP5 simulation with the same model version. The initial conditions were set to a 2005 state from a similar CMIP5 simulation of the model. The uncoupled simulations were run for 60 years, while all coupled simulations were run for 180 years to allow the model to adjust to the imposed forcings. The output of the coupled and uncoupled simulations were analysed for the last 80 and 50 years, respectively. We used the student's *t*-test at a significance level of 0.05 to evaluate the statistical significance of the differences in climate responses between our scenarios. The aerosol concentration fields used in our simulations are based on offline simulations with the atmospheric chemistry and transport model TM5 (Huijnen et al., 2010; van Noije et al., 2014). Detailed information about the use of the TM5 aerosol concentration fields in EC-Earth can be found in chapter 3.

Simulation	**BC concentrations**	**OC concentrations**	**SO_4 concentrations**	**SST and SI Conditions**
LOW uncoupled	Low	Low	Low	fixed 2005
HIGH uncoupled	High	High	High	fixed 2005
LOW-BC uncoupled	Low	High	High	fixed 2005
LOW-SO_4 uncoupled	High	High	Low	fixed 2005
LOW coupled	Low	Low	Low	Changing
HIGH coupled	High	High	High	Changing
LOW-BC coupled	Low	High	High	Changing
LOW-SO_4 coupled	High	High	Low	Changing

Table 4.1. Overview of the uncoupled and coupled EC-Earth simulations performed in this study. where SST and SI are the sea surface temperature and sea ice cover boundary conditions.

4.2.4 Efficacy of climate forcing calculations

In this study we use the F_s measure of climate forcing (Hansen et al., 2005) to calculate the efficacy of different aerosol forcing agents. Here, F_s is given as:

$$Fs = Fo + \delta To / \lambda, \quad (4.1)$$

where F_o and δT_o are the global mean flux change at the TOA and the global mean change in surface air temperature (usually taken at 2 meter), in response to the forcing perturbation with SST and sea ice held constant, and λ the model equilibrium climate sensitivity to CO_2. The efficacy E_s is then defined as the global mean temperature response per unit forcing relative to the response per unit forcing of CO_2 for the same unperturbed climate state:

$$Es = \frac{\Delta Ts}{\lambda \times Fs}, \quad (4.2)$$

where ΔT_s is the global mean equilibrium climate response from the coupled simulations. In our calculations, we use a climate sensitivity λ=1.1 K/(W m^{-2}) for a 4xCO_2 perturbation in EC-Earth (Lacagnina et al., 2014). The difference in climate sensitivity between 4xCO_2 and 2xCO_2 is expected to be small, as CO_2 has a long residence time in the atmosphere and is very homogeneously distributed (see Hansen et al., 2005).

4.3 Results

4.3.1 Aerosols effects in atmosphere-only simulations

Fig. 4.1 shows the differences in the clear-sky contribution to the annual mean radiative imbalance at the TOA in 2050 as a result of perturbations in aerosol concentrations. The effect of sulphate, black carbon and organic aerosol combined is calculated as the difference between the HIGH and LOW air pollution scenarios (left) and the contribution from SO_4 aerosols only as the difference between the HIGH and the SO_4-LOW scenarios (right). The results indicate that the aerosol induced TOA radiative perturbation is dominated by sulphate notably in the NH subtropics and mid-latitudes. The largest clear-sky contribution to the radiative forcing imbalance, with negative values down to -4.3 Wm^{-2}, are found in parts of China and India where aerosol concentration are substantially higher in the HIGH scenario relative to the LOW and SO_4-LOW. We also find significant contributions in some parts of the United States, Mexico, Europe, South America and Africa. The higher aerosol forcing in the NH is likely to give rise to different feedbacks and climate responses (discussed below) compared to CO_2, which is more uniformly distributed.

Globally, we find an increase in the top net solar radiation for the combined aerosols, and for SO_4 and BC only under all-sky conditions (Table 4.2). For the combined aerosol and SO_4-only perturbations, the clear-sky contribution to this flux is negative (-0.34 and -0.35 Wm^{-2}, respectively), and the increase in the all-sky flux is due to the contribution from the cloudy part of the sky. In Fig. 4.2 we present zonally averaged changes in TOA net shortwave (SW) solar (left panels) and longwave (LW) thermal (right panels) radiation due to aerosol perturbations under all-sky conditions together with the contributions from the clear and cloudy parts of the sky. Clearly, the aerosol perturbation to the incoming solar radiation is

highest at NH mid-latitudes. We find a reduction in the clear-sky contribution to the zonal mean TOA net solar radiation reaching up to 1 Wm^{-2} mostly due to the scattering effect of sulphate (Fig. 4.2 left top and bottom panels). The opposite picture emerges under all-sky conditions where we estimate an increase in zonally averaged TOA net solar radiation of maximally 0.6 Wm^{-2}, notably between 30° N to 60° N. Further analysis shows an even higher increase in the cloudy-sky contribution (up to 1.2 Wm^{-2}) under HIGH relative to LOW and SO_4-LOW. The increase in TOA solar radiation is partially compensated by thermal cooling at the same latitudes (Fig. 4.2, right panels and Table 4.2).

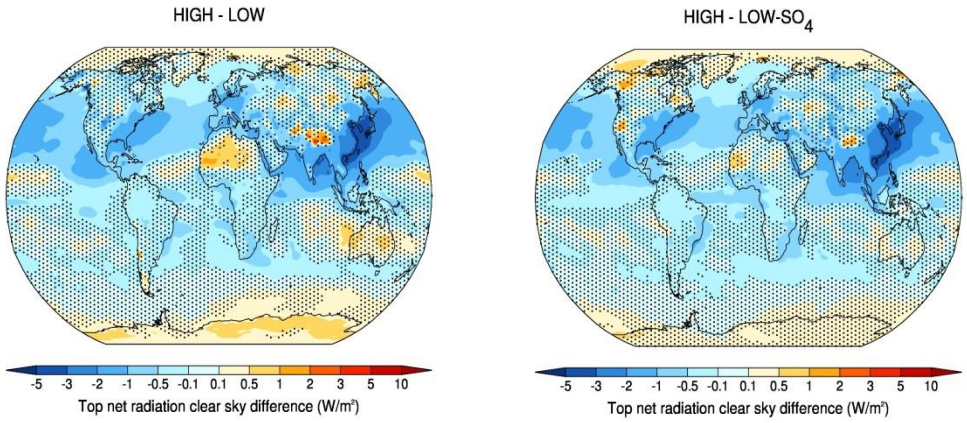

Fig. 4.1. Changes in the clear-sky contribution to the annual mean TOA net radiative flux (measured positive in the downward direction) in response to aerosol perturbations in 2050, under the HIGH compared to the LOW and LOW-SO_4 respectively, in the atmosphere-only simulations. The stippled areas show regions where the differences are not significant at the 5% level.

	TSR	**TSRC**	**TTR**	**TTRC**	**Fo**	**FoC**
Aerosols	0.066	-0.339	-0.085	-0.017	-0.020	-0.357
BC	0.013	0.008	0.024	0.031	0.032	0.039
SO_4	0.026	-0.353	-0.076	-0.025	-0.051	-0.378

Table 4.2. Global annual mean changes in TOA net solar radiative flux (TSR and TSRC), TOA net thermal radiative flux (TTR and TTRC) and TOA total net radiative flux (Fo and FoC) in response to aerosol perturbations in 2050, for the combined aerosols (HIGH-LOW), BC (HIGH- LOW-BC) and SO_4 (HIGH- LOW-SO_4), in the atmosphere-only simulations. Here TSR, TTR and Fo denote all-sky fluxes and TRSC, TTRC and FoC are the corresponding contributions from the clear parts of the sky. All fluxes (W/m^2) are measured as positive in the downward direction.

The zonal mean radiative effects of BC changes at the TOA are small compared to those of sulphate and the combined aerosols (see Fig. 4.2, middle panels). This can partly be explained by the fact that under clear-sky conditions the absorption of solar radiation by BC does not have a substantial impact at the TOA over dark ocean surfaces. The effect of BC at the TOA is stronger when the absorption takes place over bright reflective surfaces or cloud layers. Since BC changes the distribution of radiation within the atmosphere, the climate impact of BC is not necessarily well reflected in the TOA forcing (Bond et al., 2013). Changes in the distribution of clouds due to the semi-direct effect of BC as well as circulation

changes may explain part of the simulated net TOA flux change as a function of latitude. On a global scale, the cooling caused by sulphate increases is only partially compensated by the warming caused by BC increases (see Table 4.3).

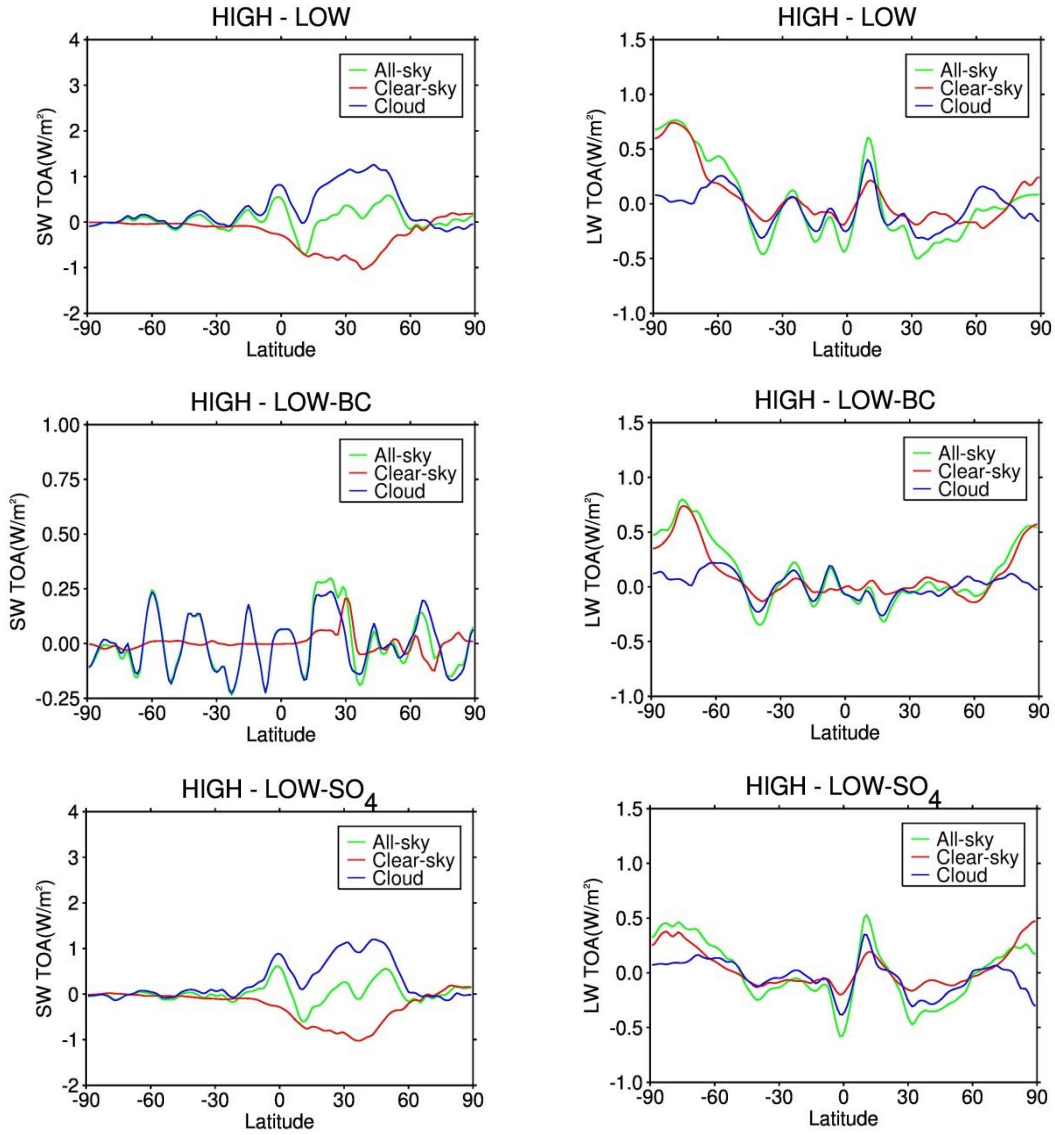

Fig. 4.2. Changes in annual mean TOA net shortwave (SW) solar (left panels) and longwave (LW) thermal (right panels) radiative fluxes (measured positive in the downward direction) in response to aerosol perturbations in 2050, for the HIGH scenario compared to the LOW, LOW-BC and LOW-SO_4 respectively, in the atmosphere-only simulations. Results for all-sky fluxes are presented together with the corresponding contributions from the clear and cloudy parts of the sky.

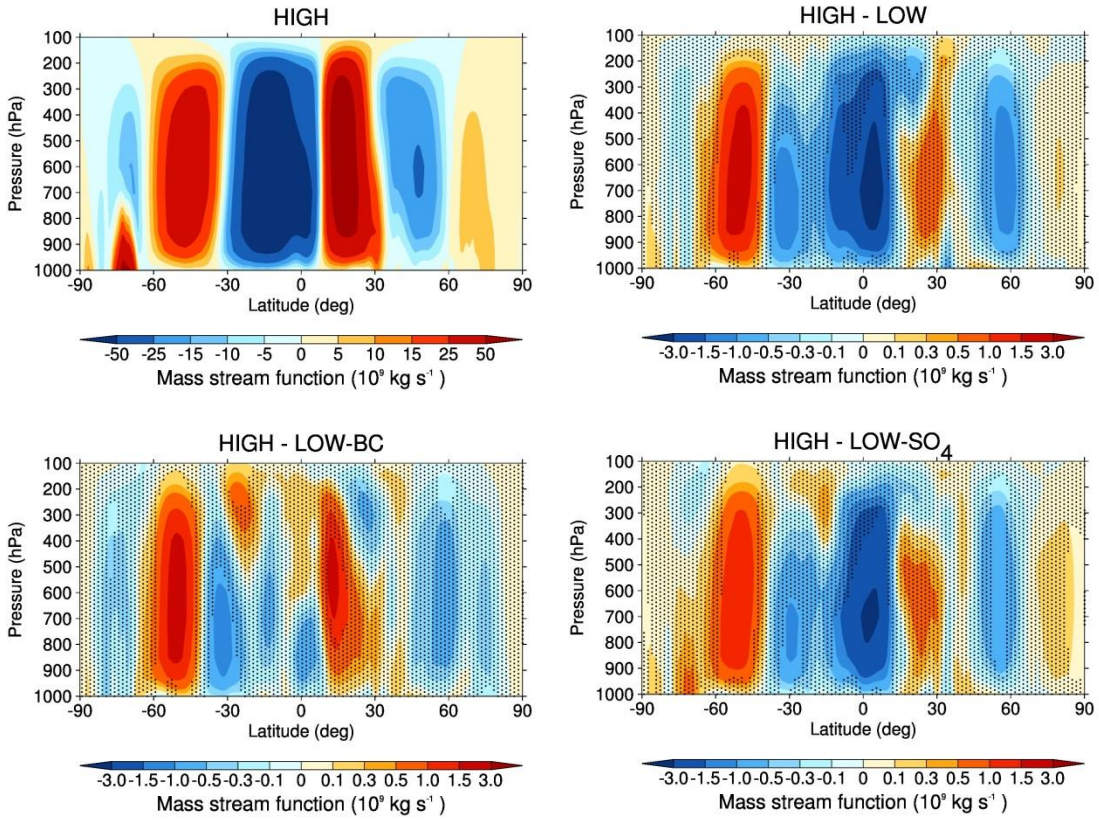

Fig. 4.3. Zonally integrated annual mean mass stream function under the HIGH scenario in 2050 (top panel) and changes in response to perturbations under the HIGH compared to the LOW (top right panel), LOW-SO_4 (bottom right panel) and LOW-SO_4 (bottom left panel) respectively, in the atmosphere-only simulations. Negative values indicate counter clockwise and positive values clockwise circulations.

	δTo (°C)	**Fs (W/m^2)**	**ΔTs (°C)**	**Es**	**Es***
Aerosols	0.014	-0.007	-0.023	2.86	1.10
BC	0.002	0.034	0.015	0.41	0.81
SO_4	0.015	-0.037	-0.046	1.12	1.04

Table 4.3. Global annual mean radiative forcings and efficacies for the combined aerosols (HIGH-LOW), BC (HIGH- LOW-BC) and SO_4 (HIGH- LOW-SO_4). Here δT_o is the global annual mean surface air temperature change after the forcing is applied with SSTs and SI held constant, ΔT_s global surface air temperature response to the climate forcing agent, F_s is the climate forcing defined in Sect. 2.4, and E_s and E_S*(obtained from Hansen et al., 2005) are the corresponding efficacies of different forcing agents.

Clearly, the dominant contributor to the SW changes at the TOA is the cloud response which is likely related to changes in the dynamics. In a broader context, the aerosol induced cloud response has been associated with changes in circulation patterns in the tropics (Boucher et al., 2013). In Fig. 4.3 we present the global annual mean meridional overturning mass streamfunction under the HIGH scenario, HIGH with respect to the LOW, BC-LOW and SO_4-LOW for our fixed SST runs. The strong interhemispheric differences in aerosol forcings result in the strengthening of the ascending branch of the Hadley cell circulation in

the NH for both the combined aerosol and sulphate-only perturbations. In the case of BC, although the interhemispheric differences in BC forcings are small (see Fig. 4.2, middle panels), our results indicate that the descending branch in the NH also becomes stronger (Fig. 4.3 bottom left). As mentioned above, BC situated above a bright reflective surface also absorbs solar radiation reflected from that surface, therefore heating the atmosphere and reducing the amount of sunlight that reaches the surface which can alter the hydrological cycle through changes in convection and circulation patterns. The stronger Hadley circulation that we find is consistent with the changes in zonal mean specific humidity (Fig. 4.4, top panels) and precipitation (Fig. 4.4, middle panels) in the NH equatorial region. We even find an indirect response of the Ferrell cell associated to the changes in the Hadley cell circulation. The negative aerosol radiative forcings in the NH induce changes in atmospheric circulation, which gives rise to decreases in cloud cover, notably between 30° N and 60° N (Fig. 4.4 bottom left). This results in the reduction in the solar radiation that is reflected back to space and an increase in outgoing thermal radiation.

4.3.2 Climate response in coupled simulations

Results of the aerosol-induced long-term climate response based on the coupled EC-Earth simulations, have already been presented in chapter 3. Here, we discuss additional results with respect to the fixed SST runs and previous studies. Fig. 4.5 shows the zonal mean changes in TOA net solar radiation induced by the aerosol perturbations under all-sky conditions, together with the contributions from the clear and cloudy parts of the sky. The perturbations in SW radiative fluxes in the coupled runs are similar to those presented above for fixed SST. The signs of the global mean change in the TOA net radiative flux are consistent with the signs of the long-term global mean surface air temperature response (see Table 4.3). For instance, sulphate aerosol causes a reduction in the global mean TOA net radiative flux of -0.037 Wm^{-2}, which results in a global cooling of -0.046 °C. However, in our fixed SST simulations we find a small global annual mean warming (up to 0.015 °C) even for sulphate (see Table 4.3) mainly as a result of the suppression of the ocean response to aerosol induced changes in surface forcing and the subsequent atmospheric response.

The global mean equilibrium air temperature response is determined not just by the magnitude of the forcing but also by climate feedbacks. Our results show that a reduction of clouds at northern mid-latitudes dominates the global mean all-sky TOA net radiation. Water vapour and lapse rate feedbacks, which are also involved in moist atmospheric processes associated with clouds, are likely to be important as well. It is clear that the aerosol induced negative forcing notably in the NH tropics decreases the specific humidity (Fig. 4.6) and evaporation. Our results are consistent with the results of Ocko et al. (2014) who also found aerosol induced decreases in specific humidity notably in the NH tropics. We also find a slight warming of the free troposphere relative to the surface (Fig. 4.7). These vertical variations of the temperature response are associated with a positive lapse-rate feedback, since the warming of the free troposphere relative to the surface leads to enhanced longwave radiative cooling (e.g. Lacagnina et al., 2014) in response to a globally net cooling forcing perturbation. Even though the radiative perturbations are dominated by sulphate, our results

show that the temperature in the free troposphere responds differently to perturbations in the combined aerosols than to changes inSO_4 only. These results suggest an enhancement in climate response through non-linear interactions between scattering and absorbing aerosols (see Kim et al., 2013).

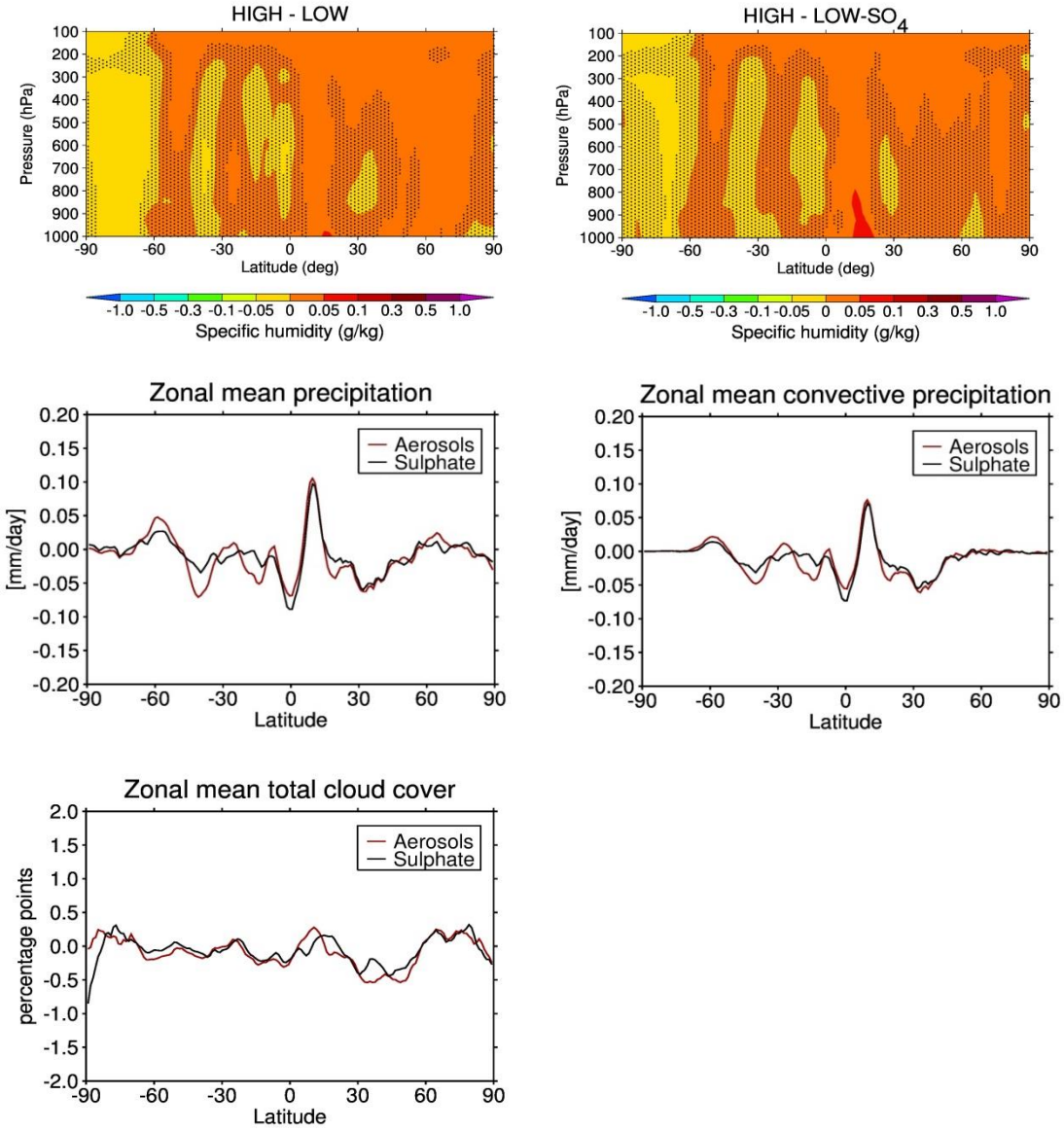

Fig. 4.4. Changes in zonal annual mean specific humidity (top panels), total precipitation (middle left panel), convective precipitation (middle right panel) and total cloud cover (bottom left panel) in response to aerosol perturbations in 2050, for the HIGH compared to the LOW and LOW-SO_4 respectively, in the atmosphere-only simulations.

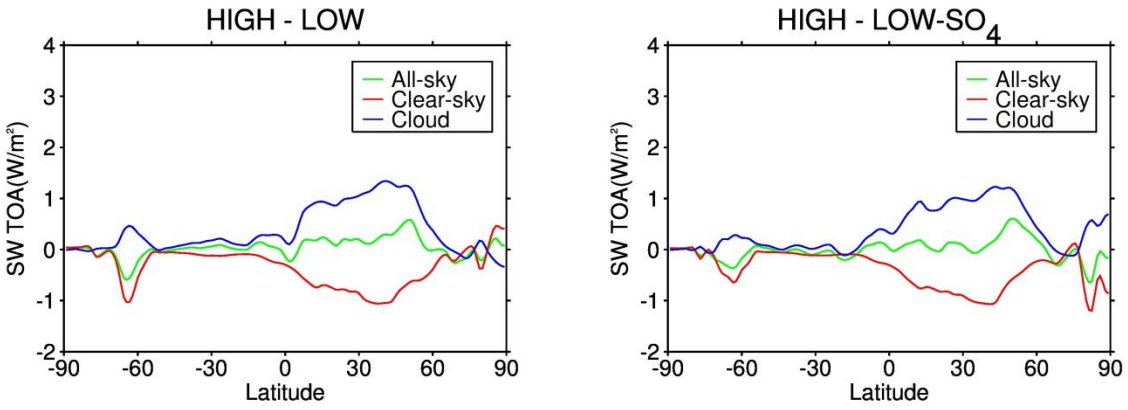

Fig. 4.5. Changes in annual mean top net solar radiation (left panel) in response to aerosol perturbations in 2050, for the HIGH compared to the LOW and LOW-SO_4 respectively, in the coupled EC-Earth runs. Results for all-sky fluxes are presented together with the corresponding contributions from the clear and cloudy parts of the sky.

Like in the fixed SST runs, we also found changes in the Hadley cell circulation, especially during the NH boreal summer (see Fig. 3.5 in chapter 3). The large aerosol concentrations in the NH hemisphere lead to a response of atmospheric circulation and associated precipitation patterns. As demonstrated in previous studies, the ITCZ shifts southward (Ming and Ramaswamy, 2009; Ocko et al., 2014) but not in all studies (Yoshimori and Broccoli, 2008) resulting in increases precipitation in the SH and decreases in the NH tropics. Here, we find that the maximum increases in precipitation are smaller in the coupled simulations shown in chapter 3 compared to the fixed SST runs and occur mostly around the equator. This reduces cloud cover notably around latitude 30° N (Fig. 4.6), which is qualitatively similar to what was reported in previous studies (Yoshimori and Broccoli, 2008; Ming and Ramaswamy, 2009; Ocko et al., 2014). Most of the changes in precipitation occur primarily in southeast and south Asia (see chapter 3).

4.3.3 Climate forcing efficacies of aerosols

Table 4.3 shows the global efficacies (E_s) for the combined aerosols and for SO_4 and BC only, using the F_s approach outlined above. Our computed efficacies for SO_4 and the combined aerosols especially, are greater than unity. The radiative forcing perturbation for BC is not indicative of the climate response as the estimated global efficacy is much smaller than unity. This implies that the combined aerosols and SO_4 are more effective and BC less efficient in causing climate change relative to CO_2. Furthermore, our calculated efficacies are higher (combined aerosols and SO_4) and lower (BC) than the values obtained by Hansen et al. (2005). Also, we find an F_s of about -0.007 Wm^{-2} for the combined aerosols, which is much smaller than the estimate of -0.22 Wm^{-2} for F_a from chapter 2, obtained using a simple calculation following the MAGICC6 approach. In that study, a present-day radiative forcing field from Hansen et al. (2005) was used and a simple linear scaling was applied based on the anthropogenic contributions to the optical depths of different aerosol components as simulated by the TM5 model (see chapter 2). Apparently there are large model differences

between EC-Earth and the GISS model used in Hansen et al. (2005). The larger sensitivity in EC-Earth is likely due to differences in climate feedbacks between the models.

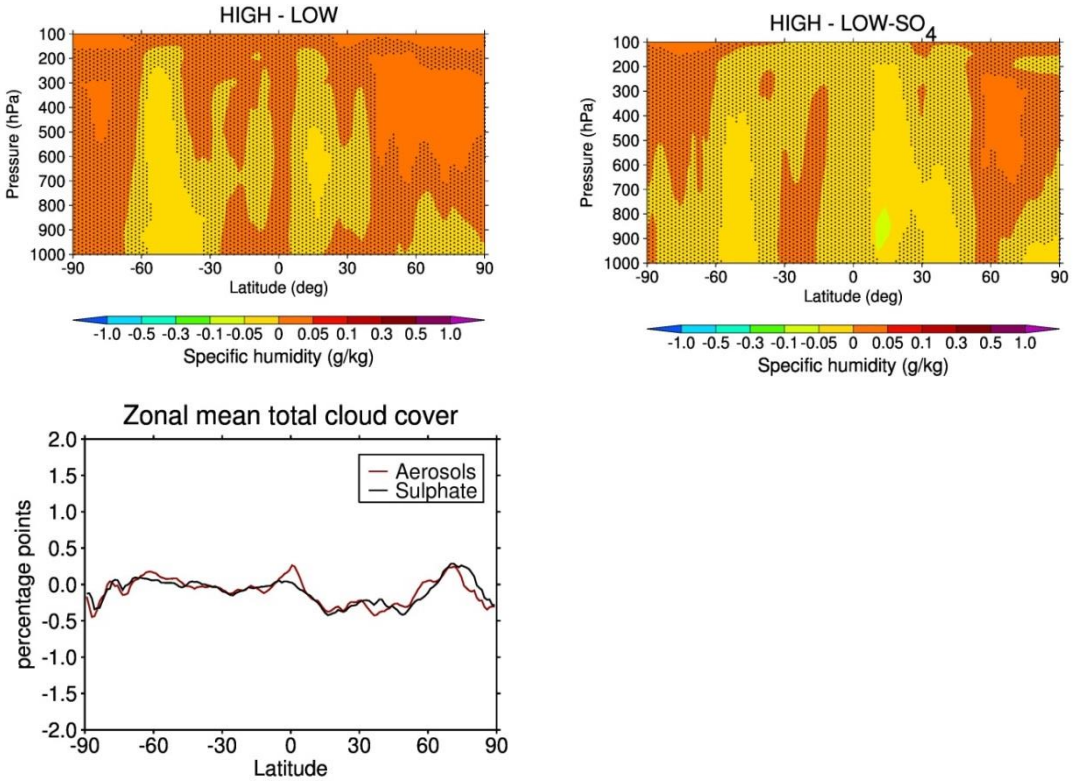

Fig. 4.6. Changes in zonal annual mean specific humidity (top panels) and total cloud cover (bottom left panel) in response to aerosol perturbations in 2050, for the HIGH compared to the LOW and LOW-SO_4, in the coupled EC-Earth runs.

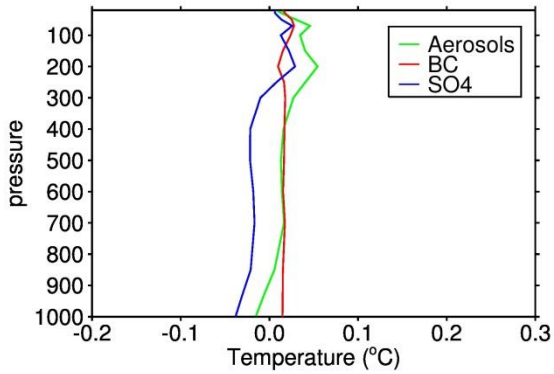

Fig. 4.7. Changes in global annual mean temperature in response to aerosol perturbations in 2050, for the HIGH compared to the LOW, LOW-BC and LOW-SO_4, in the coupled EC-Earth runs.

4.4 Discussion and Conclusions

Climate efficacy expresses the effectiveness of a forcing agent in causing a surface air temperature response on a global scale relative to CO_2. Since different forcing agents produce different spatial forcing patterns, they trigger different feedbacks in the climate system and thus produce a different response in global mean temperature at the same global forcing strength. As a result, especially for short-lived forcing agents, efficacies can differ substantially from unity. In previous studies, the efficacies of different aerosol components were computed based on a limited number of models where results show a significant spread. Here, we evaluate the efficacies of different aerosol components using different RCP-like scenarios in the climate model EC-Earth (Hazeleger et al., 2012). We performed both prescribed SST and fully coupled atmosphere-ocean simulations with fixed boundary conditions in order to characterize radiative forcings and the long-term climate response associated with aerosol perturbations in 2050. By comparing the different fixed SST simulations, we are able to estimate the net radiative forcing change at the TOA due to perturbations in anthropogenic aerosols (in our case SO_4, BC and organic aerosols) combined, as well as the separate contributions of SO_4 and BC. The associated equilibrium climate responses are computed by comparing the different coupled EC-Earth runs. It is important to note only the direct radiative effects of the aerosols are included in our model simulations.

We find that the TOA radiative forcing induced by the aerosol perturbations is dominated by sulphate, especially in the NH subtropics and mid-latitudes. The largest forcings are seen in parts of India and China, where aerosol concentrations are projected to increase the most. The computed global mean forced SST radiative forcings F_s due to changes in aerosol concentrations is much smaller than the estimates for the corresponding adjusted forcing F_a calculated in chapter 2, which were obtained by scaling of present-day adjusted forcing fields from Hansen et al. (2005). This may be related to the fact that changes in aerosol trigger much stronger cloud responses in EC-Earth than in the GISS model used in Hansen et al. (2005).

In our simulations, we find that a forcing induced by a perturbation in the different anthropogenic aerosol components together is much more effective in producing a global mean temperature change than CO_2, resulting in an efficacy of 286%. For BC and SO_4 , on the other hand, we find an efficacy smaller and greater than unity respectively, which is consistent with previous studies (e.g. Hansen et al., 2005; Yoshimori and Broccoli, 2008). The low efficacy computed for BC (41%) is likely related to a large negative cloud response which depends on the vertical distribution of black carbon (Hansen et al., 2005; Yoshimori and Broccoli, 2008). The slightly higher efficacy of sulphate (112%) is probably linked to the interhemispheric differences in sulphate forcings, which give rise to different climate responses compared to CO_2 which is more uniformly distributed. As indicated by Hansen et al. (2005), a high efficacy value for the combined aerosols is to be expected as the combination of positive (BC) and negative (SO_4) forcings can give rise to a small net forcing (in this case -0.007 Wm^{-2}) and the resulting efficacy can take on a large range of values. In

addition, the calculated efficacies are higher (aerosols and SO_4) and lower (BC) than the those of Hansen et al. (2005) and Yoshimori and Broccoli (2008). One plausible explanation for these differences is the variation in the strength of different feedbacks which influence the climate responses to the forcing and therefore the efficacy. Moreover, the aerosol perturbations applied in our simulations are different from those applied in other studies.

Although the spatial distribution of sulphate dominates the forcing perturbation and climate response that we find in our RCP6.0-like scenarios, under the RCP2.6-like scenarios (e.g. see chapter 2) with stronger climate policies, the vertical distribution of BC and associated feedbacks might become more important as BC emissions could be much less affected by climate policies compared to sulphate, which is being significantly reduced by climate policies.

In our simulations, we find strong circulation changes in response to the applied aerosol perturbations, especially in the tropics. These circulation changes are consistent with the computed zonal mean changes in specific humidity and precipitation, especially in the NH. The aerosol-induced changes in circulation lead to a decrease in cloud cover at northern mid-latitudes, which provides a negative climate feedback.

This study illustrates that the response of the climate system to inhomogeneous aerosol forcings is determined by the fact that these forcings are concentrated in the NH, where they evoke different feedbacks that cause the global mean surface temperature response to be much different from that induced by a more uniformly distributed CO_2 forcing of the same overall magnitude. This results in climate efficacies that are less (BC) or greater (SO_4 and anthropogenic aerosols combined) than unity. Further study will be needed to better quantify the strength of the different climate feedbacks induced by spatially heterogeneous aerosol forcings.

Acknowledgements
The authors would like to thank Frank Selten for helping with the setting up of the experiments.

CHAPTER 5

Global impacts of surface ozone changes on crop yields and land use

Abstract

Exposure to surface ozone has detrimental impacts on vegetation and crop yields. In this study, we estimate ozone impacts on crop production and subsequent impacts on land use in the 2005-2050 period using results of the TM5 atmospheric chemistry and IMAGE integrated assessment model. For the crops represented in IMAGE, we compute relative yield losses based on published exposure-response functions. We examine scenarios with either constant or declining emission factors in a weak climate policy future (radiative forcing target of 6.0 W/m^2 at the end of the century), as well as co-benefits of stringent climate policy (targeted at 2.6 W/m^2). Without a large decrease in air pollutant emissions, higher ozone concentrations could lead to an increase in crop damage of up to 20% locally in 2050 compared to the situation in which the changes in ozone are not accounted for. This may lead to a 2.5% global increase in crop area, and a regional increase of 8.9% in Asia. Implementation of air pollution policies could limit crop yield losses due to ozone to maximally 10% in 2050 in the most affected regions. Similar effects can be obtained as a result of co-benefits from climate policy (reducing ozone precursor emissions). We also evaluated the impact of the corresponding land-use changes on the carbon cycle. Under the worst-case scenario analysed in this study, future ozone increases are estimated to increase the cumulative net CO_2 emissions between 2005 and 2050 by about 3.7 Pg C, which corresponds to about 10% of baseline land use emissions over the same period.

This chapter has been published as: Chuwah, C.D., van Noije, T., van Vuuren, D.P., Stehfest, E., Hazeleger, W., 2015. Global impacts of surface ozone changes on crop yields and land use, Atmospheric Environment 106, 11-23.

5.1 Introduction

Anthropogenic emissions of ozone precursors have increased surface ozone concentrations in many areas of the world (Royal Society, 2008). It has been demonstrated in field experiments conducted mostly in Europe and North America that exposure to elevated ozone concentrations has detrimental effects on plants (e.g., Heck et al., 1983; Fuhrer et al., 1997; Pleijel et al., 2002; Karlsson et al., 2007; González-Fernández et al., 2008; De Bock et al., 2011). This ozone impact on plants has different implications: Firstly, it affects the productivity of crops and thus the global production of food. Secondly, it also negatively impacts natural vegetation. This may reduce biodiversity and contribute to global warming by reducing the CO_2 uptake by plants (Sitch et al., 2007). Finally, ozone impacts on crops may also necessitate the need for additional agricultural cropland to meet food demand thus resulting in land use changes.

Future changes in surface ozone are expected to vary regionally depending on the evolution of ozone precursors emissions. It is expected that the implementation of stringent air pollution policies will lead to a reduction in episodic peak ozone concentrations in Europe and North America (Ellingsen et al., 2008; Royal Society, 2008). At the same time, surface ozone concentrations are projected to increase in regions with rapidly growing economies in South and East Asia, at least in the near term. Young et al. (2013) presented multi-model projections of surface ozone concentrations based on the representative concentration pathways (RCPs). In chapter 2, we presented projections based on an extended set of RCP-like scenarios and showed that both air pollution and climate policy could significantly affect ozone precursor emissions and consequently ozone concentrations in the coming decades.

There have been a number of studies on present-day ozone impacts on crop yields, such as the global studies of Van Dingenen et al. (2009) and Avnery et al. (2011a) and the regional study for the United States by Yue and Unger (2014). In addition, scenario studies have investigated the possible impacts of future ozone levels on crop yields, such as the global studies by Avnery et al. (2011b; 2013) and the regional study for Asia by Wang and Mauzerall (2004), both based on the IPCC SRES scenarios (Nakićenović et al., 2000), the global study by Van Dingenen et al. (2009) based on emission scenarios from the International Institute for Applied Systems Analysis (IIASA), and the global study of Tai et al. (2014) based on the Representative Concentration Pathways (RCPs). Other studies have looked at the impacts of future changes in land use on ozone precursor emissions and ozone concentrations (Lathière et al., 2006; Ganzeveld et al., 2010; Wu et al., 2012). However, no attention has been given to the impacts of changes in surface ozone on land use via crop yield losses. In this study, we use a wider set of scenarios with respect to air pollution (see chapter 2) developed using the Integrated Model to Assess the Global Environment (IMAGE, Bouwman et al., 2006) to assess the possible impacts of ozone concentration changes on future crop yields and consequently land use under different climate and air pollution policy regimes.

To do so, we make use of established exposure-response functions (ERFs) based on field experiments. The relative yield loss (RYL) factors for different crop types have been calculated from hourly ozone fields simulated with the atmospheric chemistry and transport model TM5 (Huijnen et al., 2010; van Noije et al., 2014). The resulting crop production losses and the subsequent impact on land use were calculated by feeding back the results to the IMAGE model. This modelling setup allows us to assess the potential of different scenarios in reducing crop losses and subsequent impacts on land use for the first half of the century.

The paper is structured as follows: Section 5.2 describes the methodology. In Section 5.3 we present results on the simulated ozone indicators. Results on ozone impacts on crop production and land use, and the associated net CO_2 emissions for the different scenarios are presented in Section 5.4. A discussion and conclusions of our results are given in Section 5.5.

5.2 Methodology

5.2.1 Models and emission scenarios

The ozone concentrations used in this study were calculated in chapter 2 using TM5, driven by present-day meteorological fields. This is justified by the fact that in most regions the impacts of climate change on ground-level ozone concentrations are expected to be much smaller than the impacts of future changes in ozone precursor emissions (see e.g. Fiore et al., 2012).

The three emission and land-use scenarios considered in this study have been developed using the IMAGE model, as described in chapter 2. We consider two scenarios that are similar to the RCP6.0 and RCP2.6, which lead to a radiative forcing of 6.0 and 2.6 W m^{-2} in 2100 respectively (Van Vuuren et al., 2011). The scenarios, called IM6.0 and IM2.6, differ in terms of energy use and land use as a consequence of the assumed climate policy. The IM6.0 is a scenario with very mild climate policy, while the IM2.6 scenario resembles the most ambitious climate policy scenarios in the literature. To assess the importance of air pollution policy we designed variants of these two climate scenarios with different trends in emission factors for ozone precursor gases and other short-lived air pollutants (see chapter 2). The low air pollution scenarios assume that emission factors will decline following the implementation of currently formulated air pollution legislation up to 2030, followed by a further decline assuming that increasing levels of welfare lead to a higher valuation of air quality (similar to the Kuznets hypothesis). This is similar to the original RCPs, used in climate research (see Van Vuuren et al., 2011). In the high-pollution variants of these scenarios, current and planned legislation is assumed to be implemented until 2010, after which emission factors are taken to be constant. In this study, the following three scenarios are considered:

1) IM6.0-high (RCP6.0 type scenario, i.e. weak climate policy with high air pollutant emissions)

2) IM6.0-low (RCP6.0 type scenario, i.e. weak climate policy with low air pollutant emissions)
3) IM2.6-low (RCP2.6 type scenario, i.e. stringent climate policy with low air pollutant emissions).

TM5 is a global atmospheric chemistry and transport model which was configured to run on a horizontal resolution of 3 x 2 degrees (longitude x latitude) with 34 vertical levels. Hourly ozone concentrations were calculated for the present day (2005) and for two future time slices (2020 and 2050). All TM5 simulations were driven by meteorological data from the ERA-Interim reanalysis (Dee et al., 2011) of the European Centre for Medium-Range Weather Forecasts (ECMWF) for the year 2005, and thus do not account for possible impacts of future climate change on ozone concentrations.

The scenarios used in this study are derived from the OECD reference scenario (OECD, 2012). This scenario is based on medium assumptions for main drivers such as population, income growth, technology development and related trends in energy and land use. The hypothetical assumption of constant emission factor in the first scenario forms an upper bound of possible emission trajectories, and provides a reference level to assess the potential impacts of air pollution policy. The emissions of long-lived greenhouse gases (LLGHGs) in the first two scenarios are the same but air pollutant emissions are significantly different as a result of the varying assumptions on emission factors. Therefore, the difference between the first and second scenario highlights the potential impact of air pollution control. The difference between the second and third scenario, in turn, shows the potential co-benefits from climate policy on air pollutant emissions. Finally, the scenarios together enable us to assess the range of potential ozone damage on crop yield and the implications for future land use. A harmonization procedure is applied to ensure that the projections start from the ACCMIP emission inventories for present day (Lamarque et al., 2010). The methane concentrations are computed following the MAGICC6 parameterization (see chapter 2 and references therein).

The terrestrial biosphere is modelled with the Terrestrial Environment System in IMAGE 2.4 (Bouwman et al., 2006), which consists of a number of sub-models wherein computations are performed on a 0.5 x 0.5 degrees (longitude x latitude) grid. The changes in natural vegetation patterns and the carbon cycle are based on an implementation of the BIOME model in IMAGE (Leemans and van den Born, 1994). In IMAGE the productivity of seven different food crops (rice, maize, tropical cereals, temperate cereals, pulses, oil crop, and root and tuber), grass and four energy crop types are calculated based on the version of FAO's GAEZ (Global AgroEcological Zones) model implemented in IMAGE (Alcamo et al., 1994). The GAEZ-IMAGE approach evaluates land suitability for agricultural production and estimates the potential crop yield. Within this approach, climatic variables such as temperature and precipitation are used to estimate the start and length of the growing season. For instance, growth only takes place at temperatures above 5°C if soil moisture is not

limiting. The characterization of soil moisture for the growing period is more complex and is based on the approach of FAO (1978). The GAEZ approach does not account for ozone impacts, which can therefore be introduced independently as discussed below.

Land-use and land-cover changes in IMAGE are estimated by first calculating the required agricultural production and allocating it to a 0.5 x 0.5 grid. The demand for agricultural land is calculated for each region based on changes in the demand for food, feed and changes in yield as a result of human management (a so called management factor representing the relation between actual and potential yield due to management effects like fertiliser application) or natural factors (soil quality and climate change). Subsequently, at grid cell level the allocation rules are based on the suitability of the land, the distance to existing agricultural and urban areas, rivers and a random factor (see Alcamo et al., 1998). If the current agricultural land is insufficient, then increases in the demand for agriculture land (as a result of increased food demand, but also, for instance, due to significant decline in crop yield) will lead to land conversion of natural land to agricultural use. At the regional level, the IMAGE model is used in conjunction with the agro-economic LEITAP model to estimate changes in demand for agricultural products, trade and investment in agricultural productivity (Bouwman et al 2006). In LEITAP, the regional crop production is estimated based on population growth, economic development, dietary preferences, agricultural trade regimes and technological change. The supply of agricultural land depends on the availability of suitable land for agriculture from IMAGE (based on the GAEZ sub model, see above), institutional factors (e.g. policies on protected areas) and land prices. The output from LEITAP is used in IMAGE to compute changes in actual crop yields due to improved management, the demand for land and the environmental consequences of crop production. It should be noted that in this study, the interaction with LEITAP was used to calculate the initial regional production and land allocation, but was not used for the scenarios accounting for ozone-concentration based yield losses. The agricultural part of IMAGE is calibrated historically to FAO data (see also below, section 2.3). For the scenario period, IMAGE and LEITAP have been evaluated against FAO projections (Bruinsma 2003), and show similar overall trends in a reference scenario (Stehfest et al. 2013). This means that, for simplification, the assumption was made that agricultural trade patterns remained unchanged.

IMAGE crop types	Crop types used for ERFs	Ozone indicator	ERFs used for RYL calculation	References
Rice	Rice	AOT40	0.00415*AOT40	Mills et al. (2007)
		M7	$Exp[-(M7/137)^{2.34}]/exp[-(25/137)^{2.34}]$	Wang and Mauzerall (2004)
Maize	Maize	AOT40	0.00356*AOT40	Mills et al. (2007)
		M12	$Exp[-(M12/124)^{2.83}]/exp[-(20/124)^{2.83}]$	Wang and Mauzerall (2004)
Temperate cereals	Barley	AOT40	0.00061*AOT40	Mills et al. (2007)
Tropical cereals	Barley/wheat	AOT40	0.00061*AOT40	Mills et al. (2007)
Pulses	Pulses	AOT40	0.0172*AOT40	Mills et al. (2007)
Oil crop	Soybean	AOT40	0.0113*AOT40	Mills et al. (2007)
Grass	Ryegrass/clover mixture	AOT40	0.00003*AOT40	González-Fernández et al. (2008)
Root and Tuber	Potato	AOT40	0.0058*AOT40	Mills et al. (2007)
Sugar cane	Cotton	AOT40	0.0150*AOT40	Mills et al. (2007); Grantz et al. (2008)
Woody bio-fuel crops	Broadleaves and conifers	AOT40f	0.00162*AOT40f	Karlsson et al. (2007)
Non-woody bio-fuel crops	Maize	AOT40	0.00356*AOT40	Van Dingenen et al. (2009)

Table 5.1. Overview of crop types in IMAGE, the different ozone indicators used to estimate ozone impacts and the exposure-response functions (ERFs) used to evaluate the relative yield loss (RYL). The mean of the RYL based on AOT40 and M7or M12 has been taken in the cases of rice and maize. Note that maize is both a food and energy crop in IMAGE.

The sources and sinks of carbon resulting from natural and anthropogenic perturbations are computed in the Terrestrial Carbon Cycle sub-model of IMAGE. The dynamics of the sources and sinks of carbon are driven by factors such as changes in land cover, physical climate parameters and atmospheric CO_2 concentrations (see Klein Goldewijk et al., 1994). Initially, the Terrestrial Carbon Cycle model is assumed to be in equilibrium with the atmosphere. This implies that there is no net release of carbon into the atmosphere. Perturbation of this equilibrium state (for instance through increases in agricultural demand that lead to an expansion of agricultural land at the expense of natural vegetation) will result in an increase in the net atmospheric CO_2 concentrations. On the other hand, reforestation or the growth of natural vegetation following abandonment of crop land gradually reduces the net atmospheric carbon stock as the converted land (re-growth of natural vegetation) now acts as a sink for carbon till a new biomass equilibrium is reached (Stehfest et al., 2009). Global totals for some key ozone precursors are presented in Fig. S5.1.

5.2.2 Calculation of ozone indicators and relative yield loss factors

To calculate crop yield losses due to exposure to ozone, we made use of ERFs for different crop types derived from large field experiments such as the National Crop Loss Assessment Network (NCLAN) in the United States and the European Open-Top Chamber Programme (see Table 5.1). In this study, the ozone indicators AOT40 (Mills et al., 2007), AOT40f (Karlsson et al., 2007), M7 and M12 (Wang and Mauzerall, 2004) were used (see Table 5.2). AOT40 (ppmv·h) is defined as the cumulative hourly ozone volume mixing ratio above a threshold of 40 ppbv during 12-hour daylight (8:00 – 19:59) over the course of the growing season (normalized to 3 months). The definition of AOT40f (ppmv·h), used in the case of forests, is similar to AOT40 except that it is normalized to 6 months. M7 and M12 (ppbv) are defined as the 7-hour (09:00–15:59) and 12-hour (08:00–19:59) daytime mean ozone mixing ratio, respectively, during the growing season.

Many of the ERFs based on AOT40 are taken from the synthesis paper by Mills et al. (2007). Following van Dingenen et al. (2009), we have scaled the AOT40 and AOT40f based ERFs for the different crop types such that they equal unity at AOT40(f)=0 (see Table 5.1). The indices M7 and M12 are both considered in this study and other studies simply because the ERFs for rice are expressed as a function of M7 and those for maize as a function of M12. For rice and maize we follow the approach of van Dingenen et al. (2009) and take the average between the ERFs based on M7 and M12, respectively, and that based on AOT40.

For other crop types that are modelled in IMAGE but not covered by Mills et al. (2007), we applied the ERFs from published literature. In the case of grass, though a lot of studies have looked at the effect of ozone on grass (Fuhrer, 2009; González-Fernández et al., 2008), developing ERFs can be very complex because of varying responses of different species (Fuhrer, 2009). In this study, the ERF of rye grass/clover mixtures from González-Fernández et al. (2008) is used, which show relatively small sensitivity to ozone. For woody bio-fuel plants, we use the ERF for conifer and broadleaves from Karlsson et al. (2007).

For some of the crop types modelled in IMAGE, no suitable ERFs were found in the literature. For these crop types, we applied the ERFs of crops from Mills et al. (2007) with broadly similar plant functional type classification. For instance, in the case of temperate cereals (where no suitable ERFs were found), we applied the ERF of barley (Mills et al., 2007). With regard to tropical cereals, which show moderate sensitivity to ozone, we used the average of the ERFs of wheat and barley. For root and tuber, we use the ERF of potato. For the non-woody bio-fuel crops, we use the ERF of maize, which is one of the crops used in producing bio-fuel. With respect to sugar cane, no suitable ERF was found. However, Grantz and Vu (2009) reported that sugar cane exhibits the same sensitivity to ozone as cotton at moderate levels of exposure and as tomato at high levels of exposure. Therefore, we used the ERF of cotton for sugar cane.

The same ERFs derived from field experiments in Europe and North America are applied globally as very little information was available on ERFs in the tropics.

Definition	References
$AOT40(ppmh) = \sum_{i=1}^{n}([O_3]_i - 40), [O_3] \geq 40\, ppbv$	Mills et al., 2007
08:00-19:59	
$AOT40\,f\,(ppmh) = \sum_{i=1}^{n}([O_3]_i - 40), [O_3] \geq 40\, ppbv$	Karlsson et al., 2007
08:00-19:59	
$M12(ppbv) = \frac{1}{n}\sum_{i=1}^{n}[O_3]_i$	Wang and Mauzerall, 2004
08:00-19:59	
$M7(ppbv) = \frac{1}{n}\sum_{i=1}^{n}[O_3]_i$	Wang and Mauzerall, 2004
09:00-15:59	

Table 5.2. Definition of the different ozone indicators used in the computation of crop relative yield. Here $[O_3]$ represents hourly ozone concentration, i is the hour index, and *n* depicts the number of hours in the growing season.

However, a comparison of crop sensitivities from a small scale study in Asia and North America revealed that Asian crops are more sensitive than North American crops (Aunan et al., 2000; Emberson et al., 2009). Thus our estimates of ozone effects on Asian crops are likely conservative.

The ozone indicators are calculated using the local growing season as determined in IMAGE. Thus, we estimated the ozone indicators by averaging (M7 and M12) or summing (AOT40 and AOT40f) hourly ozone fields between the start and end of the growing season. Following their definitions, AOT40 and AOT40f were then normalized to 3 months (van Dingenen et al., 2009) and 6 months (Karenlampi and Skärby 1996), respectively. The resulting ozone

indicators were used to calculate the RYL factors for the various crops used in IMAGE (see Table 5.1). It is important to note that the growing season used in the calculation of the ozone indicators in this study is fixed to 2005 conditions, which implies that only the impacts of changes in ozone precursor emissions on the ozone indicators and the resulting RYL factors are explored. The RYL factors are calculated based on simulated ozone mixing ratios for the years 2005, 2020 and 2050. For the intermediate years, the RYL factors are obtained by linear interpolation in time.

5.2.3 Calculation of crop production loss

In IMAGE, the simulated crop productions and crop areas are calibrated to FAO crop production and resource data from 1970 to present-day to ensure that they are consistent with aggregated agricultural statistics at national and global levels by adjusting the so-called management factor representing the human influence on crop yields (details on this can be found in Bouwman et al., 2006). In fact, in this way IMAGE implicitly accounts for ozone impacts for the present-day as these are implicitly included in the FAO production statistics. To correct for this effect, we apply the following formula to calculate the ozone impact on the crop production per grid cell in IMAGE:

$$CP_i(year) = \frac{1 - RYL_i(year)}{1 - RYL_i(2005)} \times CP_i^o(year). \qquad (5.1)$$

Here CP_i is the potential crop yield of crop type *i* in a particular year that explicitly accounts for ozone impacts, and CP_i^o is the corresponding yield derived from the original IMAGE model, i.e. without explicit ozone impacts. In the paper, we only use this equation to estimate the relative future losses compared today. Crop production loss (CPL_i) per grid cell for the different food crops represented in IMAGE are equal to:

$$CPL_i(year) = \frac{RYL_i(year)}{1 - RYL_i(year)} \times CP_i(year). \qquad (5.2)$$

5.2.4 Simulations for estimating the impacts on land use and the carbon cycle

At regional and global scales our IMAGE simulations meet the same required crop production irrespective of whether or not the impacts of changes in surface ozone are accounted for. This means that the crop yield loss or gain due to ozone changes is compensated through expansion or abandonment of agricultural land. To estimate this indirect effect of ozone on future land use and the carbon cycle, we have performed five simulations using our three IMAGE scenarios: two control runs with IM2.6-low and IM6.0-low, indicated by IM6.0-orig and IM2.6-orig, in which the impacts of future ozone changes on crops are not explicitly included, and the three runs for IM6.0-high, IM6.0-low and IM2.6-low wherein these impact are explicitly accounted for (Table 5.3). By comparing simulations with and without impacts of future ozone changes on crops for the same climate forcing scenario, we can separate the ozone impacts on crops from other drivers, such as climate change. Since the regional and global crop production is determined by the food demand, in calculating the crop production loss due to ozone effects using the equation given above, we

assume that the crop production is the same as in IM6.0-orig and IM2.6-orig, respectively, thereby neglecting small differences in crop production at the local scale.

Simulations	Changing ozone damage on crops
IM6.0-orig	No
IM2.6-orig	No
IM6.0-high	Yes
IM6.0-low	Yes
IM2.6-low	Yes

Table 5.3. Overview of the IMAGE simulations performed for this study.

5.3 Results on ozone indicators

5.3.1 Evaluation of ozone indicators for present day

Simulated surface and tropospheric ozone concentrations from TM5 have been extensively evaluated against observations (Huijnen et al., 2010; van Noije et al., 2014). Here, we evaluate the model with respect to its ability in capturing the ozone indicators introduced in the previous section as well as the corresponding monthly values for the year 2005. To this end, we have selected rural background stations providing hourly surface ozone measurements. We considered stations from the European Monitoring and Evaluation Programme (EMEP), the European air quality database (AIRBASE), the Clean Air Status and Trends Network (CASTNET) and the World Data Centre for Greenhouse Gases (WDCGG). We selected only stations which provided data at least 90% of the time during the growing season, as determined from the IMAGE model for the selected year. In Europe and the United States (US) there is sufficient data coverage to enable a regional comparison between the modelled and observations based ozone indicator. The locations of the remaining stations used in our evaluation and the demarcation of the regions used in our regional analysis are shown in Fig. 5.1. The simulated ozone data are linearly interpolated to the station locations. Additionally, we account for station heights by interpolating to the station pressure based on a standard atmosphere. Regional means are calculated by taking the mean over all stations within a given region.

The monthly 12-hour averaged ozone mixing ratio (M12) from the model and the selected background stations for different regions are presented in Fig. 5.2. A similar comparison for AOT40 is shown in the supplementary material (Fig. S5.2). The error bars show one standard deviation of the values obtained for the individual stations. In addition, ratios between the regionally averaged measured and simulated ozone indicators averaged (M7 and M12) or summed (AOT40 and AOT40f) over the full growing season are listed in Table 5.4. This comparison shows that the amplitude of the monthly M12 metric is generally well captured by TM5. In general, the model shows a positive offset in the summer in all considered regions in Europe and the US. The biases in Europe can be as high as about 15 ppbv in the summer months. The largest biases are found in the US. In summer they reach 25 ppbv in the northeastern US, which is highly significant compared to the variability among the stations included for this region. For Japan, TM5 systematically over-predicts the 12-hour daytime mean surface ozone by up to 30 ppbv at the two selected stations in the spring and summer

months. Averaged over the whole growing season the model reproduces M12 to within 13% in Europe and 21% in the US.

AOT40 and AOT40f are more sensitive to model biases because of the 40 ppbv threshold. While TM5 captures the observed AOT40 reasonably well in Europe, the results in the US are less robust as our modelled AOT40 is approximately twice as high as the observed values (Table 5.4). The reasons for the observed mismatches especially in the US can have various causes related to representation of chemical and physical processes in the model. Biases in the applied emissions of ozone precursors and the relatively coarse horizontal resolution of the model (Wild et al., 2006) likely also contribute substantially to the observed discrepancies.

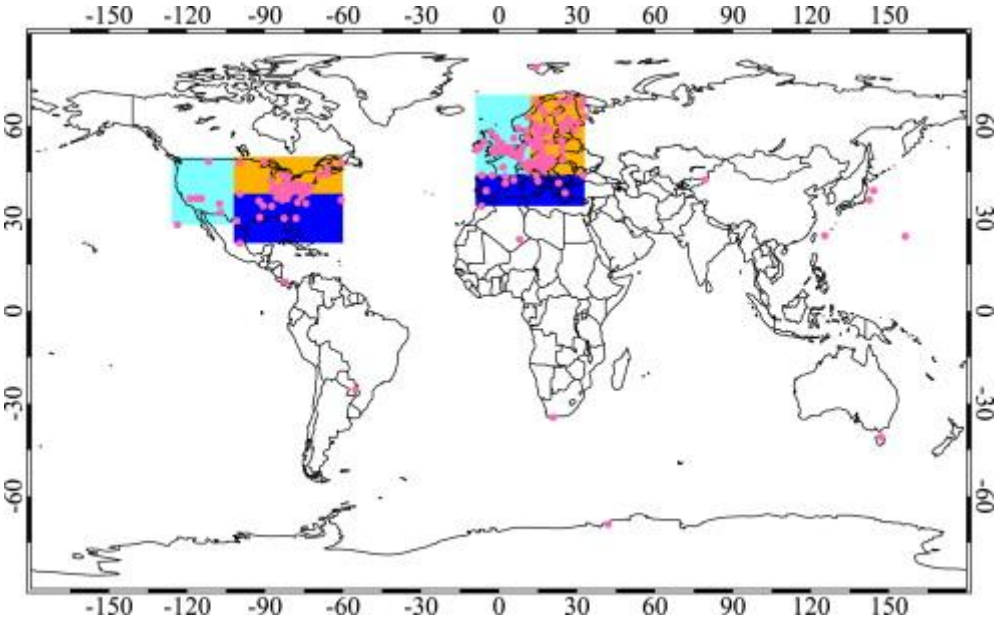

Fig. 5.1. Spatial distribution of the selected ozone measurement stations providing hourly ozone concentrations for northwestern Europe (9°W-12°E × 44°N-68°N), northeastern Europe (12°E-30°E × 44°N-68°N), Southern Europe (9°W-30°E × 34°N-44°N), the northeastern US (63°W-102°W × 38°N-48°N), the southeastern US (63°W-102°W × 22°N-38°N) and the western US (102°W-126°W × 28°N-50°N).

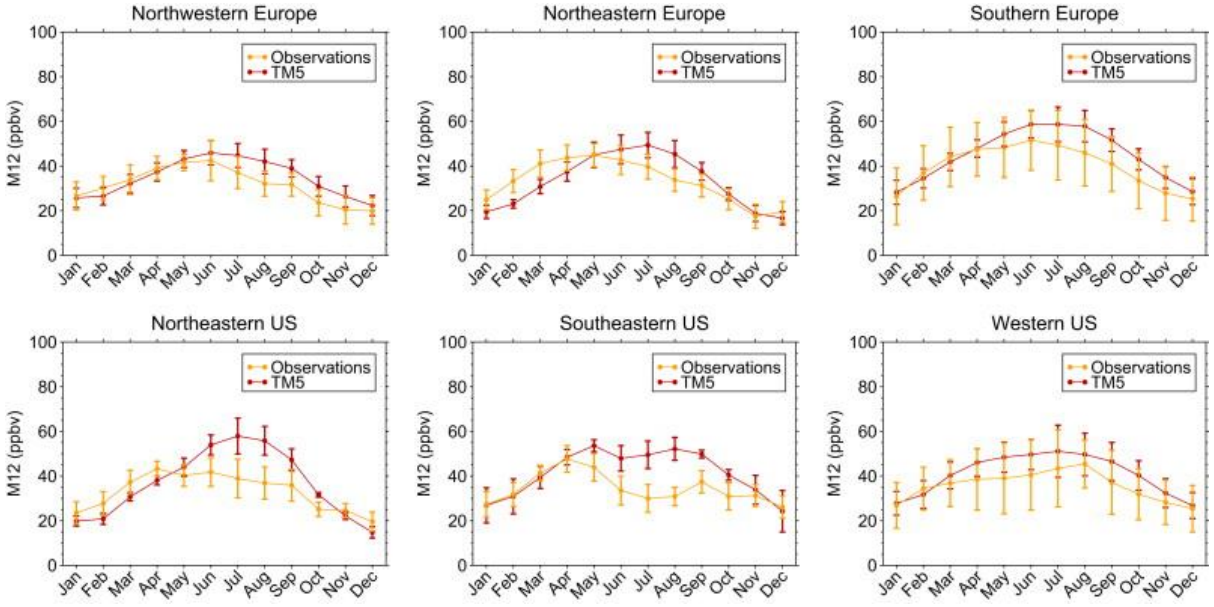

Fig. 5.2. Regional monthly 12-hour averaged ozone concentrations (M12) from the selected background measurement stations compared to TM5. The error bars on the measurements and simulation show one standard deviation of the monthly means for the different station locations in a given region.

The observed biases between measured and observed ozone especially for AOT40 is of great importance as calculated RYL might be significantly overestimated in the US. To reduce this error, we applied a correction to the model results for the different ozone indicators. This is achieved by scaling the simulated ozone indicators, obtained per grid cell for the whole growing season. The scale factor is obtained on a regional level as the ratio of the regional mean observed to modelled value for the corresponding ozone indicator. We are not able to perform a similar bias correction in Asia, Africa and South America because of the lack of representative networks of measurement stations of hourly surface ozone data for 2005. This implies that the estimated RYL calculated in these regions are sensitive to model biases. However, when considering the impacts of future changes in ozone concentrations, biases in present-day and future ozone concentrations partially cancel each other.

5.3.2 Future projections of ozone indicators

Fig. 5.3 shows the simulated M12 and AOT40 fields and changes in 2050 relative to 2005 under the IM2.6-low, IM6.0-low and IM6.0-high scenarios. The data shown for Europe and the US are the model results after the application of the bias correction. Results for present-day seasonal mean ozone concentrations (M12) are typically around 40-60 ppbv in the northern hemisphere industrialized regions, with values reaching around 60 ppbv in parts of India and China. In most of the northern hemisphere mid-latitudes and central Africa, we find AOT40 values higher than the 3 ppmv·h limit necessary to curtail ozone impact on crops (see Karenlampi and Skärby 1996). Under the IM6.0-high scenario, we find a strong increase in surface ozone concentrations exceeding 20 ppbv for M12 and 15 ppmv·h for AOT40. The increase is principally strong in the Indian subcontinent. However, we also see decreases in surface ozone concentrations mostly in the Congo and Amazon basins.

Comparison of simulated ozone concentrations under the different scenarios shows that future changes in surface ozone strongly depend on the assumed level of air pollution control and climate policy. For instance, the implementation of all current and planned legislation and additional air pollution abatement measures (IM6.0-low) decreases both M12 and AOT40, as seen most noticeably in the eastern United States, part of the Mediterranean, northwestern Europe and central Eurasia. If more stringent climate and air pollution measures are put in place (IM2.6-low), both indicators will be reduced over the entire globe – with reductions up to about 15 ppbv and15 ppmv·h, respectively, simulated in northern mid-latitudes.

5.4 Ozone impact on crops, land use and the carbon cycle

5.4.1 Ozone impacts for the present day

Fig. 5.4 shows the results for the ozone induced relative yield loss for maize and rice, two important crop types in IMAGE. These two crops have already been assessed on a global scale by Van Dingenen et al. (2009) and Avnery et al. (2011a). This enables a comparison of our results to their findings. Based on present-day (2005) ozone levels, a RYL of up to about 10% is estimated for both crops especially in parts of the Middle East, India and China where high ozone concentrations are simulated during the growing season. Comparison of our RYL estimates for maize and rice with the results of Van Dingenen et al. (2009) for the present-day reveals similar global patterns with RYL factors also reaching values around 10% locally. In Europe and the US where our results are less affected by model biases, we estimate RYL factors of maximally about 4% for maize in both regions and for rice in the US which is lower than the maximum values of about 10% computed by Van Dingenen et al. (2009) and 6% found for maize by Avnery et al. (2011a). Part of this discrepancy is due to the fact that we have corrected for biases in the simulated ozone concentrations. Without this bias correction, we find maximal RYL of about 8% in parts of Europe and the US (Fig. S5.3). Differences are also caused by the fact that we used the growing season from IMAGE in our computation of the ozone indicators, while the crop calendar from the US Department of Agriculture was used in the studies by Van Dingenen et al. (2009) and Avnery et al. (2011a).

Regions	**M7**	**M12**	**AOT40**
Northwestern Europe	0.89	0.87	0.89
Northeastern Europe	0.85	0.88	0.77
Southern Europe	0.91	0.90	0.93
Northeastern US	0.85	0.79	0.54
Southeastern US	0.88	0.84	0.60
Western US	0.87	0.83	0.51

Table 5.4. Ratio of regional averages of the measured to simulated ozone indicators between the start and end of the growing period.

The estimated crop production loss varies regionally and between crop types as they portray different sensitivities to ozone (Fig. 5.5). The corresponding crop production from which CPL is computed is presented in the supplementary material (Fig. S5.4). For 2005, we

estimate losses of up to 5 metric tons/km^2 for maize and rice in Asia which is akin to the present-day estimate of Van Dingenen et al. (2009). Similarly, we find small CPLs in the US for rice. However, for maize our computed CPL (0.5 metric tons/km^2) in the northeastern US is smaller than the 5 metric tons/km^2 estimated by Van Dingenen et al. (2009). Without the bias correction, estimated CPL for maize reaches 1 metric tons/km^2 in this region (Fig. S5.5). While these differences stem partly from the applied bias correction, they are also associated with the fact that the estimated maize production in Van Dingenen et al. (2009) for this region is higher than that simulated in IMAGE. Though there are spatial and temporal differences, the present-day ozone impact on maize production averaged over the US decreases by 48% when the bias correction was applied and by 27% in Europe. For rice, we find a decrease of about 40% in the US and 16% in Europe after the application of bias correction.

5.4.2 Future impacts of ozone on crops

The effect of future ozone-induced crop losses can also be seen in Fig. 5.4 and 5.5. Under the scenario with little air pollution control (IM6.0-high), we find for both crops high RYLs exceeding 20% in 2050 in most parts of the Middle East, India and China. Avnery et al. (2011b) using the A2 scenario also estimated RYL for maize of up to 20% in these regions in 2030 for M12. The implementation of stringent air pollution policy results in a decrease in projected RYL for maize and rice compared to 2005 values especially in the US, southern Europe, the Middle East, India and China. Despite the stringent air pollution policy in place, we still find RYL exceeding 15% mainly in some parts of India and China in 2050.

If air pollution policies are not tightened (IM6.0-high) in 2050, CPL might get up to 10 metric tons/km^2 especially in Asia. At the same time, crop production losses up to 2 metric tons/km^2 for maize are also noted in the US (up to 5 metric tons/km^2 without bias correction), Southern Europe and central Africa. In contrast, the implementation of air pollution mitigation measures leads to lower CPL under IM6.0-low compared to IM6.0-high, most noticeably in parts of the US and Southern Europe. Irrespective of the stringent policy in place, CPL in some parts of India and China still gets up to 10 metric tons/km^2

5.4.3 Impact on land use

Fig. 5.6 shows global and regional (see Bouwman et al. 2006 for regional definition) ozone impacts on land use through crop yield losses and the resulting expansion in agricultural areas under the three scenarios evaluated in this study and also two simulations without changes in ozone effects (IM2.6-orig and IM6.0-orig). In the latter simulations ozone impacts are only included implicitly based on FAO crop production data for the present day. The difference between the solid and dashed lines gives the impacts of future ozone changes on land use via crop yield loss. If air pollution measures are not enforced as assumed in IM6.0-high, crop yield losses due to ozone changes will lead to an increase in global crop area of approximately 1.3 million km^2 (2.5%) in 2050. Regionally, we find the highest increases of up to 8.9% in Asia, 2.7% in Western Europe and 1.1% in North America. Without bias correction, we estimate higher increases in regional crop area in North America (1.6%) and Western Europe (3.2%). Implementation of current and planned air pollution legislation till

2030 and additional abatement measures thereafter (IM6.0-low), leads to small impacts of crop yield losses on crop area globally and in most regions except in Asia, where increases in crop area of up to 3.6% are estimated in 2050. This implies that additional measures to control the emissions of ozone precursors would be needed in order to further curb the impact of surface ozone on crop yield and land use.

5.4.4 Impacts of climate policy on crop yields and land use

The effect of climate policy on ozone-induced crop losses can be evaluated by comparing the IM6.0-low and IM2.6-low scenarios (Fig. 5.4, 5.5 and 5.6). Interestingly, these Figures show that climate policy can has significant co-benefits by reducing the ozone impacts on crop yields. For instance, in India and China, which are the most affected regions, we find RYL reaching 10% for maize and 8% for rice under IM2.6-low compared to 15% or more for maize and rice under IM6.0-low. The co-benefits of climate policy can also be seen in the lower CPL especially in the US and Southern Europe. Even without bias correction, the CPL is still relatively low in these regions. Also in Asia, CPL decreases from a maximum of about 10 metric tons/km^2 to approximately 5 metric tons/km^2 following the implementation of climate policy.

It should be noted that while the climate mitigation scenario (IM2.6-low) requires less land in response to ozone damage, it needs more land use for bio-energy production that forms part of the mitigation portfolio. Overall, this leads to an increase of agricultural area of 4.8% globally. Regionally, significant increases in crop area are found most notably in Eurasia (14.2%), North America (9.3%), Asia (5.5%) and Western Europe (3.9%). In IMAGE, bio-energy crops are cultivated mostly on abandoned agricultural land and grassland mainly in OECD countries and the former Soviet Union in the first half of the century (see van Vuuren et al., 2007). The indirect impact of ozone on land use (depicted by the difference between (IM2.6-low and IM2.6-org) is small because stringent climate and air pollution policies measures assumed under these scenarios lead to a reduction of the emission of ozone precursors and hence limit the severity of ozone damage on crops.

5.4.5 Impact on the carbon cycle

Table 5.5 gives the cumulative net CO_2 emissions to the atmosphere from land use between 2005 and 2050. We estimate negative cumulative CO_2 emissions for all our scenarios in North America and Western Europe as re-growth of vegetation on abandoned agricultural land leads to significant uptake of carbon. The indirect impact of ozone changes on CO_2 emissions through changes in land use is rather small in most parts of the globe. On a global scale, we find the highest increase in the cumulative CO_2 emissions due to impacts of ozone changes on crops under the IM6.0-high scenario, where we estimate an increase of about 3.7 Pg C (10.4%) compared to the case without ozone changes. Compared to the anthropogenic CO_2 emissions from fossil fuel combustion and cement production (9.5±0.8 Pg C in 2011; Ciais et al. 2013) these are relatively small numbers. However, in Asia a significant increase of the cumulative CO_2 emissions from land use can be noticed due the impacts of ozone increases under both the IM6.0-low (26.2%) and IM6.0-high (52.4%) scenarios. The impact of ozone changes on CO_2 emissions is relative small in Eurasia, South America, Africa, the

Middle East and Oceania. Hence, the 10% increase under IM6.0-high is dominated by the increased land-use emissions in Asia.

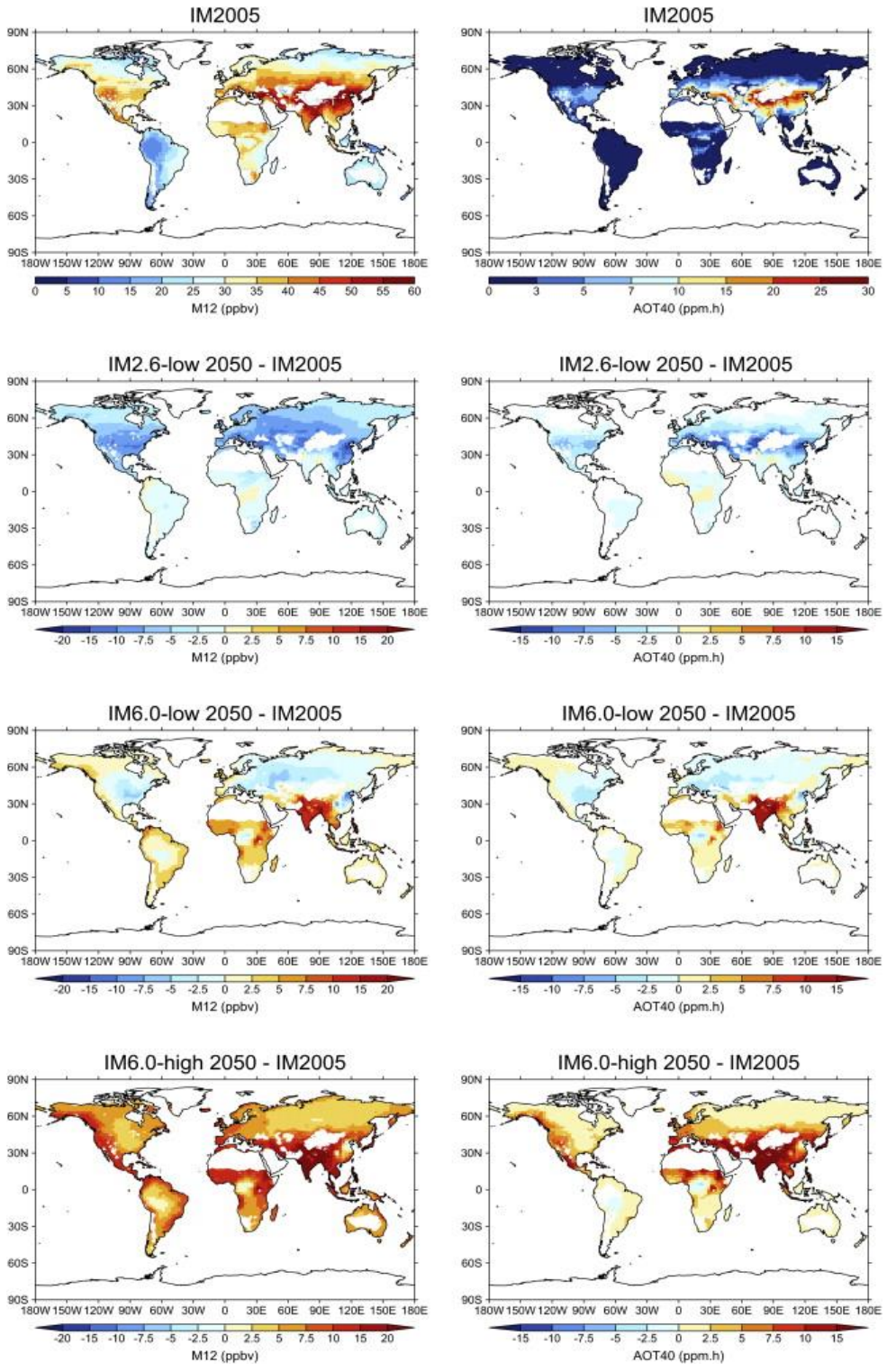

Fig. 5.3. Simulated global distributions of M12 and AOT40 for the year 2005 and the changes in 2050 relative to 2005 under the different scenarios (IM2.6-low, IM6.0-high and IM6.0-low) after mean bias correction in Europe and North America.

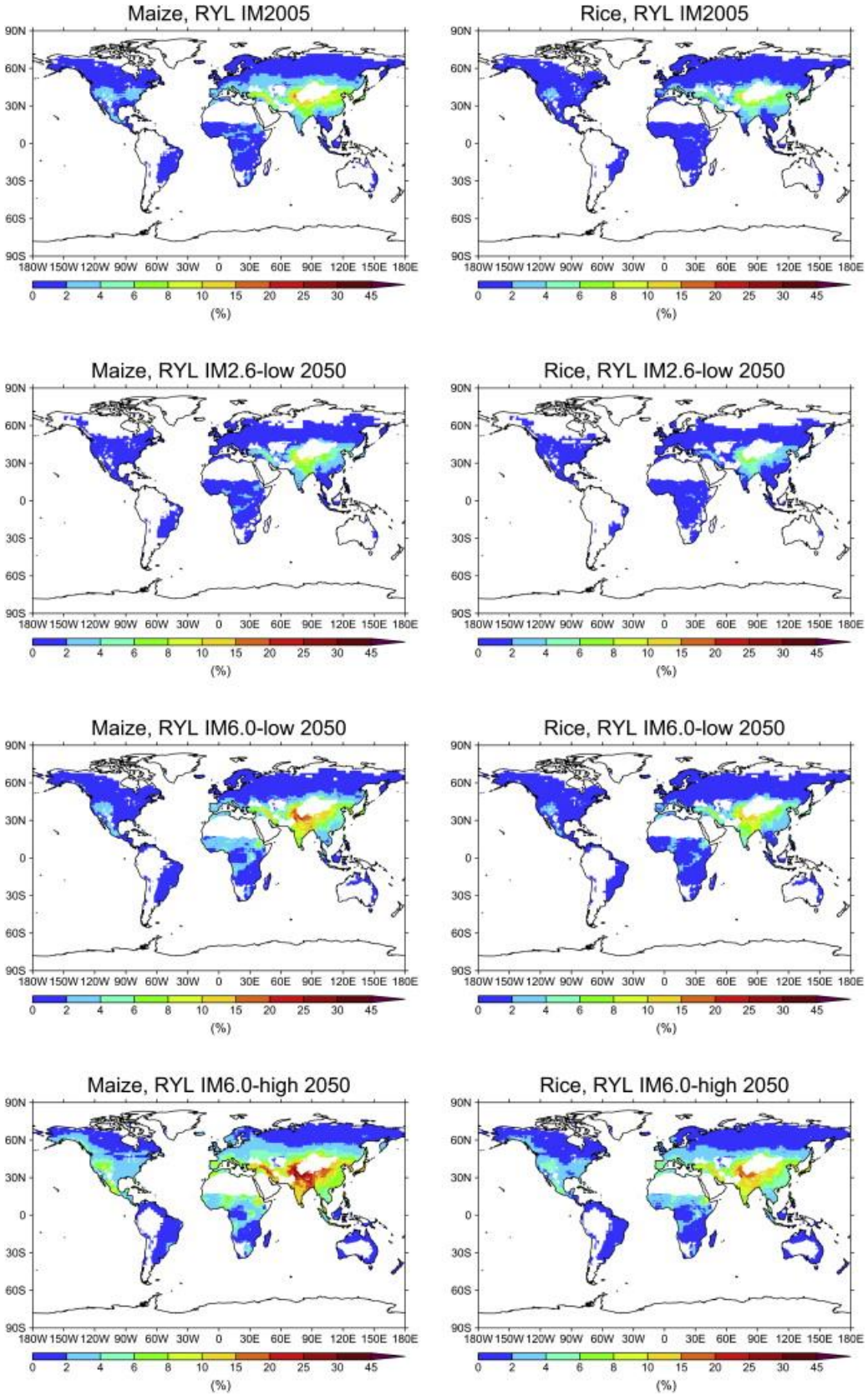

Fig. 5.4. Estimated relative yield loss for maize and rice for the present day (2005) and three scenarios for 2050.

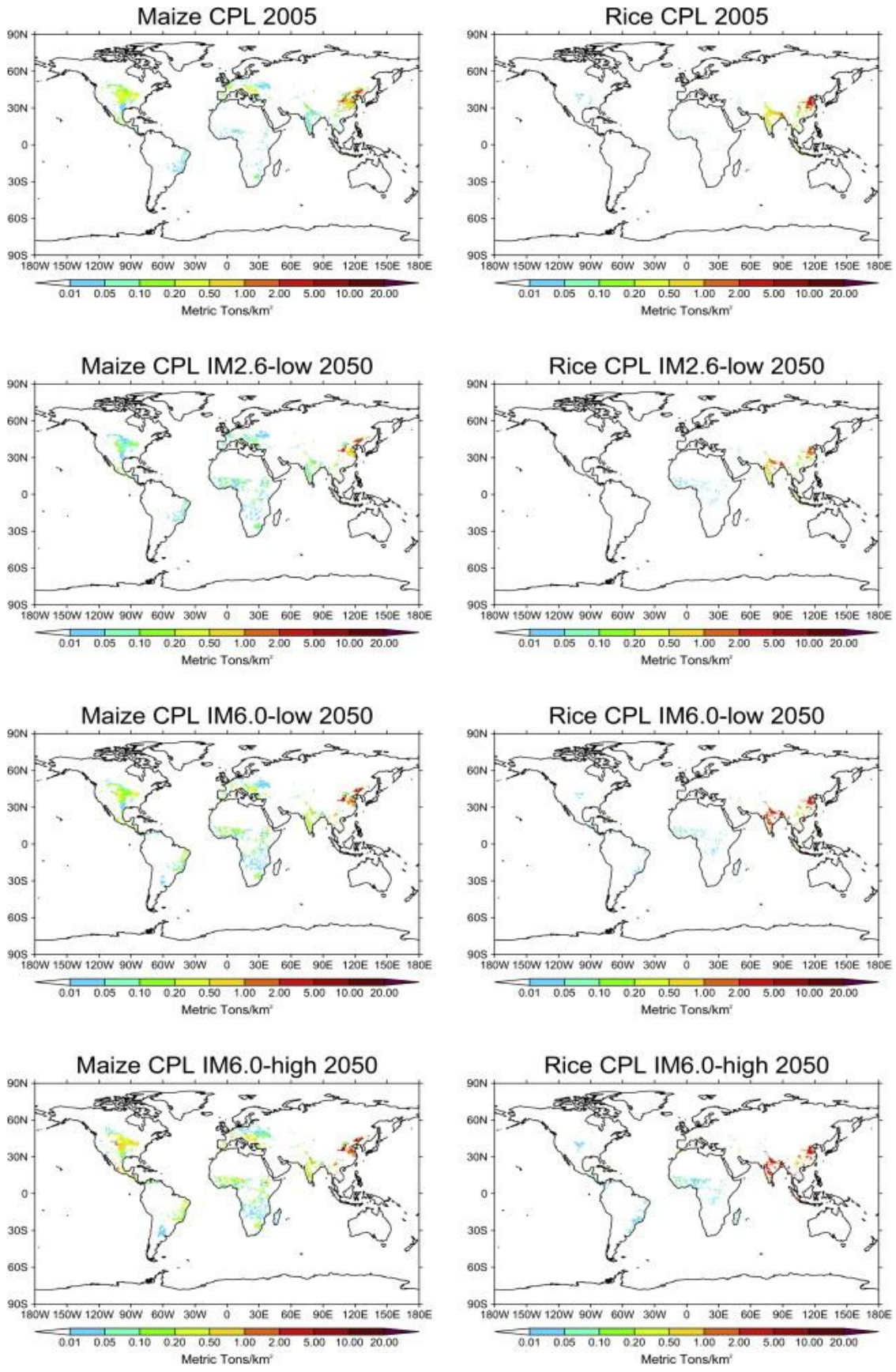

Fig. 5.5. Crop production loss (CPL) for 2005 and 2050, under IM2.6-low, IM6.0-low and IM6.0-high for maize and rice.

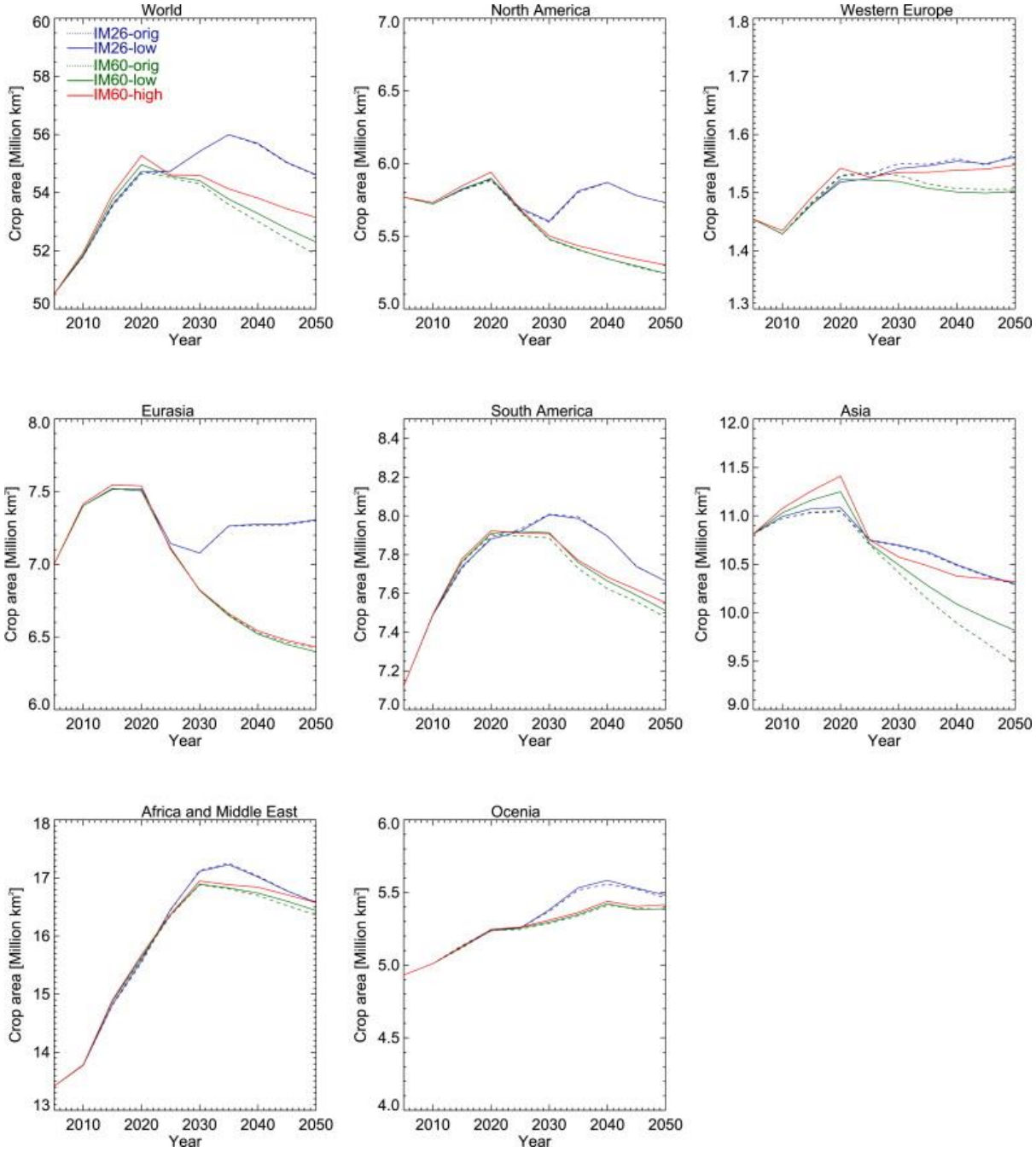

Fig. 5.6. Global and regional crop area under IM2.6-low, IM6.0-low and IM6.0-high. The dash lines show simulations in IMAGE without ozone changes (IM2.6-orig and IM6.0-orig), while the solid lines correspond to simulations that account for impacts of ozone changes.

Regions	IM2.6-orig	IM2.6-low	IM6.0-orig	IM6.0-low	IM6.0-high
North America	-0.57	-0.43	-1.19	-1.02	-0.91
Western Europe	-1.13	-1.11	-1.13	-1.11	-1.07
Eurasia	3.37	3.43	3.75	3.70	3.68
Asia	4.25	4.55	3.93	4.96	5.99
South America	9.68	9.67	8.96	8.98	9.47
Africa and Middle East	21.3	21.4	20.5	20.2	21.2
Oceania	0.89	0.85	0.76	0.85	0.95
World	37.8	38.4	35.6	36.6	39.3

Table 5.5. Regional and global cumulative net CO_2 emission (Pg C) to the atmosphere from land use between 2005 and 2050.

5.5 Discussion and conclusions

Using the IMAGE integrated assessment model and the global chemistry and transport model TM5, we estimated the impacts of plant exposure to ozone on crop production for the present day (2005) and for three RCP-like scenarios for the first half of the century. Moreover, we have evaluated the subsequent impacts of the corresponding future ozone changes on land use and the carbon cycle. By comparing the different scenarios we have been able to assess possible future impacts of air pollution control and climate change mitigation policy. Some important conclusions can be drawn.

For many crop types the relative yield loss (RYL) and crop production loss (CPL) caused by present-day ozone levels is found to be substantial. According to our calculations the relative yield losses for maize and rice may be reaching 10% in parts of the Middle East, India and China. These percentages are in line with the results found by Van Dingenen et al. (2009), but may be affected by biases in ozone concentrations in TM5. In Europe and the US, where our estimates are less affected by model biases because of the applied mean bias correction in these regions, we find RYL factors of maximally about 4% for both maize and rice which is below the estimates of Van Dingenen et al (2009) and Avnery et al (2011a).

The associated crop production losses for both maize and rice reaches 5 metric tons/km^2 in Asia, which is similar to the present-day estimate of Van Dingenen et al. (2009). Similarly, we estimate small CPLs in the US and Europe for rice. In the case of maize, our computed CPL (0.5 metric tons/km^2) in the northeastern US is lower than the 5 metric tons/km^2 calculated by Van Dingenen et al. (2009). The differences in the estimated CPL are mainly related to the bias correction applied in this study, and the high maize production assumed in Van Dingenen et al. (2009) for this region compared to that simulated in IMAGE.

Without air pollution and climate policies, increasing ozone precursors emissions could lead to higher crop yield losses. Both air pollution and climate policies could reduce these losses by reducing surface ozone concentrations. If control on air pollution policies is not strengthened, crop yield losses could be considerably higher especially in Asia, where we find up to 20% losses in 2050 compared to a reference situation without ozone changes. Our results also show that significant yield loss can be avoided by reducing emissions of ozone precursors. This can be achieved through air pollution control measures, as co-benefit of climate mitigation policies or by a combination of both.

Reducing ozone damage leads to increased crop productivity, and, possibilities for reducing cultivated area. This, in turn, could lead to a reduction of emissions associated with land-use change. In the worst-case scenario analysed in this study, future ozone increases will increase the global crop area by 2.5% and the cumulative net CO_2 emissions from land use between 2005 and 2050 by about 3.7Pg C or 10.4% compared to the case without changes in ozone. The ozone induced changes in land use are more substantial in regions where severe ozone crop damage is estimated. This is especially the case in Asia, where we find a 8.9% expansion of the crop area in 2050 and a 52.4% increase in the cumulative net CO_2 emissions between 2005 and 2050. It should be noted that the implementation of climate mitigation

policies by itself may result in an increase in crop area, if a significant contribution of bio-energy forms part of the mitigation portfolio.

In some regions the extra crop production as a result of reduced ozone impacts on yields due to climate mitigation is substantial. For instance, the maize and rice yield gains as a result of lower ozone concentrations could reach 10% in Asia. For comparison, Easterling et al. (2007) estimate that climate change impacts on the yield of maize and rice could be in the order of 40% for maize and 20% for rice for local temperatures increases above 3^{o}C. Recently, Tai et al., (2014) showed similar to this study that air pollution policies have the potential to partially offset the crop production reduction caused by climate change.

This study provides a first exploration of the effects using relatively simple methods to estimate crop damage. Some limitations of this integrated approach to crop yield loss assessment have already been highlighted in previous studies (Van Dingenen et al., 2009; Avnery et al., 20011a and 2001b). Below we indicate the key limitations of this study.

- Our methodology uses an exposure-based approach which has been widely used to assess ozone damage on crops. However, the applicability of this approach is limited because it does not explicitly account for crucial environmental factors (such as temperature, water availability and plant defence), which are important in evaluating the rate of ozone uptake by plants and the eventual damage. For this reason, a mechanistic flux-based method has been designed in recent years (Emberson et al., 2000; Sitch et al., 2007, Yue and Unger, 2014). In this approach the yield loss is calculated from the flux of ozone through the stomata. This requires information on environmental factors like aerodynamic and boundary layer resistance, which affect the stomatal conductivity and uptake of ozone by plants. Flux-based methods are not suitable for the kind of large-scale assessment of crop losses undertaken in this study because of lack of sufficiently reliable data to characterize plant sensitivities (Avnery et al., 2011a; Van Dingenen et al., 2009). More so, experimental data needed for the computation of ozone stomatal flux are only available for a limited number of crops.

- In this study, we have only accounted for the impacts of future changes in emissions on ozone concentrations, without considering any possible effects of future climate change on ozone. Future changes in climatic factors like temperature, precipitation and changes in the large-scale circulation are likely to also affect surface ozone concentrations. However, in most regions emission changes are the main factor influencing the concentrations of ozone in the troposphere in the first half of the century (Fiore et al, 2012; Young et al., 2013). A further source of uncertainty not accounted for is the effect of climate change on biogenic emissions of ozone precursors.

- Also, we have not considered possible impacts of climate change on growing season, as we use a fixed present-day start and length of the growing season in our calculations of ozone indicators. Changes in the crop calendar is likely to have a small

impact on crop production losses and land use on a global scale but might be significant on a local scale (van Dingenen et al., 2009). Furthermore, we do not model the ozone and CO_2 interaction in IMAGE but rather simulate the effects of ozone changes on the carbon cycle via crop yield. In reality, the reduction in stomatal conductance that follows elevated atmospheric CO_2 concentrations suppresses the ozone effects on plants (see Sitch et al., 2007).

- An additional uncertainty is due to biases in the simulated ground-level ozone concentrations. We therefore applied a bias correction to the model-based ozone indicators in Europe and the US. This tends to reduce the present-day ozone impacts on maize production in the US and Europe by on average 48% and 26%, respectively. In other regions, our calculation of the present-day ozone impacts on crop production is affected by model biases. The bias correction effect is generally smaller than the bias itself because the present-day bias and future bias partially offset each other, and we expect that errors outside of the US and Europe due to these biases to be similar in size to the US and European errors.

- Finally, we assume no changes in agricultural trade regimes in IMAGE. However, future changes in trade patterns will have impacts on agricultural production and land use. For instance trade liberation will lead to an increase in trade of agricultural products and economic benefits in most parts of the world, but to an increase in environmental pressures (increases in land use) especially in developing exporting regions. Also, the introduction of ozone resistant species or intensification of agricultural practices on current crop land could limit the impacts of ozone on land use.

The limitations mentioned above have little influence on the qualitative conclusions of this study.

Acknowledgements
The authors would like to thank Rita van Dingenen, Håkan Pleijel, Max Posch, and Maurits van den Berg for useful comments.

Electronic Supplementary Material C

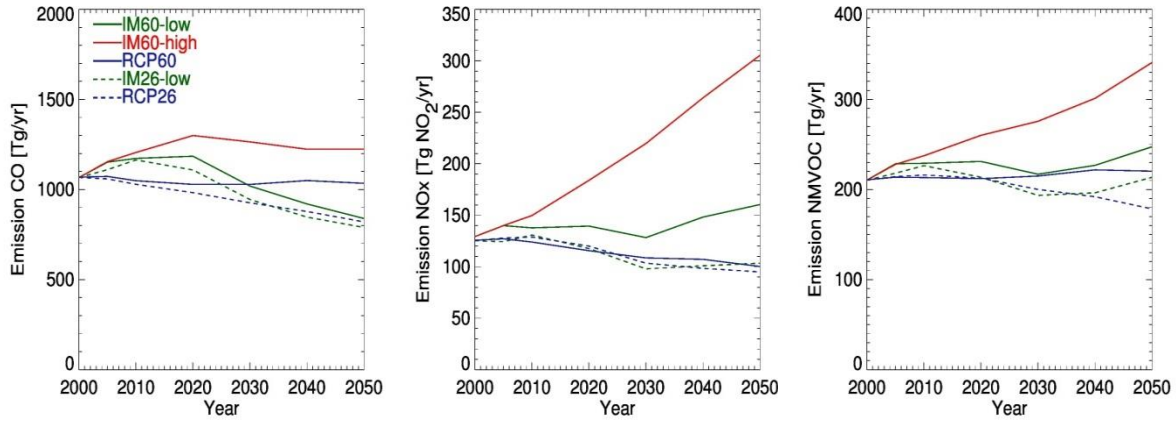

Fig. S5.1. Annual total anthropogenic emissions of CO, NOx and NMVOC in the IMAGE scenarios and corresponding RCPs. Emissions from biomass burning are included in the totals.

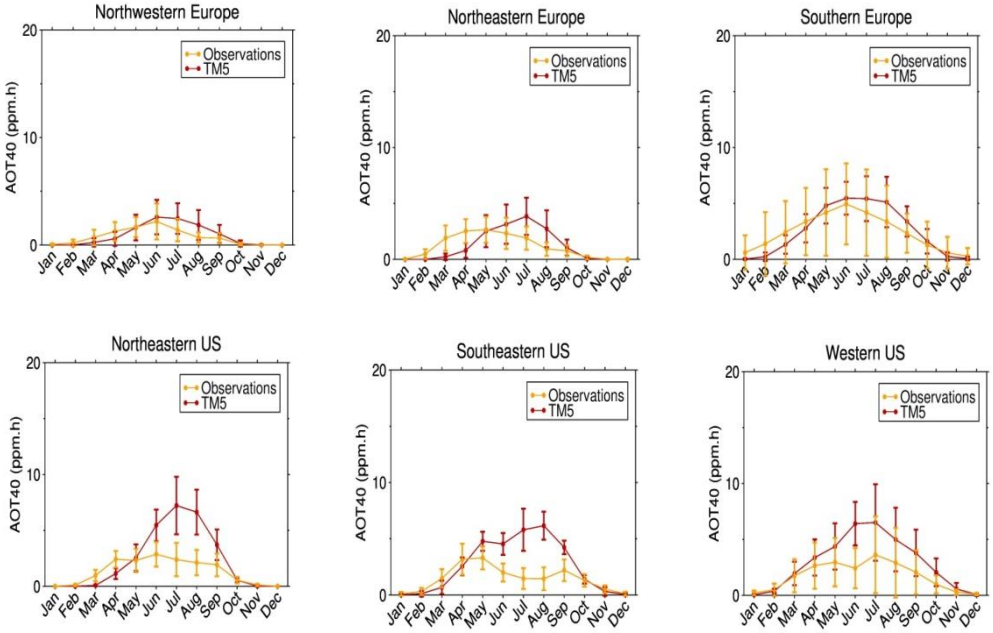

Fig. S5.2. Regional monthly accumulated AOT40 from the selected background measurement stations compared to TM5. The error bars on the measurements and simulation show one standard deviation of the monthly accumulated AOT40 for the different station locations in a given region.

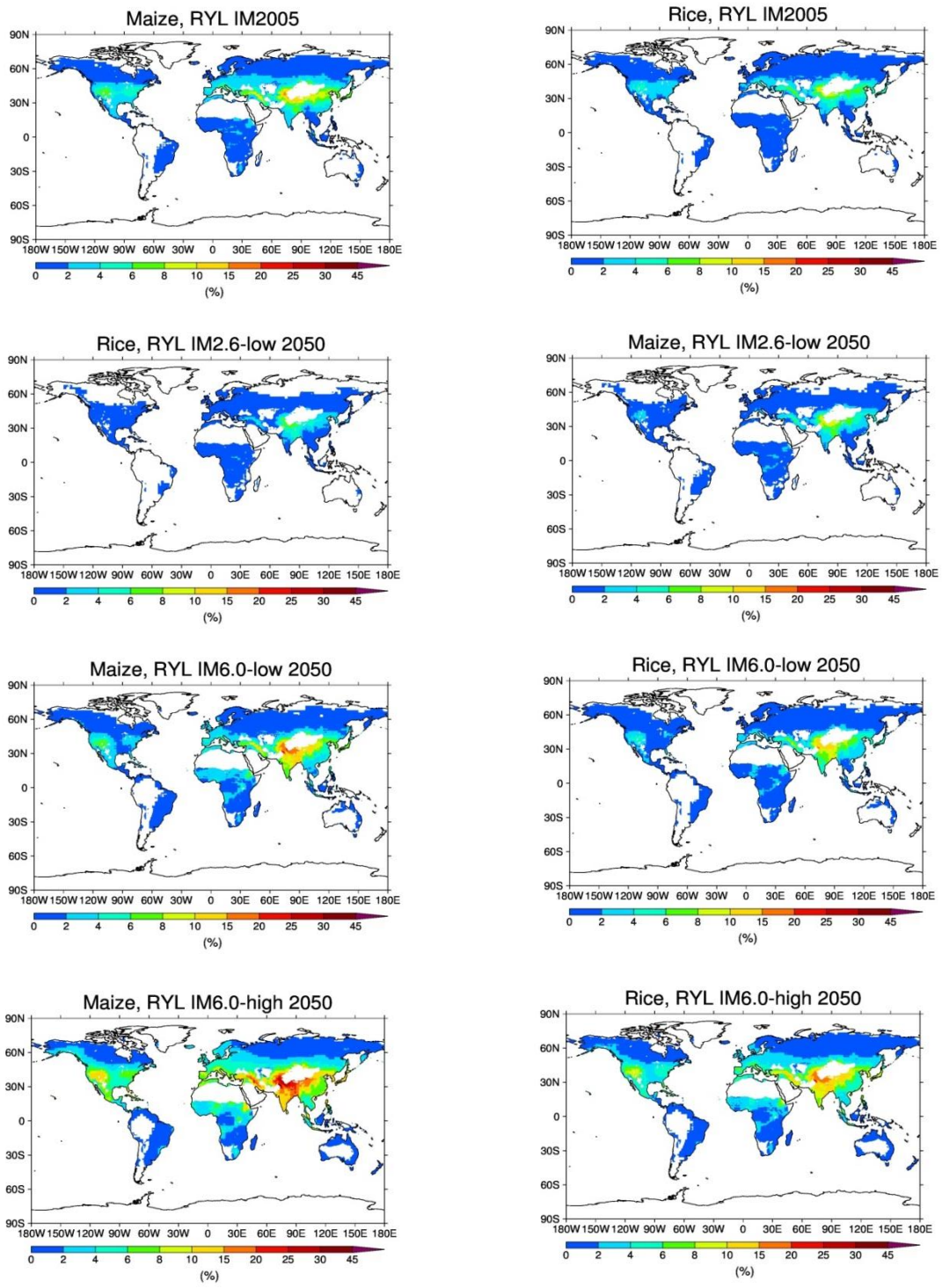

Fig. S5.3. Estimated relative yield loss for maize and rice for the present day (2005) and three scenarios for 2050, for the case without bias correction.

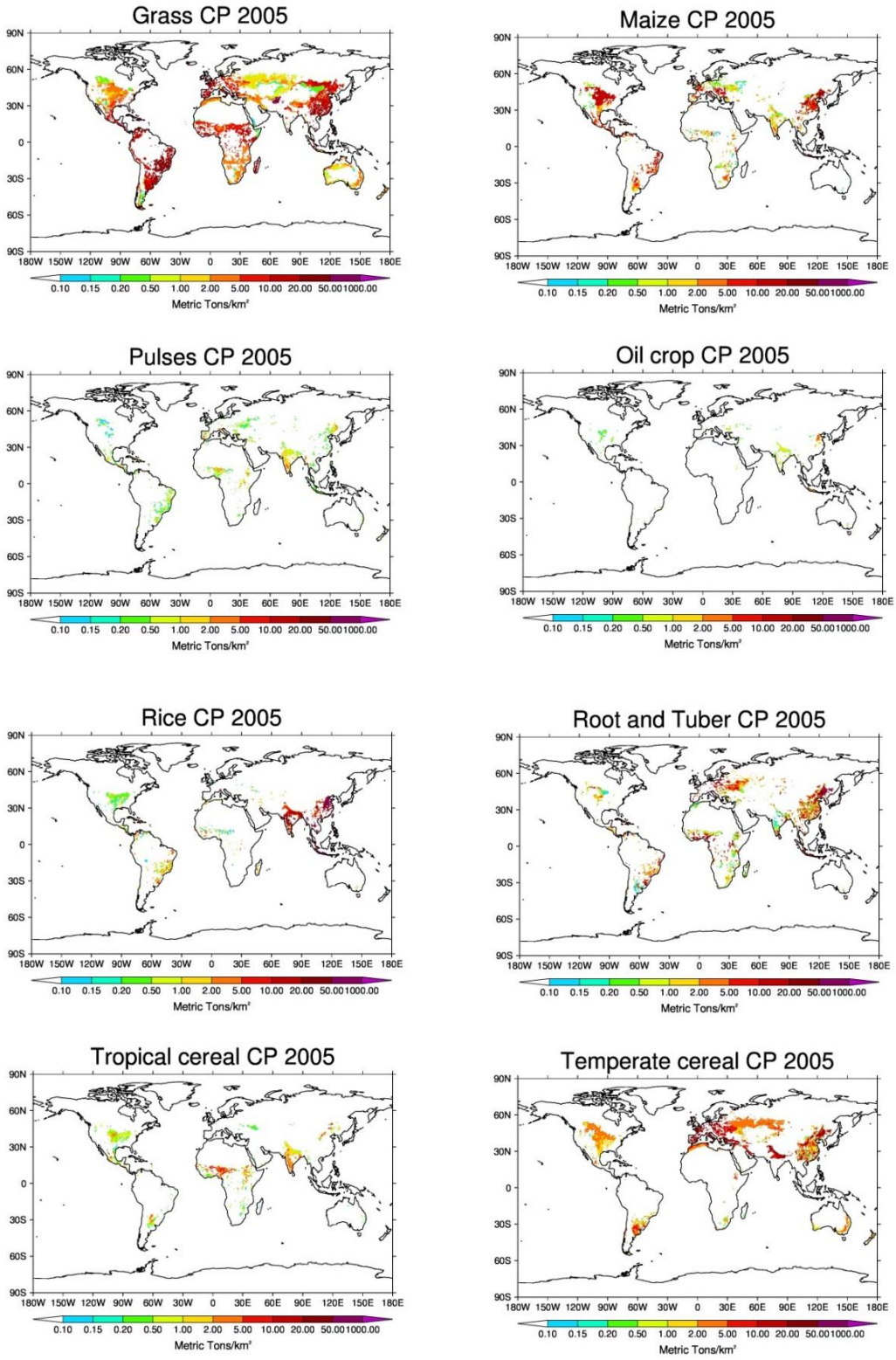

Fig. S5.4. Crop production (CP) for present day (2005) for different crop types simulated in IMAGE.

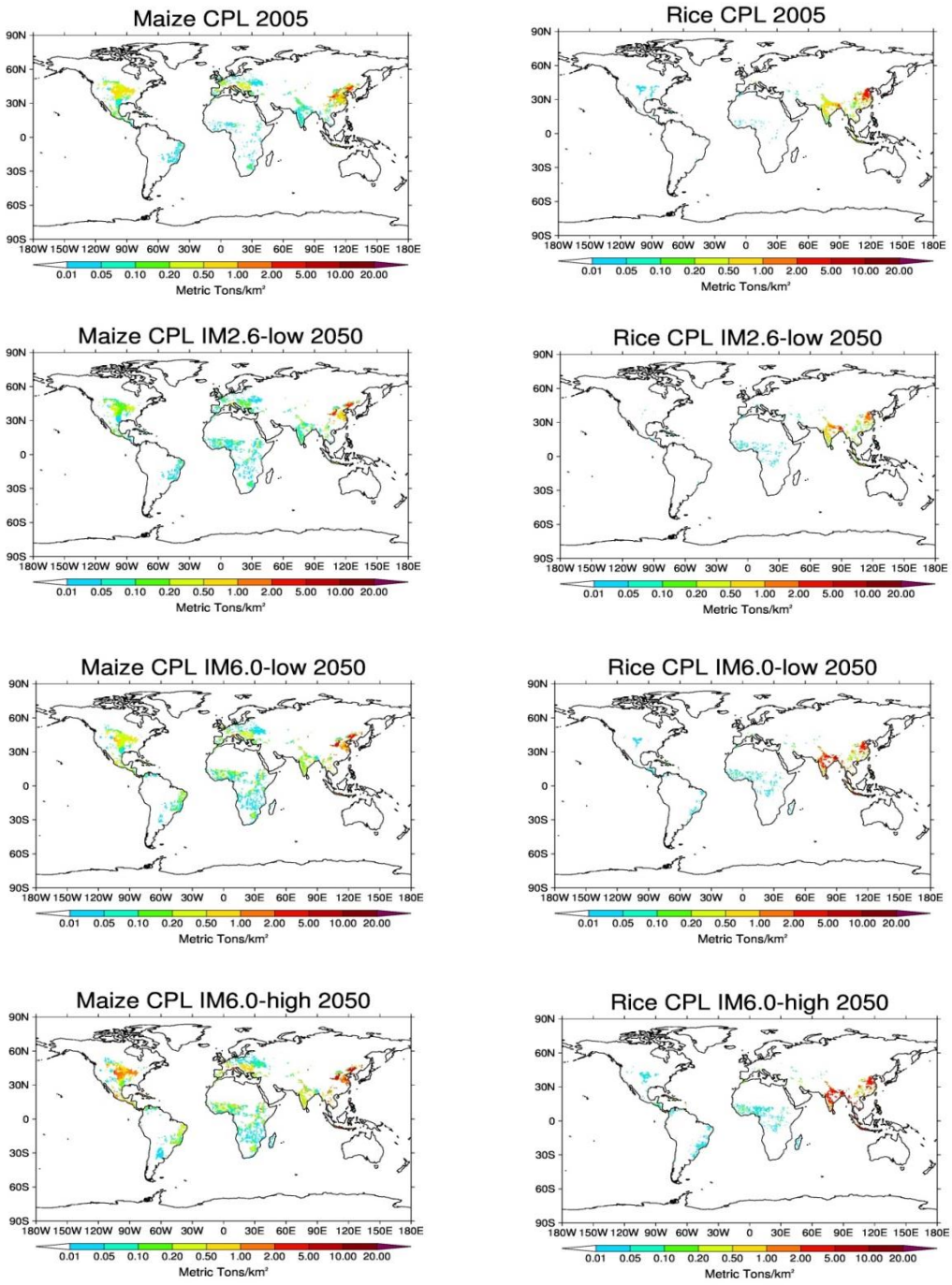

Fig. S5.5. Crop production loss (CPL) for 2005 and 2050, under IM2.6-low, IM6.0-low and IM6.0-high for maize and rice, for the case without bias correction.

CHAPTER 6

Synthesis

6.1 Overview of the research presented in this thesis

The research presented in this dissertation is aimed at exploring important relationships between anthropogenic activities and emissions of air pollutants on the one hand, and atmospheric composition and the response of the climate system on the other hand. We combined information from an integrated assessment model, a global chemistry transport model, and a global climate model to investigate the consequences of air pollution control for air quality, climate change, crop production and land use in the 21st century. In this concluding chapter we return to the research questions posed in Chapter 1 and address them using the results of the previous chapters. We also provide an outlook for future research.

Implications of alternative assumptions regarding future air pollution control in scenarios similar to the Representative Concentration Pathways

The Representative Concentration Pathways (RCPs) are a set of emission and concentration projections that were selected for use in the Coupled Model Intercomparison Project (CMIP5), which formed a key input to the Fifth Assessment Report (AR5) of the IPCC. The RCPs were selected to represent the full range of greenhouse gas emission, concentration and land-use scenarios in the literature. The whole set of information (i.e. emissions, concentration and climate outcomes) forms a major database for climate research and assessment by providing a wide set of possible trajectories for the 21st century, ranging from a stringent mitigation scenario to a very high level of climate change. The scenarios are also used for assessment of possible trajectories for air pollutants; however, it was found that the emission range for these specific species is limited. While the narrow range in the RCPs may well represent the most likely trajectories of future air pollutant emissions, it does not cover the extreme scenarios in which only few new air pollution control measures are introduced. In Chapter 2 we investigated how a wider range of assumptions on future air pollution policy could lead to different concentrations of air pollutants for two scenarios that in terms of the assumed climate policies are similar to RCP2.6 and RCP6.0.

In order to do so, we used the IMAGE integrated assessment model to produce low and high air pollution variants of the scenarios with radiative forcing targets of 2.6 W/m^2 and 6.0 W/m^2 in 2100, leading to a much broader range of possible outcomes with respect to the future evolution of air pollutants compared to the existing RCP scenarios. The TM5 model was used to estimate the effect of future emission changes on the concentrations of air pollutants, aerosol optical depth and associated global mean direct radiative forcing of the different air pollutants. *The results show that climate mitigation and air pollution control policies both have large-scale effects on pollutant concentrations. Regionally, the impacts*

are often of similar magnitude. In 2050, air pollution control is projected to change the combined global mean direct radiative forcing from methane, ozone and aerosols (mostly due to reductions in the sulphate). Clearly, if no further air pollution policies would be implemented, pollution levels could be considerably higher than in the RCPs in some parts of the world. For instance, in our most extreme scenario the annual mean surface concentrations of SO_4 are projected to increase by more than 25 $\mu g/m^3$ in India and China in 2050 relative to 2005. Further tightening of air pollution standards, notably in Asia, would be needed to avoid this. Also, the co-benefits of climate policy on air quality, by stimulating a transition towards a cleaner energy system, can contribute to achieving further improvement in air quality. For example, the stringent climate policy assumptions in the high mitigation scenarios could limit the increase in surface SO_4 concentrations to about 5 $\mu g/m^3$ in 2050 compared to 2005. Furthermore, the global climate effect of worldwide implementation of air pollution control is determined by the balance between the reduced warming by ozone and black carbon (BC) versus the reduced cooling by sulphate and the enhanced warming by methane. Interestingly, in the scenarios the overall impacts are much smaller than those for individual components due to a strong cancellation of the contributions of methane, ozone and aerosols to the total global mean direct radiative forcing. In the most extreme scenario, we estimate a net cooling effect of about -0.44 W/m^2 for aerosols which is partially offset by the warming of methane and ozone (0.41 W/m^2) resulting in a net total radiative forcing of about -0.033 W/m^2**.**

It is important to note that the simulations of future changes in the concentrations of air pollutants are based on present-day physical climate conditions. In reality, the future climate will change depending on the scenario assumed for emissions and land use, and this will have an effect on future air quality as well. Emission changes are nevertheless the most important driver of changes in tropospheric ozone and aerosols in the coming decades. The effects of climate change are still very uncertain and model dependent, but are generally expected to be smaller than emission changes (Stevenson et al., 2006; Lamarque et al., 2011; Fiore et al., 2012; Young et al., 2013).The adjusted radiative forcing shown in this chapter have their limitations, and these have been reexamined in chapter 4 where we used EC-Earth with fixed SSTs to calculate the radiative forcing.

Global and regional climate impacts of future aerosol mitigation in an RCP6.0-like scenario in EC-Earth

In Chapter 3 we evaluated the climate impacts of the different air pollution scenario assumptions made in Chapter 2, with focus on the effects of aerosols. To do so, we made long climate simulations for perpetual 2050 conditions, using the global atmosphere-ocean coupled climate model EC-Earth, which includes only aerosol direct radiative effects. In these simulations, the concentrations of sulphate and carbonaceous aerosols were prescribed based on the low and high air pollution variants of the RCP6.0-like scenario. Our primary objective was to investigate the long-term climate response to future changes in individual and combined anthropogenic aerosol components for different air pollution assumptions in the RCP6.0-like scenarios.

The results show that reduction of aerosol and precursor emissions through air pollution control measures result in significant brightening and warming at the surface in some parts of the tropics and NH mid-latitudes. The aerosol-induced brightening at the surface increases affects major climate patterns and diabatic heating in the tropics as evident in the changes in the Hadley cell circulation and associated changes in precipitation in the low latitudes. Our results show that the brightening at the surface, may reach about 10 W/m^2 most notably in Asia. This signal is dominated by the reduced cooling effect of sulphate which in some areas, is partially compensated by the decreased warming effect of black carbon. The mitigation of aerosols and concomitant brightening at the surface results in an increase of up to 0.5°C in surface temperature in parts of the North America, India and China.

Aerosol reductions can significantly affect the climate at high latitudes especially in the winter. The strong surface temperature response in the high latitudes is likely related to local ice albedo feedbacks and nonlocal effects through atmospheric teleconnections. Chapter 3 shows that part of the strong surface temperature response that is seen during the winter at the poles is likely related to the local ice albedo feedback carried over from the summer. The reduced sea ice cover in the summer enhances the warming of the ocean surface, which further enhances sea ice retreat and allows energy uptake by the ocean which is then released in the winter.

The results reveal increases in zonal mean precipitation of up to about 0.07 mm per day , especially in the NH tropics, which might cause anomalies in high-level wind divergence which acts as a Rossby wave source (Hoskins and Karoly, 1981). The results show that changes in aerosol concentrations alter the Hadley cell circulation, precipitation and cloud cover in the NH tropics. The simulated changes in the Hadley cell circulation in our coupled runs with EC-Earth are consistent with the changes found in previous studies (Ming and Ramaswamy, 2009; Yoshimori and Broccoli 2008, Ocko et al., 2014). The anomalies in geopotential height indicate a Pacific-North American (PNA) response in the Northern Hemisphere (see Wallace and Gutzler 1981).

Efficacy of aerosol forcings in an RCP6.0-like scenarios

The objective of Chapter 4 was to estimate the effectiveness of different aerosol components in causing climate change compared to carbon dioxide. To this end, we considered the same aerosol perturbations as in Chapter 3, and applied them in EC-Earth simulations with prescribed SSTs and sea ice. This allowed us to estimate the efficacies associated with the direct radiative forcing of sulphate and black carbon individually, as well as of a combined perturbation in sulphate and carbonaceous aerosols. Although a number of studies (Hansen et al., 2005; Yoshimori and Broccoli 2008; Kummer and Dessler, 2014) have estimated the efficacy of different aerosols forcing agents, the number of climate models for which such an analysis has been carried out is limited.

Our results reveal a broad range of efficacies for different anthropogenic aerosol components. The results show that the heterogeneous distribution of aerosol forcings evokes regional clouds feedbacks that cause the global mean surface temperature response to be

much different from that induced by a more uniformly distributed CO_2 forcing of the same overall magnitude. As such, the efficacies for the aerosol perturbations investigated here differ from unity. We find an aerosol efficacy of 286% for the combined aerosols, 112% for sulphate and 41% for black carbon.

We found higher radiative forcing (-0.22 Wm^{-2}) associated with these aerosols reductions in Chapter 2, based on a simple calculation following the MAGICC6 approach. In Chapter 2, we used present-day radiative forcing fields from Hansen et al. (2005) and applied a simple linear scaling based on the anthropogenic contributions to the optical depths of the different aerosol components as simulated by the TM5 model. The fixed SST forcing estimates obtained in Chapter 4 (about -0.007 Wm^{-2} for the combined aerosols) using fixed SST EC-Earth simulations are much lower than the adjusted forcing estimate obtained in chapter 2. Part of the difference between the adjusted and fixed SST forcings stem from the fact that the latter include more feedbacks compared to the former. Clearly, there are large model differences between EC-Earth and the GISS model used in Hansen et al. (2005) that might explain part of the differences between the estimated adjusted and fixed SST forcings. For instance, the scattering and absorption efficiencies per unit aerosol mass are likely to be different in both models due to differences in the way the aerosol optical properties are computed.

In our EC-Earth simulations in Chapter 3 and Chapter 4, we used prescribed monthly aerosols fields from the CAM model, and scaled the concentrations of sulphate, black carbon and organic aerosols from their CAM values for 2005 to the target values for 2050, using the corresponding concentration ratios simulated by TM5 model for the different scenarios. The use of prescribed monthly aerosol fields neglects correlations introduced by synoptic variability, for instance related to wet removal and interactions with clouds. This tends to decrease the simulated aerosol direct radiative effects under clear-sky conditions, and in the case of BC above clouds. It is important to note that other models in CMIP5 (Taylor et al., 2012) also used prescribed monthly aerosol fields and did not simulate aerosols interactively. Also, we did not take into consideration the nitrate aerosol forcing. The impact of nitrate on future climate will likely become more important, as ammonia emissions are projected to increase (van Vuuren et al., 2011). Bellouin et al. (2011) indicated that nitrate aerosols are likely to become the dominant aerosol component in Europe and Asia and decelerate the decrease in aerosol cooling on a global scale. Nitrate concentrations are quite difficult to model, especially with global models, because of the strongly localized pattern of ammonia emissions and the semi-volatile character of nitric acid.

The climate responses presented in Chapters 3 and 4 only take into account the direct radiative effects of the imposed aerosol changes. Aerosols also affect the climate indirectly by modulating cloud microphysical processes that influence cloud properties such as albedo, lifetime and precipitation efficiency (Boucher et al., 2013). Other studies (e.g. Kloster et al., 2010, Levy et al., 2013, Shindell et al., 2013, Boucher et al., 2013) have taken into account the indirect aerosol effects on cloud albedo and cloud lifetime. Including the aerosol indirect effect would likely make the sulphate effects more important relative to other aerosols like

black carbon. For instance, Levy et al. (2013) found that both the temperature and the precipitation show much stronger responses when aerosol indirect effects are included, but uncertainties on the physical processes and representation in numerical models are very large and require further research. The EC-Earth model used in chapters 3 and 4 has a higher spatial resolution than most climate models used in CMIP5 and represents dynamics better than most other models (see Zappa et al., 2013).

Global impacts of surface ozone changes on crop yields and land use

In Chapter 5 we estimated ozone impacts on crop production and subsequent impacts on land use in the 2005-2050 period using results of the TM5 atmospheric chemistry model and the IMAGE integrated assessment model. For the crops represented in IMAGE, we computed the relative yield losses based on published exposure-response functions. The main objective of this study was to estimate the impacts of future changes in surface ozone on agricultural yields and land use under different assumptions of future air pollution and climate policies. Although a number of studies (e.g. van Dingenen et al., 2009; Avnery et al., 2011) have looked at the impact of surface ozone on crops, hardly any attention has yet been paid to the subsequent impact on land use. We use the set of scenarios presented in Chapter 2 to assess the possible impacts of ozone concentration changes on future crop yields and consequently land use.

This study shows that the higher ozone concentrations resulting from the scenario without additional air pollution control or climate policy would lead to an increase in crop damage in 2050. Both air pollution policies or climate policies (through co-benefits) could limit crop yield losses due to ozone in the most affected regions as a result of lower emissions of ozone precursors. The increase in ozone induced crop damage resulting from the scenario assuming no improvement in current air pollution policies (IM6.0-high) in 2050 would be around 20% (up to 10 metric tons/km^2) for maize and rice in India and China relative to 2005. The implementation of air pollution policies (IM6.0-low) could limit future crop yield losses due to ozone to maximally 10% in the most affected regions in 2050. Reductions in crop yield losses can also be achieved as a result of co-benefits from implementing stringent climate policy. For instance, in Asia crop production loss decreases from a maximum of about 10 metric tons/km^2 to approximately 5 metric tons/km^2 following the implementation of climate policy. Interestingly, the co-benefit of climate policy in terms of reduced ozone-damage on crop yields can be of similar magnitude as the avoided crop damage as a direct result of the reduced temperature and precipitation change.

Ozone impacts on crops may also impact the land-use change and thus emissions from land use. If air pollution measures are not enforced as assumed in the IM6.0-high scenario, crop yield losses due to ozone changes would require an increase in global crop area of approximately 1.3 million km^2 in 2050 in order to produce the same amount of food. However, the development of less sensitive ozone cultivars will likely result in a decrease in crop area needed to produce a given amount of food. The implementation of current and planned air pollution legislation until 2030, and additional abatement measures thereafter as assumed under IM6.0-low, have a clear yield impact in Asia and smaller impacts in other

parts of the world. Assuming that the same amount of food is produced, the abatement policies would reduce crop area in 2050, mostly in Asia. The indirect impact of ozone on land use under the high mitigation scenarios (IM2.6-low) is small because the stringent climate and air pollution policies measures assumed under these scenario. Although the high climate mitigation scenario requires less land in response to ozone damage, it needs more land use for bio-energy production that forms part of the mitigation portfolio. In IMAGE, bio-energy crops are cultivated mostly on abandoned agricultural land and grassland. This occurs mainly in the Organisation for Economic Co-operation and Development (OECD) countries and the former Soviet Union in the first half of the century (see van Vuuren et al., 2007).

The possible feedback of changes in ozone concentrations on land-use related CO_2 emissions was found to be rather small in most parts of the globe. The highest increase in the cumulative CO_2 emissions between 2005 to 2050 due to the impacts of ozone changes on crops is found for the IM6.0-high scenario, where we estimate an increase of about 3.7 Pg C compared to the case without ozone changes, which is 1 Pg C of total CO_2 emission during this period. However, in Asia a significant increase of the cumulative CO_2 emissions from land use can be noticed due the impacts of ozone increases under both the IM6.0-low and IM6.0-high scenarios.

In the calculation of the ozone impact on the different crop types in IMAGE, we made use of the exposure-based approach which has been widely used to assess ozone damage on crops. The applicability of this approach is limited, however, because it does not explicitly take into account crucial environmental factors (e.g. temperature, water availability and plant defence), which are important in assessing the rate of ozone uptake by plants and the subsequent impact. As such, a mechanistic flux-based method has been developed in recent years (Sitch et al., 2007, Yue and Unger, 2014), where crop yield loss is calculated from the flux of ozone through the stomata. Flux-based methods are not yet suitable for the kind of large-scale assessment of crop losses undertaken in this study because of lack of sufficiently reliable data to characterize plant sensitivities (Avnery et al., 2011; Van Dingenen et al., 2009). More so, experimental data needed for the computation of ozone stomatal flux are only available for a limited number of crops.

One of the major sources of uncertainty relates to biases in the simulated ground-level ozone concentrations. We applied a bias correction to the model-based ozone indicators in Europe and the US, where we found reliable ground measurement data. In other regions, our calculation of the present-day ozone impacts on crop production are affected by model biases. The bias correction effect is generally smaller than the bias itself because the present-day bias and future bias partially offset each other.

6.2 Further research

The research presented in this dissertation aimed to explore some important linkages between anthropogenic activities and the atmospheric composition and climate system and crop yield loss. Further research could be geared toward expanding the research on feedbacks and linkages between IAMs and ESMs in a more consistent way. Firstly, the consistent modelling

framework we used, from the IAM (IMAGE) to the CTM (TM5) to the ESM (EC-Earth), and also back to the IAM, should be extended to other models. The results of such studies can then be compared to those reported in this thesis to see if they have similar behaviour like the models used in this study. This can provide the foundation for further development of ESM and IAM coupling in a more robust framework.

Secondly, there are additional feedbacks and linkages between IAMs and ESMs (e.g. see van Vuuren et al., 2012) that have not yet been evaluated and need further investigation. For instance, Isaac and van Vuuren (2009) showed that climate change could lead to a decrease energy demand for heating and an increase in demand for energy for cooling. A first calculation showed that the additional GHG emissions from the energy demand associated with these changes are small. However, apart from GHGs, future changes in energy demand as a resulting changing heating and cooling patterns are expected to give rise to changes in the emissions of air pollutants. Due to their inhomogeneous spatial distributions, their impacts on regional climate as shown in Chapter 4 can be much larger.

The results presented in Chapter 2 can be extended to include the impact of future changes in climate on air pollution levels and the impact of climate change on biogenic VOC and other natural emissions. This would require an interactive simulation of atmospheric chemistry and aerosols, as has recently become possible through integration of TM5 in EC-Earth (van Noije et al., 2014). Such a simulation will also enable a more consistent simulation of the climate effects of aerosols (Chapter 3 and Chapter 4). Such simulations are planned for the upcoming CMIP6 simulations. The new EC-Earth version that will be used for CMIP6 will include both aerosol-radiation interactions and aerosol-cloud interactions. It is important to note that the computation of aerosol forcing in climate models is still associated with large uncertainties (Boucher et al., 2013 and references therein). For instance, Stevens et al. (2015) showed that climate models can still not adequately simulate the aerosol forcings over the historical period. As such, further improvements in aerosols models are required.

In the future, a more mechanistic flux based approach should be used to assess the ozone impact on crops in place of the exposure-response approach used in this thesis (Chapter 5). In EC-Earth, such an approach can be made possible by coupling TM5 to the dynamic vegetation model LPJ-GUESS (Smith et al., 2014). This will also make it possible to simulate the impact of ozone on natural vegetation, which likely presents a significant climate forcing, as illustrated by Sitch et al. (2007). To be able to do so, additional experimental data would be needed for the computation of the ozone stomatal flux, which are currently only available for a limited number of crops.

Future efforts to fully coupled IAMs and ESM would have to balance the competing needs between scientific and policy oriented assessment. For instance, a coupled IAMs-ESMs meant to be used as a policy tool need to be computationally efficient to allow multiple experiments assessing different policy options to be performed in the shortest time possible, while coupled IAMs-ESMs system to be used as a scientific tool require more details and may operate much slower. The appropriate level of details such as the spatial scale of the

assessment and the degree of parametrization of the physical process modelled to be included must be defined at each stage of the integration.

In this dissertation, we have indicated that there is a need for further integration of IAMs and ESMs research efforts to better understand interactions between human activities and the climate system. Further cooperation between IAM and ESM research communities in the future is likely to give rise to more complex model linkages. While the full integration of IMAGE and EC-Earth would enable more consistent simulations, it would also result in a more complex modelling framework with less flexibility and less opportunities for exploring uncertainty. Simplified couplings of IAMs and ESMs components might therefore be sufficient to investigate many of the existing linkages and feedbacks of interest to climate research.

Acknowledgements

This thesis would not be complete without expressing my gratitude to my supervisors, colleagues, friends and family who contributed in different ways toward the completion of this thesis.

Firstly, a big thank you to my supervisor Twan van Noije and promotors Wilco Hazeleger and Detlef van Vuuren for the many useful comments and constructive criticisms in the course of my PhD. I am also grateful for the efforts you put in reading my manuscripts and the feedbacks you gave were very helpful. Secondly, I wish to express my sincere gratitude to Philippe Le Sager and Oostenrijk Rineke for their technical support. Special thanks to some of my colleagues for their insightful suggestions and valuable comments on my work. A big thank you to all my colleagues who made my time at the KNMI and PBL enjoyable.

Finally, my heartfelt thanks to my friends for their encouragement and support throughout my PhD. A big thank you to my family for providing me with the foundation and showing interest in my studies and work.

References

Van Aardenne, J., Dentener, F., Van Dingenen, R., Maenhout, G., Marmer, E., Vignati, E., Russ, P., Szabo, L., 2010. Climate and air quality impacts of combined climate change and air pollution policy scenarios. Joint Research Centre Scientific and Technical Research Reports, EUR 24572 EN, 71 pp.

Alcamo J., Leemans, R., Kreilemen, E. (Eds.), 1998. Global change scenarios of the 21st century. Results from the IMAGE 2.1 model. Elsevier Science, Oxford.

Alcamo, J., Kreileman, G.J.J., Krol, M.S., Zuidema, G., 1994. Modeling the global society-biosphere-climate system: Part 1: Model description and testing. Water Air and Soil Pollution 76, 1–35.

Aunan, K., Berntsen, T.K., Seip, H.M., 2000. Surface ozone in China and its possible impact on agricultural crop yields. A Journal of the Human Environment 29, 294–301.

Averny, S., Mauzerall, D., Liu, J., Horowitz, L.W., 2011a. Global crop yield reductions due to surface ozone exposure: 1. Year 2000 crop production losses and economic damage. Atmospheric Environment 45, 2284–2296.

Averny, S., Mauzerall, D., Liu, J., Horowitz, L.W., 2011b. Global crop yield reductions due to surface ozone exposure: 2. Year 2030 potential crop production losses and economic damage under two scenarios of O3 pollution. Atmospheric Environment 45, 2297–2309.

Avnery, S., Mauzerall, D., Fiore, A.M., 2013. Increasing global agricultural production by reducing ozone damages via methane emission controls and ozone resistance. Global Change Biology 19, 1285–1299.

Bellouin, N., Rae, J., Jones, A., Johnson, C., Haywood, J., Boucher O., 2011. Aerosol forcing in the Climate Model Intercomparison Project (CMIP5) simulations by HadGEM2-ES and the role of ammonium nitrate, Journal of Geophysical Research-Atmospheres 116, D20206.

De Bock, M., Op de Beeck, M., De Temmerman, L., Guisez, Y., Ceulemans, R., Vandermeiren, K., 2011. Ozone dose-response relationships for spring oilseed rape and broccoli, Atmospheric Environment 45, 1759–1765.

Bollasina, M.A., Ming, Y., Ramaswamy, V., Schwarzoopf, M.D., Nalk, V., 2014. Contribution of local and remote aerosols to the twentieth century weakening of the South Asia Monsoon, Geophysical Research Letter 41, 680–687.

Bond, T.C., Doherty, S.J., Fahey, D.W., Forster, P.M., Berntsen, T., DeAngelo, B.J., Flanner, M.G., Ghan, S., Kärcher, B., Koch, D., Kinne, S., Kondo, Y., Quinn, P.K., Sarofim, M.C., Schultz, M.G., Schulz, M., Venkataraman, C., Zhang, H., Zhang, S., Bellouin, N., Guttikunda, S.K., Hopke, P.K., Jacobson, M.Z., Kaiser, J.W., Klimont, Z., Lohmann, U., Schwarz, J.P., Shindell, D., Storelvmo, T., Warren, S.G., Zender, C.S., 2013. Bounding the role of black carbon in the climate system: A scientific assessment. Journal of Geophysical Research 118, 1–173.

Bondeau, A., Smith, P.C., Zaehle S., Schaphoff, S., Lucht, W., Cramer, W., Gerten D.E., Lotze-Campen, H., Muller, C., Reichstein, M., Smith, B., 2007. Modelling the role of

agriculture for the 20th century global terrestrial carbon balance, Global change Biology 13,679–706.

Boucher, O., Randall, D., Artaxo, P., Bretherton, C., Feingold, G., Forster, P., Kerminen, V-M., Kondo, Y., Liao, H., Lohmann, U., Rasch, P., Satheesh, S.K., Sherwood, S., Stevens, B., Zhang X.Y., 2013. Clouds and Aerosols Climate Change 2013: The Physical Science Basis, edited by Stocker T.F., Qin, D., Plattner G.-K., Tignor, M., Allen, S.K., Boschung, J., Nauels, A., Xia, Y., Bex, V., Midgley, P.M., pp. 571–657, Cambridge University Press, Cambridge, United Kingdom and New York, NY, USA.

Bouwman, A.F., Kram, T., Klein Goldewijk, K., 2006. Integrated modelling of global environmental change. An overview of IMAGE 2.4. Netherlands Environmental Assessment Agency (MNP), Bilthoven, The Netherlands.

Aan de Brugh, J.M.J., Schaap, M., Vignati, E., Dentener, F., Kahnert, M., Sofiev, M., Huijnen, V., Krol, M.C., 2010. The European aerosol budget in 2006. Atmospheric Chemistry and Physics 11, 1117–1139.

Aan de Brugh, J.M.J., 2013. The Generic Aerosol Optics Toolbox: an aerosol optics module for any atmospheric model, in: Aerosol processes relevant for the Netherlands, Ph.D. thesis, Wageningen University, Wageningen, The Netherlands, pp. 117-134.

Bruinsma, J.E. (Eds.), 2003. World Agriculture: Towards 2015/2030. An FAO Perspective. Earthscan, London.

Chalmers, N., Highwood, E.J., Hawkins, E., . Sutton, T., Wilcox L.J., 2012. Aerosol contribution to the rapid warming of near-term climate under RCP2.6, Geophysical Research Letter 39(18), L18709.

Charlson, R.J., Langner, J., Rodhe H., 1990. Sulphate aerosol and climate, Nature 348, 22.

Charlson, R.J., Langner, J., Rodhe, H., Leovy, C.B., Warren S.G., 1991. Perturbation of the northern hemispheric radiative balance by backscattering from anthropogenic sulfate aerosol, Tellus 43(AB), 152–163.

Charlson, R. J., Schwartz, S. E., Hales, J. M., Cess, R. D., Coakley, J. A. Jr., Hansen, J. E., Hofmann, D. J., 1992. Climate Forcing by Anthropogenic Aerosols. Science 255, 423–430.

Chen, W.-T., Liao, H., Seinfeld, J. H., Future climate impacts of direct radiative forcing of anthropogenic aerosols, tropospheric ozone, and long-lived greenhouse gases, Journal of Geophysical Research 112, D14209.

Ciais, P., Sabine, C., Bala, G., Bopp, L., Brovkin, V., Canadell, J., Chhabra, A., De Fries, R., Galloway, J., Heimann, M., Jones, C., Le Quéré, C., Myneni, R.B., Piao S., Thornton, P., 2013. Carbon and Other Biogeochemical Cycles. In: Climate Change 2013: The Physical Science Basis. Contribution of Working Group I to the Fifth Assessment Report of the Intergovernmental Panel on Climate Change. Stocker, T.F., Qin, D., Plattner, G.-K., Tignor, M., Allen, S.K., Boschung, J., Nauels, A., Xia, Y., Bex V., Midgley P.M. (Eds.), Cambridge University Press, Cambridge, United Kingdom and New York, NY, USA.

Dee, D.P., Uppala, S.M., Simmons, A.J., Berrisford, P., Poli, P., Kobayashi, S., Andrae, U., Balmaseda, M.A., Balsamo, G., Bauer, P., Bechtold, P., Beljaars, A.C.M., van de Berg, L., Bidlot, J., Bormann, N., Delsol, C., Dragani, R., Fuentes, M., Geer, A.J., Haimberger, L., Healy, S.B., Hersbach, H., Hólm, E.V., Isaksen, L., Kållberg, P.,

Köhler, M., Matricardi, M., McNally, A.P., Monge-Sanz, B.M., Morcrette, J.-J., Park, B.-K., Peubey, C., De Rosnay, P., Tavolato, C., Thépaut, J.-N., Vitart, F., 2011. The ERA-Interim reanalysis: configuration and performance of the data assimilation system. Quarterly Journal of the Royal Meteorological Society 137, 553–597.

Dentener, F., Stevenson, D., Ellingsen, K., van Noije, T., Schultz, M., Amann, M., Atherton, C., Bell, N., Bergmann, D., Bey, I., Bouwman, L., Butler, T., Cofala, J., Collins, B., Drevet, J., Doherty, R., Eickhout, B., Eskes, H., Fiore, A., Gauss, M., Hauglustaine, D., Horowitz, L., Isaksen, I.S.A., Josse, B., Lawrence, M., Krol, M., Lamarque, J.F., Montanaro, V., Müller, J.F., Peuch, V.H., Pitari, G., Pyle, J., Rast, S., Rodriguez, J., Sanderson, M., Savage, N.H., Shindell, D., Strahan, S., Szopa, S., Sudo, K., Van Dingenen, R., Wild, O., Zeng, G., 2006a. The global atmospheric environment for the next generation. Environmental Science and Technology 40, 3586–3594.

Dentener, F., Kinne, S., Bond, T., Boucher, O., Cofala, J., Generoso, S., Ginoux, P., Gong, S., Hoelzemann, J.J., Ito, A., Marelli, L., Penner, J.E., Putaud, J.-P., Textor, C., Schulz, M., Van der Werf, G.R., Wilson, J., 2006b. Emissions of primary aerosol and precursor gases in the years 2000 and 1750 prescribed data-sets for AeroCom. Atmospheric Chemistry and Physics 6, 4321–4344.

Van Dingenen, R., Dentener, F.J., Raes, F., Krol, C.K., Emberson, L., Janusz, C., 2009. The global impact of ozone on agricultural crop yields under current and future air quality legislation. Atmosphere Environment 43, 604–618.

Easterling, W.E., Aggarwal, P.K, Batima, P., Brander, K.M., Erda, L., Howden, S.M., Kirilenko, A., Morton, J., Soussana, J.-F., Schmidhuber J., Tubiello, F.N., 2007. Food, fibre and forest products. In: Climate Change 2007: Impacts, Adaptation and Vulnerability. Contribution of Working Group II to the Fourth Assessment Report of the Intergovernmental Panel on Climate Change, Parry, M.L., Canziani, O.F., Palutikof, J.P., van der Linden P.J., Hanson, C.E. (Eds.), Cambridge University Press, Cambridge, UK, 273-313.

Ehhalt, D., Prather, M.J., Dentener, F., Derwent, R., Dlugokencky, E., Holland, E., Isaksen, I., Katima, J., Kirchhoff, V., Matson, P., Midgley, P., Wang, M., 2001. Atmospheric Chemistry and Greenhouse Gases, in: Houghton J.T., Ding, Y., Griggs, D.J., Noguer, M., van der Linden, P.J., Dai. X., Maskell, K., Johnson, C.A. (Eds.), Climate Change 2001: The Scientific Basis. Contribution of Working Group I to the Third Assessment Report of the Intergovernmental Panel on Climate Change, Cambridge University Press, Cambridge, United Kingdom and New York, NY, USA, pp. 239–287.

Ehrlich, P., Holdren, J., 1971. Impact of population growth. Science 171, 1212–1217.

Ellingsen, K., Gauss, M., Van Dingenen, R., Dentener, F.J., Emberson, L., Fiore, A.M., Schultz, M.G., Stevenson, D.S., Ashmore, M.R., Atherton, C.S., Bergmann, D.J., Bey, I., Butler, T., Drevet, J., Eskes, H., Hauglustaine, D.A., Isaksen, I.S.A., Horowitz, L. W., Krol, M., Lamarque, J.F., Lawrence, M.G., van Noije, T., Pyle, J., Rast, S., Rodriguez, J., Savage, N., Strahan, S., Sudo, K., Szopa, S., Wild, O., 2008. Global ozone and air quality: A multi-model assessment of risks to human health and crops. Atmospheric Chemistry and Physics Discussion 8, 2163–2223.

Den Elzen, M.G.J., van Vuuren, D.P., 2007. Peaking profiles for achieving long-term temperature targets with more likelihood at lower costs. Proceedings of the National Academy of Sciences of the United States of America 104, 17931–17936.

Emberson, L.D., Ashmore, M.R., Cambridge, H.M., Simpson, D., Tuovinen J.-P., 2000. Modelling stomatal ozone flux across Europe, Environmental Pollution 109, 403–413.

Emberson, L.D., Büker, P., Ashmore, M.R., Mills, G., Jackson, L.S., Agrawal, M., Atikuzzaman, M.D., Cinderby, S., Engardt, M., Jamir, C., Kobayashi, K., Oanh, N.T.K., Quadir, Q.F., Wahid, A., 2009. A comparison of North American and Asian exposure-response data for ozone effects on crop yields, Atmospheric Environment 43, 1945–1953.

FAO, 1978. Report on the agro-ecological zones project, Vol. 3, Methodology and results for South and Central America. Food and Agricultural Organization of the United Nations, World Soil Resources Report 48, Rome.

Fiore, A.M., Naik, V., Spracklen, D.V., Steiner, A., Unger, N., Prather, M., Bergmann, D., Cameron-Smith, P.J., Cionni, I., Collins, W.J., Dalsøren, S., Eyring, V., Folberth, G.A., Ginoux, P., Horowitz, L.W., Josse, B., Lamarque, J.-F., MacKenzie, I.A., Nagashima, T., O'Connor, F.M., Righi, M., Rumbold, S.T., Shindell, D.T., Skeie, R.B., Sudo, K., Szopa, S., Takemura, T., Zeng, G., 2012. Global air quality and climate. Chemical Society Review 41, 6663–6683.

Frankhauser, S., Tol, R.S.J., 2005. On climate change and economic growth, Energy Economics 27, 1–17.

Forster, P., Ramaswamy, V., Artaxo, P., Berntsen, T., Betts, R., Fahey, D.W., Haywood, J., Lean, J., Lowe, D.C., Myhre, G., Nganga, J., Prinn, R., Raga, G., Schulz M., Van Dorland, R., 2007. Changes in Atmospheric Constituents and in Radiative Forcing. In: Climate Change 2007: The Physical Science Basis. Contribution of Working Group I the Fourth Assessment Report of the Intergovernmental Panel on Climate Change, edited by Solomon, S., Qin, D., Manning, M., Chen, Z., Marquis, M., Averyt, K.B., Tignor M., Miller H.L., Cambridge University Press, Cambridge, United Kingdom and New York, NY, USA.

Fuhrer, J., Skärby, L., Ashmore, M.R., 1997. Critical levels for ozone effects on vegetation in Europe. Environmental Pollution 97, 91–106.

Fuhrer, J., 2009. Ozone risk for crops and pastures in present and future climates. Naturwissenschaften 96, 173–194.

Ganzeveld, L., Bouwman, L., Eickhout, B., Lelieveld, J., Stehfest, E., van Vuuren, D.P., 2010. The impact of land use and land cover changes on atmospheric chemistry–climate interactions, Journal of Geophysical Research, 115, D23301.

Gillett, N.P., Von Salzen K., 2013. The role of reduced aerosol precursor emissions in driving near-term warming, Environmental Research Letter, 8, 034008.

González-Fernández, I., Bass, D., Muntifering, R., Mills, G., Barnes, J., 2008. Impacts of ozone pollution on productivity and forage quality of grass/clover swards, Atmospheric Environment 42, 8755–8769.

Granier, C., Bessagnet, B., Bond, T., D'Angiola, A., Denier van der Gon, H., Frost, G.J., Heil, A., Kainuma, M., Kaiser, J., Kinne, S., Klimont, Z., Kloster, S., Lamarque, J.-F., Liousse, C., Matsui, T., Meleux, F., Mieville, A., Ohara, T., Raihi, K., Schultz, M.,

Smith, S.J., Thomson, A.M., van Aardenne, J., van der Werf, G., 2011. Evolution of anthropogenic and biomass burning emissions of air pollutants at global and regional scales during the 1980–2010 period, Climatic Change 109, 163–190.

Grantz, D., and Vu, H., 2009. O_3 sensitivity in a potential C_4 bioenergy crop: Sugarcane in California. Crop Science 49, 643–650.

Gery, M., Whitten, G.Z., Killus, J.P., Dodge, M.C., 1989. A photochemical kinetics mechanism for urban and regional scale computer modeling. Journal of Geophysical Research 94, 18925–18956.

Guenther, A.B., Jiang, X., Heald, C.L., Sakulyanontvittaya, T., Duhl, T., Emmons, L.K., Wang, X., 2012. The Model of Emissions of Gases and Aerosols from Nature version 2.1 (MEGAN2.1): an extended and updated framework for modeling biogenic emissions, Geoscientic Model Development 5, 1471–1492.

Hansen, J., Johnson, D., Lacis, A., Lebedeff, S., Lee, P., Rind, D., Russell G., 1981. Climate impact of increasing atmospheric carbon dioxide, Science 213, 957–966.

Hansen, J., Sato, M., Ruedy, R., Nazarenko, L., Lacis, A., Schmidt, G.A., Russell, G., Aleinov, I., Bauer, M., Bauer, S., Bell, N., Cairns, B., Canuto, V., Chandler, M., Cheng, Y., Del Genio, A., Faluvegi, G., Fleming, E., Friend, A., Hall, T., Jackman, C., Kelley, M., Kiang, N., Koch, D., Lean, J., Lerner, J., Lo, K., Menon, S., Miller, R., Minnis, P., Novakov, T., Oinas, V., Perlwitz, J., Perlwitz, J., Rind, D., Romanou, A., Shindell, D., Stone, P., Sun, S., Tausnev, N., Thresher, D., Wielicki, B., Wong, T., Yao, M., Zhang, S., 2005. Efficacy of climate forcing. Journal of Geophysical Research 110, D18104.

Hansen, J., Ruedy, R., Sato, M., Lo, K., 2010. Global surface temperature change. Reviews of Geophysics 48, RG4004.

Hartmann, D.L., Klein Tank, A.M.G., Rusticucci, M., Alexander, L.V., Bronnimann, S., Charabi, Y., Dentener, F.J., Dlugokencky, E.J., Easterling, D.R., Kaplan, A., Soden, B.J., Thorne, P.W., Wild M., Zhai, P.M., 2013. Observations: Atmosphere and Surface. In: Climate Change 2013: The Physical Science Basis, edited by Stocker T.F., Qin, D., Plattner G.-K., Tignor, M., Allen, S.K., Boschung, J., Nauels, A., Xia, Y., Bex, V., Midgley, P.M., pp. 571–657, Cambridge University Press, Cambridge, United Kingdom and New York, NY, USA.

Heck, W.W., Adams, R.M., Cure, W.W., Heagle, A.S., Heggestad, H.E., Kohut, R.J., Kress, L.W., Rawlings, J.O., Taylor, O.C., 1983. A reassessment of crop loss from ozone, Environmental Science and Technology 17, 572A–581A.

Hess, M., Koepke, P., Schult, I., 1998. Optical Properties of Aerosols and Clouds: The software package OPAC. Bulletin of the American Meteorological Society 79, 831–844.

Huijnen, V., Williams, J., van Weele, M., van Noije, T., Krol, M., Dentener, F., Segers, A., Houweling, S., Peters, W., de Laat, J., Boersma, F., Bergamaschi, P., van Velthoven, P., Le Sager, P., Eskes, H., Alkemade, F., Scheele, R., Nédélec, P., Pätz, H.-W., 2010. The global chemistry transport model TM5: description and evaluation of the tropospheric chemistry version 3.0. Geoscientific Model Development 3, 445–473.

Hazeleger, W., X. Wang, Severijns, C., Stefanescu, S., Bintanja, R., Sterl, A., Wyser, K., Semmler, T., Yang, S., van den Hurk, B., van Noije, T., van der Linden, E., van der Wiel K., 2012. EC-Earth V2.2: description and validation of a new seamless Earth system prediction model, Climate Dynamics, 39, 2611–2629.

Heck, W.W., Adams, R.M., Cure, W.W., Heagle, A.S., Heggestad, H.E., Kohut, R.J., Kress, L.W., Rawlings, J.O., Taylor, O.C., 1983. A reassessment of crop loss from ozone, Environmental Science and Technology 17, 572A–581A.

Hoskins, B.J., Karoly D.J., 1981. The steady linear responses of a spherical atmosphere to thermal and orographic forcing. Journal of Atmospheric Sciences, 38, 1179–1196.

Huijnen, V., Williams, J., van Weele, M., van Noije, T., Krol, M., Dentener, F., Segers, A., Houweling, S., Peters, W., de Laat, J., Boersma, F., Bergamaschi, P., van Velthoven, P., Le Sager, P., Eskes, H., Alkemade, F., Scheele, R., Nédélec, P., Pätz, H.-W., 2010. The global chemistry transport model TM5: description and evaluation of the tropospheric chemistry version 3.0, Geoscience. Model Development, 3, 445-473.

IPCC 2013. Climate Change 2013: The Physical Science Basis. Contribution to Working Group I to the Fifth Assessment Report of the Intergovernmental Panel on Climate Change, edited by Stocker T.F., Qin, D., Plattner G.-K., Tignor, M., Allen, S.K., Boschung, J., Nauels, A., Xia, Y., Bex, V., Midgley, P.M., Cambridge University Press, Cambridge, United Kingdom and New York, NY, USA.

Isaac, M., van Vuuren, D.P., 2009. Modeling global residential sector energy demand for heating and air conditioning in the context of climate change. Energy Policy 37, 507–521.

Jones, P. D., Lister, D. H., Osborn, T. J., Harpham, C., Salmon, M., Morice, C. P., 2012: Hemispheric and large-scale land-surface air temperature variations: An extensive revision and an update to 2010. Journal of Geophysical Research Atmosphere, 117, D05127.

Karenlampi, L., Skärby, L. (Eds.), 1996. Critical levels for ozone in Europe: testing and finalizing the concepts. UN-ECE workshop report. Department of Ecology and Environmental Science, University of Kuopio.

Karlsson, P.E., Braun, S., Broadmeadow, M., Elvira, S., Emberson, L., Gimeno, B.S., Le Thiec, D., Novak, K., Oksanen, E., Schaub, M., Uddling, J., Wilkinson, M., 2007. Risk assessments for forest trees: The performance of the ozone flux versus the AOT concepts, Environmental Pollution 146, 608–616.

Kiehl, J.T., Briegleb B.P., 1993. The relative role of sulfate aerosols and greenhouse gases in climate forcing, Science 260, 311–314.

Kinne, S., Lohmann, U., Feichter, J., Schulz, M., Timmreck, C., Ghan, S., Easter, R., Chin, M., Ginoux, P., Takemura, T., Tegen, I., Koch, D., Herzog, M., Penner, J., Pitari, G., Holben, B., Eck, T., Smirnov, A., Dubovik, O., Slutsker, I., Tanre, D., Torres, O., Mishchenko, M., Geogdzhayev, I., Chu, D.A., Kaufman, Y., 2003. Monthly averages of aerosol properties: A global comparison among models, satellite data and AERONET ground data. Journal of Geophysical Research 108, 4634.

Kim, D., Wang, C., Ekman, A.M. L., Barth M. C., Lee, D.-I. , 2014. The responses of cloudiness to the direct radiative effect of sulfate and carbonaceous aerosols, Journal of Geophysical Research 119, 1172–1185.

Klein Goldewijk, K., van Minnen, J.G., Kreileman, G.J.J., Vloedbeld, M., Leemans, R., 1994. Simulation of the carbon flux between the terrestrial environment and the atmosphere. Water Air and Soil Pollution 76, 199–230.

Kloster, S., Dentener, F., Feichter, J., Raes, F., van Aardenne, J., Roeckner, E., Lohmann, U., Stier, P., Swart, R., 2008. Influence of future air pollution mitigation strategies on total aerosol radiative forcing. Atmospheric Chemistry and Physics 8, 6405–6437.

Kloster, S., Dentener, F., Feichter, J., Raes, F., Lohmann, U., Roeckner, E., Fischer-Bruns I., 2010. A GCM study of future climate response to aerosol pollution reductions, Climate Dynamics 34, 1177–1194.

Koornneef, J., Ramirez, A., van Harmelen, T., 2010. The impact of CO_2 capture in the power and heat sector on the emission of SO_2, NO_x, particulate matter, volatile organic compounds and NH_3 in the European Union. Atmospheric Environment 44, 1369–1385.

Kriegler, E., O'Neill, B., Hallegatte, S., Kram, T., Lempert, R., Moss, R., Wilbanks, T., 2011. Socioeconomic scenario development for climate change analysis, Centre International de Recherches sur l'Environnement et le D´eveloppement (CIRED) Working Paper, Paris.

Kummer, J.R., Dessler, A.E., 2014. The Impact of forcing efficacy on the equilibrium climate sensitivity. Geophysical Research Letter 41, 3565–3568.

Lacagnina,C., Selten, F., Siebesma A.P., 2014. Impact of changes in the formulation of cloud-related processes on model biases and climate feedbacks, Journal of Advances in Modelling Earth System 6, 1224–1243.

Lathière, J., Hauglustaine, D.A., Friend, A.D., De Noblet-Ducoudré, N., Viovy, N., Folberth, G.A., 2006. Impact of climate variability and land use changes on global biogenic volatile organic compound emissions, Atmospheric Chemistry and Physics 6, 2129–2146.

Lamarque, J.-F., Bond, T.C., Eyring, V., Granier, C., Heil, A., Klimont, Z., Lee, D., Liousse, C., Mieville, A., Owen, B., Schultz, M.G., Shindell, D., Smith, S.J., Stehfest, E., Van Aardenne, J., Cooper, O.R., Kainuma, M., Mahowald, N., McConnell, J.R., Naik, V., Riahi, K., van Vuuren D.P., 2010. Historical (1850–2000) gridded anthropogenic and biomass burning emissions of reactive gases and aerosols: methodology and application, Atmospheric Chemistry and Physics 10, 7017–7039.

Lamarque, J.-F., Page Kyle, G., Meinshausen, M., 2011. Global and regional evolution of short-lived radiatively-active gases and aerosols in the Representative Concentration Pathways. Climatic Change 109, 191–212.

Lamarque, J.-F., Shindell, D.T., Josse, B., Young, P.J., Cionni, I., Eyring, V., Bergmann, D., Cameron-Smith, P., Collins, W.J., Doherty, R., Dalsoren, S., Faluvegi, G., Folberth, G., Ghan, S.J., Horowitz, L.W., Lee, Y.H., MacKenzie, I.A., Nagashima, T., Naik, V., Plummer, D., Righi, M., Rumbold, S.T., Schulz, M., Skeie, R.B., Stevenson, D.S., Strode, S., Sudo, K., Szopa, S., Voulgarakis, A., Zeng, G., 2013. The Atmospheric Chemistry and Climate Model Intercomparison Project (ACCMIP): overview and description of models, simulations and climate diagnostics. Geoscientific Model Development 6, 179–206.

Leemans R., Solomon A.M., 1993. Modeling the potential change in yield and distribution of the earth's crops under a warmed climate. Climate Research 3, 79–96.

Leemans R, van der Born G.J., 1994. Determining the potential global distribution of natural vegetation, crops and agricultural productivity. Water Air and Soil Pollution 76, 133–161.

Levy, H., Horowitz, L., Schwarzkopf, M., Ming, Y., Golaz, J., Naik, V., Ramaswamy V., 2013. The roles of aerosol direct and indirect effects in past and future climate change, Journal of Geophysical Research-Atmospheres, 118, 4521–4532.

Lucas, P.L., van Vuuren, D.P., Olivier, J.G.J., den Elzen, M.G.J., 2007. Long-term reduction potential of non-CO_2 greenhouse gases. Environmental Science and Policy 10, 85–103.

Madec, G., 2008. NEMO ocean engine. Note du Pole de modelisation (Institut Pierre-Simon Laplace), France, No. 27 ISSN No. 1288–1619.

Masui, T., Matsumoto, K., Hijoka, Y., Kinoshita, T., Nozawa, T., Ishiwatari, S., Kato, E., Shukla, P.R., Yamagata, Y., Kainuma, M., 2011. An emission pathway for stabilization at 6 Wm^{-2} radiative forcing. Climatic Change 109, 59–76.

Meinshausen, M., Raper, S.C.B., Wigley, T.M.L., 2011a. Emulating coupled atmosphere-ocean and carbon cycle models with a simpler model, MAGICC6-Part 1: Model description and calibration. Atmospheric Chemistry and Physics 11, 1417–1456.

Meinshausen, M., Smith, S.J., Calvin, K., Daniel, J.S., Kainuma, M.L.T., Lamarque, J.-F., Matsumoto, K., Montzka, S.A., Raper, S.C.B., Riahi, K., Thomson, A., Velders, G.J.M., van Vuuren, D.P., 2011b. The RCP greenhouse gas concentrations and their extensions from 1765 to 2300. Climatic Change 109, 213–241.

Mickley, L. J., Leibensperger, E. M., Jacob, D. J., Rind D., 2012. Regional warming from aerosol removal over the United States: Results from a transient 2010-2050 climate simulation, Atmospheric Environment 46, 545–553.

Mills, G., Buse, A., Gimeno, B., Bermejo, V., Holland, M., Emberson L., Pleijel, H., 2007. A synthesis of AOT40-based response functions and critical levels of ozone for agricultural and horticultural crops. Atmospheric Environment 41, 2630–2643.

Ming, Y., Ramaswamy, V., 2009. Nonlinear climate and hydrological responses to aerosol effects. Journal of Climate 22, 1329–1339.

Mitchell, J.F.B., Johns, T.J., Gregory, J.M., Tett S.F.B., 1995. Transient climate response to Increasing sulphate aerosols and greenhouse gases, Nature 376, 501–504.

Moss, R.H., Edmonds, J.A., Hibbard, K.A., Manning, M.R., Rose, S.K., van Vuuren, D.P., Carter, T.R., Emori, S., Kainuma, M., Kram, T., Meehl, G.A., Mitchell, J.F.B., Nakicenovic, N., Riahi, K., Smith, S.J., Stouffer, R.J., Thomson, A.M., Weyant, J.P., Wilbanks, T.J., 2010. The next generation of scenarios for climate change research and assessment. Nature 463, 747–756.

Myhre, G., Samset, B.H., Schulz, M., Balkanski, Y., Bauer, S., Berntsen, T.K., Bian, H., Bellouin, N., Chin, M., Diehl, T., Easter, R.C., Feichter, J., Ghan, S.J., Hauglustaine, D., Iversen, T., Kinne, S., Kirkevåg, A., Lamarque, J.-F., Lin, G., Liu, X., Lund, M.T., Luo, G., Ma, X., van Noije, T., Penner, J.E., Rasch, P.J., Ruiz, A., Seland, Ø., Skeie, R.B., Stier, P., Takemura, T., Tsigaridis, K., Wang, P., Wang, Z., Xu, L., Yu, H., Yu, F., Yoon, J.-H., Zhang, K., Zhang, H., Zhou, C., 2013. Radiative forcing of the direct aerosol effect from AeroCom Phase II simulations. Atmospheric Chemistry and Physics 13, 1853–1877.

Myhre, G., Shindell, D., Breon, F.-M., Collins, W., Fuglestvedt, J., Huang, J., Koch, D., Lamarque, J.-F., Lee, D., Mendoza, B., Nakajima, T., Robock, A., Stephens, G., Takemura T., Zhang, H., 2013. Anthropogenic and Natural Radiative Forcing. In: Climate Change 2013: The Physical Science Basis. Contribution of Working Group I to the Fifth Assessment Report of the Intergovernmental Panel on Climate Change, edited by Stocker T.F., Qin, D., Plattner G.-K., Tignor, M., Allen, S.K., Boschung, J., Nauels, A., Xia, Y., Bex, V., Midgley, P.M., pp. 571–657, Cambridge University Press, Cambridge, United Kingdom and New York, NY, USA.

Naik, V., Voulgarakis, A., Fiore, A.M., Horowitz, L.W., Lamarque, J.-F., Lin, M., Prather, M.J., Young, P.J., Bergmann, D., Cameron-Smith, P.J., Cionni, I., Collins, W.J., Dalsøren, S.B., Doherty, R., Eyring, V., Faluvegi, G., Folberth, G.A., Josse, B., Lee, Y.H., MacKenzie, I.A., Nagashima, T., van Noije, T.P.C., Plummer, D.A., Righi, M., Rumbold, S.T., Skeie, R., Shindell, D.T., Stevenson, D.S., Strode, S., Sudo, K., Szopa, S., Zeng, G., 2013. Preindustrial to present-day changes in tropospheric hydroxyl radical and methane lifetime from the Atmospheric Chemistry and Climate Model Intercomparison Project (ACCMIP). Atmospheric Chemistry and Physics 13, 5277–5298.

Nakićenović, N., Alcamo, J., Davis, G., de Vries, B., Fenhann, J., Gaffin, S., Gregory, K., Griibler, A., Jung, T.Y., Kram, T., Lebre La Rovere, E., Michaelis, L., Mori, S., Morita, T., Pepper, W., Pitcher, H., Price, L., Riahi, K., Roehrl, A., Rogner, H.-H., Sankovski, A., Schlesinger, M., Shukla, P., Smith, S., Swart, R., van Rooijen, S., Victor, N., Dadi Z., 2000. Special Report on Emissions Scenarios. A Special Report of Working Group III of the Intergovernmental Panel on Climate Change. Cambridge University Press, Cambridge, United Kingdom and New York, NY, USA, 599 pp.

Niemeier, U., Schmidt, H., Alterskjær, K., Kristjánsson J. E., 2013. Solar irradiance reduction via climate engineering--impact of different techniques on the energy balance and the hydrological cycle, Journal of Geophysical Research 118, 11905-11917.

Van Noije, T.P.C., Le Sager, P., Segers, A.J., van Velthoven, P.F.J., Krol, M.C., Hazeleger, W., Williams, A.G., Chambers, S.D., 2014. Simulation of tropospheric chemistry and aerosols with the climate model EC-Earth, Geoscientific Model Development 7, 2435–2475.

Nordhaus, W., 1993. "Rolling the 'DICE': An Optimal Transition Path for Controlling Greenhouse Gases", Resource and Energy Economics 15, 27–50.

OECD, 2012. OECD Environmental Outlook to 2050. OECD Publishing. http://dx.doi.org/10.1787/9789264122246-en.

Ocko, I.B., Ramaswamy, V., Ming, Y., 2014. Contrasting climate response to the scattering and absorbing features of anthropogenic aerosol forcings, Journal of Climate 27, 5329–5345.

Van Oldenborgh, G.J. , Drijfhout, S., van Ulden, A., Haarsma, R., Sterl, A., Severijns, C., Hazeleger W., Dijkstra H., 2009. Western Europe is warming much faster than expected, Climate of the Past 5, 1–12.

Persad, G. G., Ming, Y., Ramaswamy V., 2012. Tropical tropospheric-only responses to absorbing aerosols, Journal of Climate 25, 2471–2480.

Pleijel, H., Danielsson, H., Vandermeiren, K., Blum, C., Colls, J., Ojanperä, K., 2002. Stomatal conductance and ozone exposure in relation to potato tuber yield results from the European CHIP programme. European Journal of Agronomy 17, 303–317.

Prather, M.J., Gauss, M., Berntsen, T., Isaksen, I., Sundet, J., Bey, I., Brasseur, G., Dentener, F., Derwent, R., Stevenson, D., Grenfell, L., Hauglustaine, D., Horowitz, L., Jacob, D., Mickley, L., Lawrence, M., Von Kuhlmann, R., Muller, J.-F., Pitari, G., Rogers, H., Johnson, M., Pyle, J., Law, K., van Weele, M., Wild, O., 2003. Fresh air in the 21st century. Geophysical Research Letters 30, 1100.

Prather, M.J., Holmes, C.D., Hsu, J., 2012. Reactive greenhouse gas scenarios: Systematic exploration of uncertainties and the role of atmospheric chemistry. Geophysical Research Letters 39, L09803.

Pleijel, H., Danielsson, H., Vandermeiren, K., Blum, C., Colls, J., Ojanperä, K., 2002. Stomatal conductance and ozone exposure in relation to potato tuber yield results from the European CHIP programme, European Journal of Agronomy 17, 303–317.

Pitman, A.J., de Noblet-Ducoudré, N., Cruz, F.T., Davin, E.L., Bonan, G.B., Brovkin, V., Claussen, M., Delire, C., Ganzeveld, L., Gayler, V., van den Hurk, B.J.J.M., Lawrence, P.J., van der Molen, M.K., Müller, C., Reick, C.H., Seneviratne, S.I., Strengers, B. J., Voldoire, A., 2009. Uncertainties in climate responses to past land cover change: First results from the LUCID intercomparison study, Geophysical Research Letter 36, L14814.

Pozzer, A., Zimmermann, P., Doering, U.M., van Aardenne, J., Tost, H., Dentener, F., Janssens-Maenhout, G., Lelieveld, J., 2012. Effects of business-as-usual anthropogenic emissions on air quality. Atmospheric Chemistry and Physics 12, 6915–6937.

Ramanathan, V., Crutzen P. J., Kiehl J. T., Rosenfeld D., 2001. Aerosols, climate, and hydrological cycle. Science 294, 2119–2124.

Ramaswamy, V., Boucher, O., Haigh, J., Hauglustaine, D., Haywood, J., Myhre, G., Nakajima, T., Shi, G. Y., Solomon, S., 2001. Radiative Forcing of Climate Change, in Climate Change 2001: The Scientific Basis: Contribution of Working Group I to the Third Assessment Report of the Intergovernmental Panel on Climate Change, edited by Houghton, J.T., Ding, Y., Griggs D.J., Noguer, M., van der Linden, P.J., Dai, X., Maskell, K., Johnson C.A., pp. 349–416, Cambridge University Press, Cambridge, United Kingdom New York, NY, USA.

Randall, D.A., Wood, R.A., Bony, S., Colman, R., Fichefet, T., Fyfe, J., Kattsov, V., Pitman, A., Shukla, J., Srinivasan, J., Stouffer, R.J., Sumi A., Taylor, K.E., 2007. Cilmate Models and their Evaluation, in Climate Change 2007: The Physical Science Basis. Contribution of Working Group I to the Fourth Assessment Report of the Intergovernmental Panel on Climate Change, edited by Solomon, S., Qin, D., Manning, M., Chen, Z., Marquis, M., Averyt, K.B., Tignor M., Miller H.L., Cambridge University Press, Cambridge, United Kingdom and New York, NY, USA.

Riahi, K., Rao, S., Krey, V., Cho, C., Chirkov, V., Fischer, G., Kindermann, G., Nakicenovic, N., Rafaj, P., 2011. RCP-8.5: Exploring the consequence of high emission trajectories. Climatic Change 109, 33-57.

Rohde, R., Muller, R.A., Jacobsen, R., Muller, E., Perlmutter, S., Rosenfeld, A., Wurtele, J., Groom, D., Wickham, C,. 2013. A new estimate of the average earth surface land

temperature spanning 1753 to 2011. Geoinformatics & Geostatistics An Overview **1**(1), 1000101.

Rotstayn, L., Collier, M., Chrastansky, A., Jeffrey, S., Luo J., 2013. Projected effects of declining aerosols in RCP4.5: unmasking global warming?, Atmospheric Chemistry Physics 13, 10883–10905.

Rotstayn, L. D., Plymin, E.L., Collier, M.A., Boucher, O., Dufresne, J.-L., Luo, J.-J., Von Salzen, K., Jeffrey, S.J., Foujols, M.-A., Ming, Y., Horowitz L.W., 2014. Declining aerosols in CMIP5 projections: Effects on atmospheric temperature structure and midlatitude jets, Journal of Climate 27, 6960-6977.

Royal Society, 2008. Ground-level ozone in the 21st century: future trends, impacts and policy implications, Policy Document 15/08, The Royal Society, London, pp. 132.

Sand, M., Berntsen, T. K., Seland, Ø., Kristjánsson J. E., 2013. Arctic surface temperature change to emissions of black carbon within Arctic or midlatitudes, Journal of Geophysical Research Atmosphere 118, 7788–7798.

Screen, J. A., Simmonds I., 2010. The central role of diminishing sea ice in recent Arctic temperature amplification, Nature 464, 1334–1337.

Schaeffer, M., Eickhout, B., Hoogwijk, M., Strengers, B., van Vuuren, D., Leemans, R., Opsteegh, T., 2006. CO_2 and albedo climate impacts of extratropical carbon and biomass plantations, Global Biogeochemistry Cycles 20, GB2020.

Schneider, S.H., 1997. Integrated assessment modeling of global climate change: Transparent rational tool for policy making or opaque screen hiding value laden assumptions? Environmental Modeling and Assessment 2, 229–249.

Segelstein, D.J., 1981. The complex refractive index of water, M.S. thesis, University of Missouri-Kansas City, Kansas City, Missouri, USA, 167 pp.

Shindell, D., 2007. Local and remote contributions to Arctic warming, Geophysical Research Letter 34, L14704.

Shindell, D.T., Faluvegi, G., 2009. Climate response to regional radiative forcing during the twentieth century, Nature Geoscience 2, 294–300.

Shindell, D., Schulz, M., Ming, Y., Takemura, T., Faluvegi, G., Ramaswamy V., 2010. Spatial scales of climate response to inhomogeneous radiative forcing, Journal of Geophysical Research 115, D19110.

Shindell, D., Kuylenstierna, J.C.I., Vignati, E., Van Dingenen, R., Amann, M., Klimont, Z., Anenberg, S.C., Muller, N., Janssens-Maenhout, G., Raes, F., Schwartz, J., Faluvegi, G., Pozzoli, L., Kupiainen, K., Höglund-Isaksson, L., Emberson, L., Streets, D., Ramanathan, V., Hicks, K., Oanh, N.T.K., Milly, G., Williams, M., Demkine, V., Fowler, D., 2012. Simultaneously mitigating near-term climate change and improving human health and food security. Science 335, 183–189.

Shindell, D., Lamarque, J.-F., Schulz, M., Flanner, M., Jiao, C., Chin, M., Young, P. J., Lee, Y. H., Rotstayn, L., Mahowald, N., Milly, G., Faluvegi, G., Balkanski, Y., Collins, W. J., Conley, A.J., Dalsoren, S., Easter, R., Ghan, S., Horowitz, L., Liu, X., Myhre, G., Nagashima, T., Naik, V., Rumbold, S. T., Skeie, R., Sudo, K., Szopa, S., Takemura, T., Voulgarakis, A., Yoon, J.-H., Lo, F., 2013. Radiative forcing in the ACCMIP historical and future climate simulations, Atmospheric Chemistry and Physics 13, 2939–2974.

Sillmann, J., Pozzoli, L., Vignati, E., Kloster, S., Feichter J., 2013. Aerosol effect on climate extremes in Europe under different future scenarios, Geophysical Research Letter 40, 2290–2295.

Smith, B., Wårlind, D., Arneth, A., Hickler, T., Leadley, P., Siltberg, J., Zaehle, S., 2014. Implications of incorporating N cycling and N limitations on primary production in an individual-based dynamic vegetation model. Biogeosciences 11, 2027-2054.

Sitch, S., Brovkin V., von Bloh W., van Vuuren D., Eickhout, B., Ganopolski, A., 2005 Impacts of future land cover changes on atmospheric CO2 and climate, Global Biogeochemistry Cycles 19, 1–15.

Sitch, S., Cox, P.M., Collins, W.J., Huntingford, C., 2007. Indirect radiative forcing of climate change through ozone effects on the land-carbon sink. Nature 448, 791–795.

Stehfest E., Bouwman, L., van Vuuren, D.P., den Elzen, M.G.J., Eickhout B., Kabat, P., 2009. Climate benefits of changing diet. Climatic Change 95, 83–102.

Stehfest E., Berg M., Woltjer G., Msangi S., Westhoek H., 2013. Options to reduce the environmental effects of livestock production - Comparison of two economic models. Agricultural Systems 114, 38–53.

Stevens, B., 2015. Rethinking the lower bound on aerosol radiative forcing, Journal of Climate, 28, 4794–4819.

Stevenson, D.S., Dentener, F.J., Schultz, M.G., Ellingsen, K., van Noije, T.P.C., Wild, O., Zeng, G., Amann, M., Atherton, C.S., Bell, N., Bergmann, D.J., Bey, I., Butler, T., Cofala, J., Collins, W.J., Derwent, R.G., Doherty, R.M., Drevet, J., Eskes, H.J., Fiore, A.M., Gauss, M., Hauglustaine, D.A., Horowitz, L.W., Isaksen, I.S.A., Krol, M.C., Lamarque, J.-F., Lawrence, M.G., Montanaro, V., Müller, J.-F., Pitari, G., Prather, M.J., Pyle, J.A., Rast, S., Rodriguez, J.M., Sanderson, M.G., Savage, N.H., Shindell, D.T., Strahan, S.E., Sudo, K., Szopa, S., 2006. Multimodel ensemble simulations of present-day and near-future tropospheric ozone. Journal of Geophysical Research 111, D08301.

Stevenson, D.S., Young, P.J., Naik, V., Lamarque, J.-F., Shindell, D.T., Voulgarakis, A., Skeie, R.B., Dalsoren, S.B., Myhre, G., Berntsen, T.K., Folberth, G.A., Rumbold, S.T., Collins, W.J., MacKenzie, I.A., Doherty, R.M., Zeng, G., van Noije, T.P.C., Strunk, A., Bergmann, D., Cameron-Smith, P., Plummer, D.A., Strode, S.A., Horowitz, L., Lee, Y.H., Szopa, S., Sudo, K., Nagashima, T., Josse, B., Cionni, I., Righi, M., Eyring, V., Conley, A., Bowman, K.W., Wild, O., Archibald, A., 2013. Tropospheric ozone changes, radiative forcing and attribution to emissions in the Atmospheric Chemistry and Climate Model Intercomparison Project (ACCMIP). Atmospheric Chemistry and Physics 13, 3063–3085.

Tai, A.P.K., Val Martin, M., Heald, C.L., 2014. Threat to future global food security from climate change and ozone air pollution. Nature Climate Change, 4, 817–821.

Taylor, K.E., Stouffer, R.J., Meehl, G.A., 2012. An overview of CMIP5 and the experiment design, Bulletin of the American Meteorological Society, 93, 485–498.

Thomson, A.M., Calvin, K.V., Smith, S.J., Kyle, G.P., Volke, A., Patel, P., Delgado-Arias, S., Bond-Lamberty, B., Wise, M.A., Clarke, L.E., Edmonds, J.A., 2011. RCP4.5: A pathway for stabilization of radiative forcing by 2100. Climatic Change 109, 77–94.

Tol, R.S.J., 1997. On the Optimal Control of Carbon Dioxide Emissions: An Application of FUND, Environmental Modelling and Assessment 2, 151–163.

Tol, R.S.J., 2002. New estimates of the damage costs of climate change: part I. Benchmark estimates, Environmental Resource Economics 2, 47–73.

Trenberth, K.E., Jones, P.D., Ambenje, P., Bojariu, R., Easterling, D., Klein A., Tank, Parker, D., Rahimzadeh, F., Renwick, J.A., Rusticucci, M., Soden, B., Zhai P., 2007. Observations: Surface and Atmospheric Climate Change. In: Climate Change 2007: The Physical Science Basis. Contribution of Working Group I to the Fourth Assessment Report of the Intergovernmental Panel on Climate Change, edited by Solomon, S., Qin, D., Manning, M., Chen, Z., Marquis, M., Averyt, K.B., Tignor M., Miller H.L., Cambridge Univ. Press, Cambridge, United Kingdom and New York, NY, USA.

UNEP 2011. Near-term Climate Protection and Clean Air Benefits: Actions for Controlling Short-Lived Climate Forcers, United Nations Environment Programme (UNEP), Nairobi, Kenya, 78pp.

Unger, M., Shindell, D.T., Koch, D.M., Streets, D.G., 2008. Air pollution radiative forcing from specific emission sectors at 2030. Journal of Geophysical Research 113, D02306.

Valcke, S., 2006. OASIS3 user guide (prism 2–5). CERFACS technical report TR/CMGC/06/73 PRISM Report No 3, Toulouse France.

Vignati, E., Wilson, J., Stier, P., 2004. M7: An efficient size-resolved aerosol microphysics module for large-scale aerosol transport models, Journal of Geophysical Research 109, D22202.

Vignati, E., Facchini, M.C., Rinaldi, M., Scannell, C., Ceburnis, D., Sciare, J., Kanakidou, M., Myriokefalitakis, S., Dentener, F., O'Dowd, C.D., 2010. Global scale emission and distribution of sea-spray aerosol: Sea-salt and organic enrichment. Atmospheric Environment 44, 670–677.

Voldoire, A., Eickhout, B., Schaeffer, M., Royer, J.F., Chauvin, F., 2007. Climate simulation of the twenty-first century with interactive land-use changes, Climate Dynamics 29, 177–93.

Von Hardenberg, J., Vozella, L., Tomasi, C., Vitale, V., Lupi, A., Mazzola, M., van Noije, T.P.C., Strunk, A., Provenzale, A., 2012. Aerosol optical depth over the Arctic: a comparison of ECHAM-HAM and TM5 with ground-based, satellite and reanalysis data. Atmospheric Chemistry and Physics 12, 6953–6967.

Van Vuuren, D.P., den Elzen, M.G.J., Lucas, P.L., Eickhout, B., Strengers, B.J., van Ruijven, B., Wonink, S., van Houdt, R., 2007. Stabilizing greenhouse gas concentrations at low levels: an assessment of reduction strategies and costs. Climatic Change 81, 119–159.

Van Vuuren, D.P., Meinshausen, M., Plattner, G.-K., Joos, F., Strassmann, K.M., Smith, S.J., Wigley, T.M.L., Raper, S.C.B., Riahi, K., de la Chesnaye, F., den Elzen, M.G.J., Fujino, J., Jiang, K., Nakicenovic, N., Paltsev, S., Reilly, J.M., 2008. Temperature increase in the 21st century mitigation scenarios. Proceedings of the National Academy of Sciences of the United States of America 105, 15258–15262.

Van Vuuren D.P., Edmonds J., Kainuma M., Riahi, K., Thomson, A., Hibbard, K., Hurtt, G.C., Kram, T., Krey,V., Lamarque, J.-F., Masui, T., Meinshausen, M., Nakicenovic, N., Smith, Steven J., Rose, S.K., 2011a. The representative concentration pathways: an overview. Climatic Change 109, 5–31.

Van Vuuren, D.P., Stehfest, E., den Elzen, M.G.J., Kram, T., van Vliet, J., Deetman, S., Isaac, M., Klein Goldewijk, K., Hof, A., Beltran, A.M., Oostenrijk, R., van Ruijven, B., 2011b. RCP2.6: Exploring the possibility to keep global mean temperature change below 2 degree C. Climatic Change 109, 95–116.

Van Vuuren, D.P., Bouwman, L.F., Smith, S.J., Dentener, F., 2011c. Global projections for anthropogenic reactive nitrogen emissions to the atmosphere: an assessment of scenarios in the scientific literature. Current Opinion in Environmental Sustainability 3, 359–369.

Van Vuuren, D.P., Batlle-Bayer, L., Chuwah, C., Ganzeveld, L., Hazeleger, W., van den Hurk, B., van Noije, T., O'Neill B., Strengers, B.J., 2012. A comprehensive view on climate change: Coupling of Earth System and Integrated Assessment Models, Environmental Research Letters 7, 024012.

Wallace, J.M., Gutzler, D.S., 1981. Teleconnections in the geopotential height field during the northern hemisphere winter. Monthly Weather Review 109, 784–812.

Wang, X., Mauzerall, D.L., 2004. Characterizing distributions of surface ozone and its impact on grain production in China, Japan and South Korea: 1990 and 2020. Atmospheric Environment 38, 4383–4402.

Wild, M., Gilgen, H., Roesch, A., Ohmura, A., Long, C.N., Dutton, E.G., Forgan, B., Kallis, A., Russak, V., Tsvetkov A., 2005. From dimming to brightening: Decadal changes in solar radiation at Earth's surface, Scieince 308, 847–850.

Wild, O., Prather, M. J., 2006. Global tropospheric ozone modeling: Quantifying errors due to grid resolution. Journal of Geophysical Research 111, D08301.

Wild, O., Fiore, A.M., Shindell, D.T., Doherty, R.M., Collins, W.J., Dentener, F.J., Schultz, M.G., Gong, S., MacKenzie, I.A., Zeng, G., Hess, P., Duncan, B.N., Bergmann, D.J., Szopa, S., Jonson, J.E., Keating, T.J., Zuber, A., 2012. Modelling future changes in surface ozone: a parameterized approach. Atmospheric Chemistry and Physics 12, 2037-2054.

Wu, S., Mickley, L.J., Kaplan, J.O., Jacob, D.J., 2012. Impacts of changes in land use and land cover on atmospheric chemistry and air quality over the 21st century, Atmospheric Environment 12, 1597–1609.

Yang, Q., Bitz, C.M., Doherty S. J., 2014. Offsetting effects of aerosols on Arctic and global climate in the late 20th century, Atmospheric Chemistry and Physics 14, 3969–3975.

Yohe, G., Andronova, N., Schlesinger, M., 2004. To hedge or not against an uncertain climate future? Science 306, 416–7.

Yoshimori, M., Broccoli, A.J., 2008. Equilibruim response of an atmosphere-mixed layer ocean model to different radiative forcing agents: global and zonal mean response, Journal of Climate 21, 4399–4423.

Young, P.J., Archibald, A.T., Bowman, K.W., Lamarque, J.-F., Naik, V., Stevenson, D.S., Tilmes, S., Voulgarakis, A., Wild, O., Bergmann, D., Cameron-Smith, P., Cionni, I., Collins, W.J., Dalsøren, S.B., Doherty, R.M., Eyring, V., Faluvegi, G., Horowitz, L.W., Josse, B., Lee, Y.H., MacKenzie, I.A., Nagashima, T., Plummer, D.A., Righi, M., Rumbold, S.T., Skeie, R.B., Shindell, D.T., Strode, S.A., Sudo, K., Szopa, S., Zeng, G., 2013. Pre-industrial to end 21st century projections of tropospheric ozone from the

Atmospheric Chemistry and Climate Model Intercomparison Project (ACCMIP). Atmospheric Chemistry and Physics 13, 2063-2090.

Yuan, X., Martinson D.G., 2000. Antarctic sea ice extent variability and its global connectivity, Journal of Climate 13, 1697–1717.

Yue, X., Unger, N., 2014. Ozone vegetation damage effects on gross primary productivity in the United States, Atmospheric Chemistry and Physics 14, 9137–9153.

Zappa G., Shaffrey, L.C., Hodges, K.I., Sansom, P.G., Stephenson D.B., 2013. A multi-model assessment of future projections of north Atlantic and European extratropical cyclones in the cmip5 climate models. Journal of Climate 26, 5846–5862.